

Department of Physics and Measurement Technology

Master's Thesis

Simulation of ion beam losses in LHC magnets

Roderik Bruce

LITH-IFM-EX-05/1514-SE

CERN-THESIS-2005-053
13/10/2005



INSTITUTE OF TECHNOLOGY
LINKÖPINGS UNIVERSITET

Department of Physics and Measurement Technology
Linköpings universitet
SE-581 83 Linköping, Sweden

Master's Thesis
LITH-IFM-EX-05/1514-SE


Simulation of ion beam losses in LHC magnets

Roderik Bruce

Supervisor: **Dr. John M. Jowett**
AB-ABP, CERN
Dr. Simone Gilardoni
AB-ABP, CERN

Examiner: **Prof. Rolf Riklund**
IFM, Linköping University

Linköping, 13 October, 2005

	Avdelning, Institution Division, Department Theory and Modelling Department of Physics and Measurement Technology Linköpings universitet SE-581 83 Linköping, Sweden	Datum Date 2005-10-13
---	--	--

Språk Language <input type="checkbox"/> Svenska/Swedish <input checked="" type="checkbox"/> Engelska/English <input type="checkbox"/> _____	Rapporttyp Report category <input type="checkbox"/> Licentiatavhandling <input checked="" type="checkbox"/> Examensarbete <input type="checkbox"/> C-uppsats <input type="checkbox"/> D-uppsats <input type="checkbox"/> Övrig rapport <input type="checkbox"/> _____	ISBN _____ ISRN LITH-IFM-EX-05/1514-SE Serietitel och serienummer ISSN Title of series, numbering _____
--	---	---

URL för elektronisk version _____

Titel Title Författare Author	Simulering av jonförluster i LHC-magneter Simulation of ion beam losses in LHC magnets Roderik Bruce
--	--

Sammanfattning Abstract <p>At the particle physics laboratory CERN, the largest accelerator ever, the Large Hadron Collider (LHC), is under construction. In the LHC ultra relativistic particles, mainly protons but also lead ions, will be brought into collision. One problem that arises in the operation is that colliding ion beams in the machine have a very large cross section for electromagnetic interactions, in particular Bound Free Pair Production (BFPP). An electron-positron pair is created by the electromagnetic field between two colliding particles and the electron is created in a bound state of one of the ions. Because of this reaction the ion changes its charge and therefore leaves the wanted trajectory and crashes in a superconducting magnet, depositing heat.</p> <p>The impact of the wrongly charged ions on the inside of the vacuum pipe was simulated with the simulation program FLUKA. It was concluded that it is not likely that enough heat is deposited in the coils of the superconducting magnet to induce a quench, although some uncertainties exist.</p> <p>A necessary safety measure that can protect against quenches due to BFPP or other beam losses is the beam loss monitor (BLM) system, which was initially designed for the proton beam. In this thesis, the ratio between the signal on the BLM and the heat deposition in the coils of the superconducting magnet was simulated for both lead ions and protons, and it was concluded that this ratio is approximately the same. This means that the same thresholds in the beam abort system can be used for both particle types, provided that the losses occur at the same places.</p> <p>Finally the response of the BLM system at the RHIC accelerator in Brookhaven to copper ions undergoing BFPP was simulated and compared with experimental data. Unfortunately the correspondence was not as good as was hoped. Several possible error sources that could cause this discrepancy were identified.</p>

Nyckelord Keywords	accelerator physics, CERN, Large Hadron Collider, quenching, superconducting magnets, Monte Carlo simulations, heat transfer
------------------------------	--

Abstract

At the particle physics laboratory CERN, the largest accelerator ever, the Large Hadron Collider (LHC), is under construction. In the LHC ultra relativistic particles, mainly protons but also lead ions, will be brought into collision. One problem that arises in the operation is that colliding ion beams in the machine have a very large cross section for electromagnetic interactions, in particular Bound Free Pair Production (BFPP). An electron-positron pair is created by the electromagnetic field between two colliding particles and the electron is created in a bound state of one of the ions. Because of this reaction the ion changes its charge and therefore leaves the wanted trajectory and crashes in a superconducting magnet, depositing heat.

The impact of the wrongly charged ions on the inside of the vacuum pipe was simulated with the simulation program FLUKA. It was concluded that it is not likely that enough heat is deposited in the coils of the superconducting magnet to induce a quench, although some uncertainties exist.

A necessary safety measure that can protect against quenches due to BFPP or other beam losses is the beam loss monitor (BLM) system, which was initially designed for the proton beam. In this thesis, the ratio between the signal on the BLM and the heat deposition in the coils of the superconducting magnet was simulated for both lead ions and protons, and it was concluded that this ratio is approximately the same. This means that the same thresholds in the beam abort system can be used for both particle types, provided that the losses occur at the same places.

Finally the response of the BLM system at the RHIC accelerator in Brookhaven to copper ions undergoing BFPP was simulated and compared with experimental data. Unfortunately the correspondence was not as good as was hoped. Several possible error sources that could cause this discrepancy were identified.

Acknowledgements

This thesis is a part of my Master of Science in Applied Physics at Linköping Institute of Technology, Sweden. The work has been carried out at the European Organization for Nuclear Research, CERN, in Geneva, Switzerland. I would like to first thank my supervisors at CERN, John Jowett and Simone Gilardoni, for all their support and for giving me the opportunity to come to CERN and work on this very interesting project. It has been a very valuable experience for me to be a part of the international environment of the LHC project. I would also like to thank my supervisor in Linköping, Rolf Riklund, for support and valuable discussions.

Furthermore, there are a number of people who have helped me during my work. I would like to thank Matteo Magistris, Alfredo Ferrari and Georg Smirnov for practical help with the FLUKA program and for giving me an understanding of some of its physical foundations.

I am also very grateful to Davide Tommasini, Daniel Leroy and Simona Bettoni for fruitful discussions and background material about quenching and superconducting magnets, and Jean-Bernard Jeanneret for interesting discussions about the heat capacity of superfluid helium among other things.

Finally I would like to express my gratitude towards Stephan Russenschuck for providing me with the magnetic field maps and temperature margin for the LHC dipoles, Ramesh Gupta, Brookhaven National Laboratory, for the magnetic field maps for the RHIC dipoles and towards Angelika Drees and the rest of the team at RHIC for the experimental data from the BFPP experiment.

Contents

1	Introduction	1
1.1	CERN	2
1.2	The accelerator complex	4
2	Ion operation at CERN	7
2.1	Operation of the LHC	7
2.2	LHC Dipole Magnets	9
2.3	Superconductivity and quenching	15
2.4	Cross sections and luminosity	18
2.5	Bound Free Pair Production (BFPP)	18
2.6	Interaction between particles and matter	23
2.7	Choice of method	27
3	Monte Carlo simulations	29
3.1	General theory of Monte Carlo simulations	29
3.1.1	Random numbers	29
3.1.2	Schematic Monte Carlo model of the present problem	30
3.1.3	The role of Monte Carlo simulations	32
3.2	The FLUKA program	33
3.2.1	General use	34
4	Simulation of ion beam losses in a LHC main dipole	37
4.1	Modelling of the dipole	37
4.2	Modelling of the beam	40
4.3	Biasing methods	41
4.4	Scoring methods and results	42
5	Quench limit and conclusion	51
5.1	Quench limit for the LHC main dipoles	51
5.2	Conclusion for the steady state case	57
5.3	BFPP Energy deposition on short timescales	63
5.3.1	Calculation without helium	65
5.3.2	Calculation with helium	67

6	The beam loss monitor system	73
6.1	Ionization chambers	73
6.2	Simulation setup	76
6.3	Results	78
7	Comparison with experimental data from RHIC	81
7.1	The BFPP experiment	81
7.2	Simulation setup	85
7.3	Results and conclusion	88
8	Concluding remarks	91
	Bibliography	93
A	Common acronyms	97

Chapter 1

Introduction

This Master's Thesis investigates a possible limitation of the performance of a future particle collider, called the Large Hadron Collider (LHC), which is currently under construction at the physics centre CERN (European Organization for Nuclear Research) in Switzerland. Here high energy beams of protons and ions will be brought into collision. At the collision point, the colliding ions might change their charge due to a process called Bound Free Pair Production (BFPP). Because of that, they leave their design trajectory and might damage the machine through a quench in one of the superconducting magnets, which form the accelerator. The first task in this thesis is to investigate how severe this effect is using computer simulations. The second task is to simulate the performance of the beam loss monitor system for ions in order to investigate if the planned design is sensitive enough for detecting the beginning of a possible quench. A quench could arise due to the BFPP process or also due to other beam losses. The last task is to simulate the signal of the beam loss monitor system at the RHIC (Relativistic Heavy ion Collider) accelerator in Brookhaven, USA, and compare this with real data.

The structure of this thesis is:

- Chapter 1 gives a short introduction to CERN and the Large Hadron Collider project, and more specifically to the ion scheme that will cause the studied effect.
- Chapter 2 describes the present problem along with some background theory that will help in understanding it. The chapter is intended also to cover subjects that could be new to someone not familiar with CERN and accelerators and that will help give a deeper understanding of the rest of the thesis. It is sufficient for a reader familiar with the background theory and CERN to read Sections 2.5 and 2.7.
- Chapter 3 presents the theory behind Monte Carlo simulations in general and the FLUKA program, which is the main tool used to study the problem. This part is not essential for the rest of the thesis and might be omitted by a reader familiar with the concepts.

- Chapter 4 describes how the impact of the lost ions from the BFPP process on the superconducting magnet was simulated. The result of the simulation gives the power deposition in the superconductors.
- In Chapter 5, an attempt is made to quantitatively understand the level of the power density that will make an LHC dipole magnet quench. This level can then be compared with the results of the simulations. Here also the results and conclusions for this problem are presented. Finally, some means to alleviate the problem are suggested.
- Chapter 6 gives an introduction to the beam loss monitor system at LHC and describes how it was simulated. Also the results of the simulation are presented, and conclusions are drawn about whether the present design initially made for protons is sensitive enough also for the ion scheme.
- Chapter 7 finally, explains how the beam loss monitor system at RHIC was simulated during operation with copper ions that undergo BFPP. The results are compared to experimental data.

1.1 CERN

CERN, the European Organization for Nuclear Research, is the world's largest particle physics centre [1]. The name CERN is an abbreviation for the French name Conseil Européen pour la Recherche Nucléaire. This name is however not used anymore — the new name is European Organization for Nuclear Research, but the abbreviation has remained. CERN was founded in 1954 by a collaboration of 12 European states. It is situated close to Geneva on the border between France and Switzerland.

At present, CERN has more than 20 member states in Europe and also a number of observer states. The member states have certain duties and privileges — they have to make financial contributions but can take part in the council meetings and decision-making. Observer states are allowed to attend the meetings but do not have the same financial duties. The research facilities constructed at CERN are often so advanced and complex that they are too expensive for a single country. Therefore the member states have to cooperate in order to realize this kind of scientific research.

Today CERN has about 3000 employees, and an additional 6500 particle physicists from over 500 universities in more than 80 countries do parts of their work here.

The primary goal of CERN is to provide physicists with the necessary tools to study the constituents of matter and the forces that hold them together. The most important tools are the accelerators and the detectors. An accelerator is a machine that uses electrical fields to accelerate electrically charged particles to high energies. When highly energetic particles collide, they may annihilate and new particles may be created from the energy set free. By colliding the accelerated particles inside a detector, scientists can assemble data to reconstruct the collision

Figure 1.1. Map showing the location of the CERN sites on the border between France and Switzerland north-west of Geneva. The large circle indicates the position of the largest accelerator at CERN, the LHC.

with great precision. In this way it is possible to identify the components of particles, calculate their masses, obtain information about how they interact, etc.

1.2 The accelerator complex

At present, the LHC (Large Hadron Collider), which will be the largest particle accelerator in the world, is being constructed at CERN. The LHC should help to clarify many mysteries in modern particle physics. In the LHC, two particle beams will circulate in opposite directions on different trajectories. Four different experiments will be built around the LHC, where the two beams will be brought together inside a huge detector, in a so-called interaction point.

Two of the constructed experiments, the CMS (Compact Muon Solenoid) [2] and ATLAS (A Toroidal LHC ApparatuS) [3], will further test the standard model of particle physics and its possible extensions. This model has so far yielded perfect agreement with existing experiments. The standard model introduces the generation of particle masses via the interaction with the Higgs particle, which scientists hope to detect in the high-energetic proton collisions in the LHC. The CMS and ATLAS experiments will also try to check theories that go beyond the standard model — for instance, researchers also hope to find supersymmetric particles. The goals of these two experiments are approximately the same, but different types of detectors will be used.

The LHCb [4] experiment will study the physics of B-mesons (mesons in which one of the constituents is a bottom quark). By measuring CP-violation in B-meson decays, scientists hope to draw conclusions about the ratio of matter and antimatter in the universe and also explain why it seems to be a very large imbalance.

The ALICE (A Large Ion Collider Experiment) [5] experiment, finally, will as main project study lead ion collisions at ultra-high energies. The goals of this project is to find and study Quark-Gluon plasma, which is a hadronic state of matter that was believed to exist just a millisecond after the big bang, and Colour Glass Condensate, which is believed to be a precursor of the Quark-Gluon plasma.

Normally quarks are locked inside bigger particles by the so called confinement law. Quarks carry colour charges, and they have to be bound together in either groups of three so that their colours blend to "white" in baryons (for instance protons and neutrons), or in pairs of quarks and anti-quarks inside mesons, where the colours and anti-colours cancel. When energy is added, instead of separating a quark from the others, new pairs of quarks and anti-quarks are created from this energy and form new bound states in baryons or mesons. This pairing process starts as soon as a quark gets separated from the other quarks that it is bound to by more than one femtometre.

Today it is however generally believed that "free" quarks must have existed in the extreme conditions of the very early universe. According to theory, the universe consisted of a very hot gas of quarks and gluons during the first 40 microseconds after the big bang. This state of matter is the so-called Quark-Gluon plasma [5].

In order to understand more about how the confinement works and how the universe has evolved, physicists want to create Quark-Gluon plasma in the labo-

ratory. This could be done in high-energy collisions of heavy ions. If the energy density is high enough, on the order of $10 \text{ GeV}/\text{fm}^3$, the collision will pack the matter so closely together, that a single quark will see numerous other quarks within a femtometre in all directions, so that the confinement will no longer matter.

In 2004, something that could be Quark-Gluon plasma was discovered in the presently largest heavy ion collider in the world, RHIC [6] (Relativistic Heavy Ion Collider, described in more detail in Chapter 7) in the USA. However, it did not behave as expected and theorists and experimentalists could not agree whether it really was Quark-Gluon plasma or not. It showed many unexpected properties—for instance, it seemed to be more a liquid than a gas. These experiments gave rise also to new theories about another kind of hadronic matter, the so-called Colour Glass Condensate. Scientists at CERN hope that the heavy ion collisions in the LHC, which will have much higher energy than the ones at RHIC, will permit the study of both these new states of matter, so that their properties can be studied with the detectors in the ALICE-experiment. Also CMS and ATLAS will study ion collisions as secondary tasks.

The lead ions, which will be used for the experiments in the LHC, will be accelerated up to $2.76 \text{ TeV}/\text{nucleon}$. Never before have heavy ions been accelerated to such high energies and with such high intensity. The operation with lead ions imposes however a lot of challenges of practical and technical nature, that have to be solved before the start-up of LHC. One of the obstacles that have to be overcome is the issue of Bound Free Pair Production, which is the main topic discussed in this report.

Chapter 2

Ion operation at CERN

2.1 Operation of the LHC

The accelerators at CERN form a chain of interlinked machines, as illustrated in figure 2.1. Each machine is larger and can accelerate particles to higher energies than the preceding one. Larger accelerators are needed in order to increase the resolution of the studied matter, and also because the probability for rare processes often increase with energy.

The particles that will be accelerated and brought into collision in the initial phase of operation in the LHC are protons and Pb^{82+} lead ions. The particles are first extracted from one of the sources and accelerated by one of two linear accelerators, called LINACs, up to an energy of 50 MeV for protons and 4.2 MeV/nucleon for ions. A LINAC is composed of a series of accelerating structures, which use a time varying electric field parallel to the direction of motion of the particles.

After that, the protons are transported and injected into the Proton Synchrotron Booster (PSB), and the ions to the Low Energy Ion Ring (LEIR). Both these machines are synchrotrons. A synchrotron is a circular accelerator, where the particles are kept on a constant orbit with bending magnets. On each lap they also pass a radio frequency cavity with an accelerating electric field. When the energy of the particle increases, the bending field has to be adjusted accordingly to keep the particle on the same orbit.

The protons are ejected from PSB when they have reached an energy of 1.4 GeV and the ions from the LEIR when they have reached 72 MeV/nucleon. After a short transport they are then injected into the Proton Synchrotron (PS). There they are accelerated up to 26 GeV for protons and 6 GeV/nucleon for ions. In the same way they continue through the Super Proton Synchrotron (SPS), where they are accelerated even more. When they leave the SPS, the protons have an energy of 450 GeV and the ions 177 GeV/nucleon. This kind of stepwise acceleration through one machine after the other is necessary since it is very hard to accelerate the particles from MeV to TeV with only one machine with fixed geometrical radius. In addition, some of the intermediate accelerators deliver particles not only to the next accelerator, but also to experiments performed at lower energies.

Figure 2.1. The CERN accelerator complex (not to scale). The accelerators discussed in this section are the Linear Accelerators (LINACs), the Proton Synchrotron Booster (PSB), the Proton Synchrotron (PS), the Super Proton Synchrotron (SPS), the Large Electron-Positron collider (LEP) and the Large Hadron Collider (LHC). At CERN also experiments with neutrinos (CNGS, CERN Neutrinos to Grand Sasso), electrons (CTF3, CLIC Test Facility 3), neutrons (n-TOF, neutrons Time Of Flight) and anti-protons (AD, Anti-proton Decelerator) are being performed.

Because of the interlinked accelerators, it is possible to perform experiments at CERN over a broad range of energies.

Until a few years ago electrons and positrons were transported farther from SPS to an even more powerful accelerator, the Large Electron-Positron collider (LEP). It was a giant circular accelerator used to accelerate and collide electrons and positrons at a center of mass energy of 204 GeV. It was situated in a tunnel 100 m underground with a circumference of 27 km. It goes through both France and Switzerland, as can be seen in figure 1.1. It was the largest scientific instrument ever used. In 1991 it was decided that LEP should be replaced by the LHC. This machine will be placed in the same tunnel that contained LEP, but as mentioned earlier it will be used to accelerate and collide protons and heavy ions instead. With this machine, it will be possible to reach much higher particle energies (7 TeV for protons and 2.76 TeV/nucleon for lead ions), which may lead to new discoveries and give answers to some of the still unsolved mysteries in particle physics. The reason why protons and ions can reach a higher energy than electrons in a machine with the same geometrical radius is that they emit less synchrotron radiation due to their larger mass. On the other hand, the protons and ions are not point-like. The collisions will be between single quarks or gluons, which means that the effective energy in the collision will be less than the energy of the particles, and also that the collisions in the LHC will be much more complex to study. LEP was shut down in November 2000 in order to start the installation of the LHC. The LHC is due to be switched on in 2007.

In figure 2.2 a more schematic layout of the experiments and facilities underground can be seen.

In the tunnel, magnetic elements will be placed, surrounding the beam. The magnets in the LHC are mainly dipoles, which produce an almost homogenous vertical field, orthogonal to the propagation direction, in order to bend the trajectories of the particles and give them a correct radius of curvature, and quadrupoles, which are used to focus and defocus the beam. The layout of the magnets in the tunnel is called the lattice. The two beams themselves will travel inside the magnets in small pipes with vacuum inside. The wall of these pipes is called beam screen. Its primary purpose is to absorb most of the synchrotron radiation emitted by the protons. A computer generated image of how it will look in the tunnel is shown in figure 2.3.

In the machine, the ions will be grouped by the radio frequency field into 592 bunches, which are a sort of packets of particles, separated in time, that have the approximate same momenta and space coordinates. At the interaction points, the beams with opposite directions will be brought together in a collision that will be observed by the detectors. The region of most interest in this report is the one around the ALICE experiment, called Interaction Point 2 (IP2).

2.2 LHC Dipole Magnets

The LHC dipoles will be described in more detail, since a dipole magnet is the main object for the simulations later on in this report. A drawing of the transverse cross

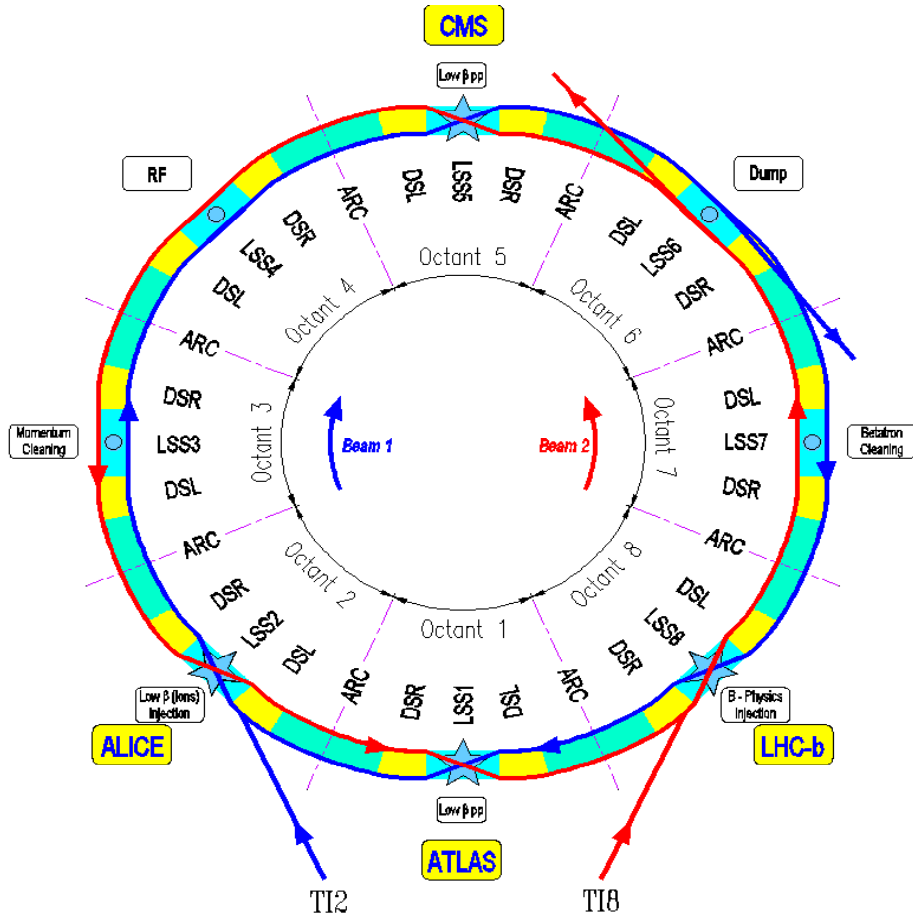


Figure 2.2. Schematic overview of the LHC. ARC stands for the regular LHC cell composed by 3 dipoles and a quadrupole. DS is the dispersion suppressor region, where the lattice has two dipoles for every quadrupole (R for right of the interaction point and L left with respect to beam 1 which is in blue). LSS stands for Long Straight Section, where the experiments are located and the beam collisions or other special sections are foreseen.

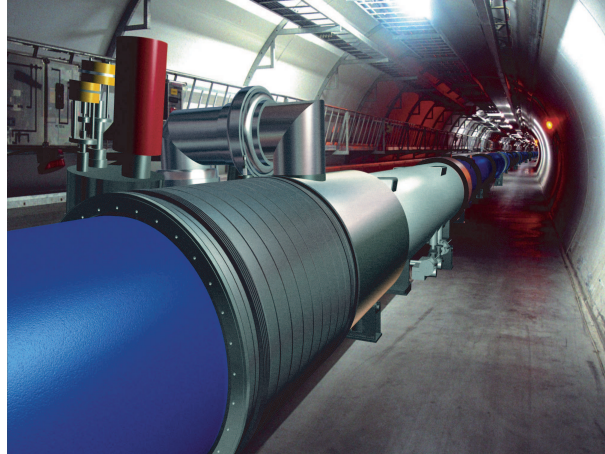


Figure 2.3. Computer generated picture of the LHC tunnel. The cylindrical construction on the left is the beamline.

section of a dipole magnet is shown in figure 2.4. An LHC dipole is 14.6 metres long and there will be 1232 dipoles placed along the tunnel to bend the beam and give it the correct radius of curvature. Since the charged particles are ultra-relativistic, a very strong vertical field with a magnitude of 8.33 T is needed in the beampipe. This is impossible to achieve with a traditional magnet that is limited by iron saturation and therefore superconducting magnets are used. Superconductivity as a physical phenomena will be described in more detail in Section 2.3.

The outermost layer of the dipole is called the cryostat or the vacuum vessel and serves as a heat insulation and vacuum barrier. It has a diameter of 91.4 cm. The next layer inside the cryostat is the thermal shield. It is there for insulation, since the inner parts of the magnet, called the cold mass, need to be cooled down to a very low temperature, 1.9 K, in order to keep the cables in their superconducting state. The air in the tunnel outside the vacuum vessel is at room temperature. The massive block inside the thermal shield is the yoke made of iron, which closes the magnetic field lines. Around the two iron beampipes, that are filled with vacuum and have an inner diameter of 5.6 cm, the superconducting coils are placed in order to create the strong field inside the pipe. This is illustrated in figure 2.5. They are kept in place by a steel collar under high pressure. Around each beam pipe there are two coils, one outer and one inner, which can be seen in figure 2.4. Each coil consists of several windings of cable. The cable itself consists of wires, so-called strands, with channels for helium between them, surrounded by an insulator. The strands are the actual current carriers. A strand has a diameter of roughly 1 mm and is made of around 8000 filaments of superconducting NbTi embedded in a copper matrix. The volume ratio of copper to superconductor is about 1.65. The composition of the cable is illustrated in figure 2.6.

In the superconducting state, all the current goes through the superconductor and not through the copper. The copper is however needed for several reasons.

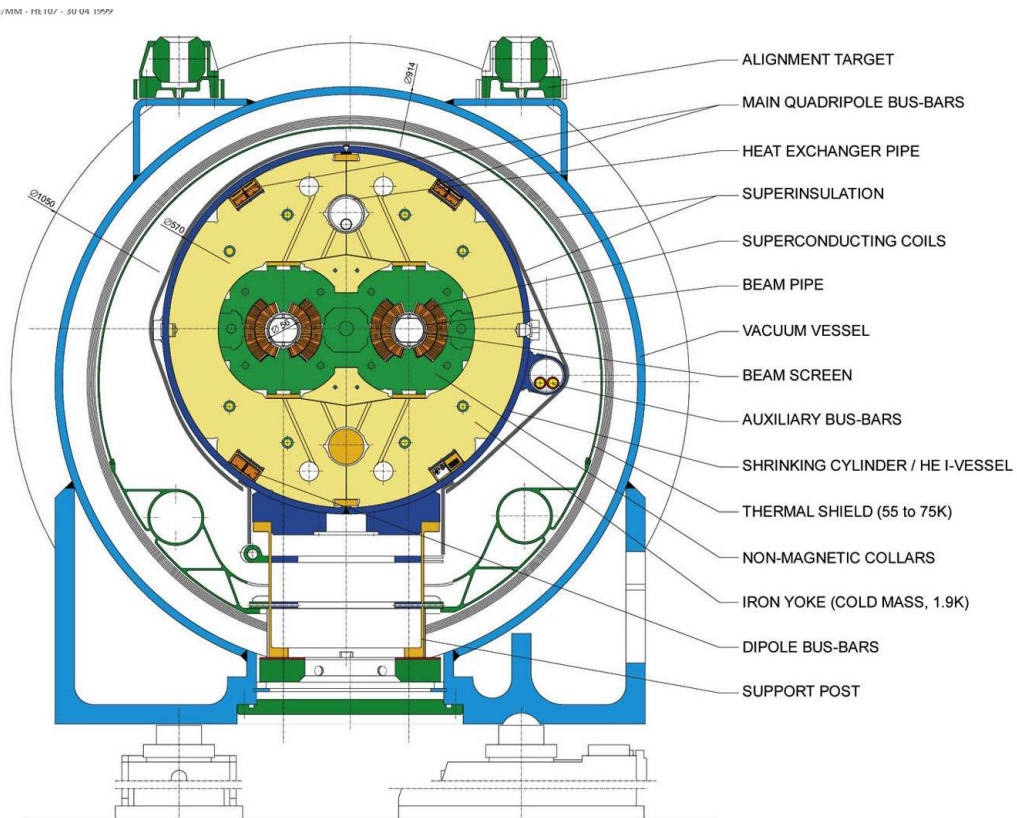


Figure 2.4. The transverse cross section of an LHC dipole magnet.

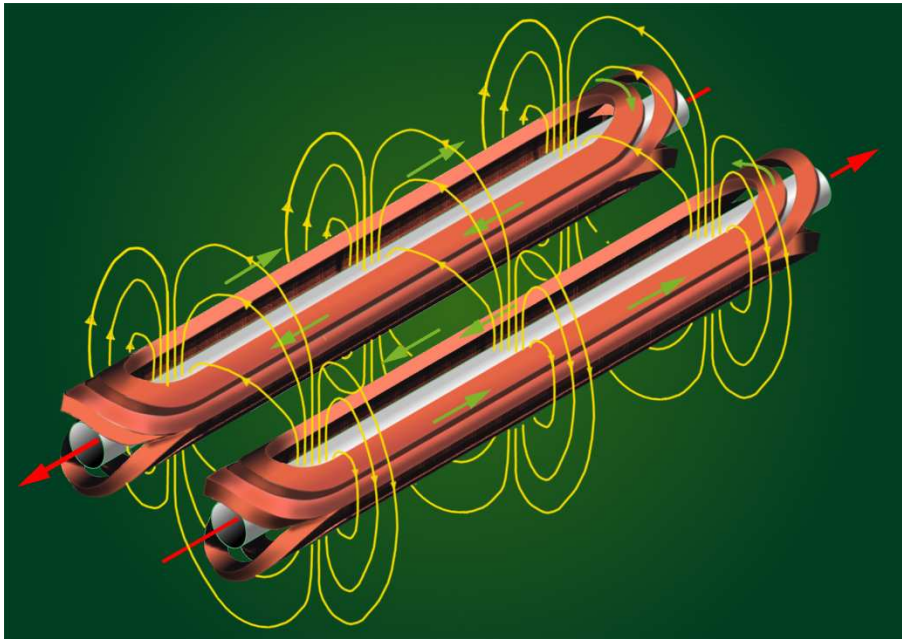


Figure 2.5. Schematic view of the coils and how they lie around the beampipes. Also the directions of the two beams (red arrows), the currents (green arrows) and the the magnetic field lines (yellow arrows) are shown.

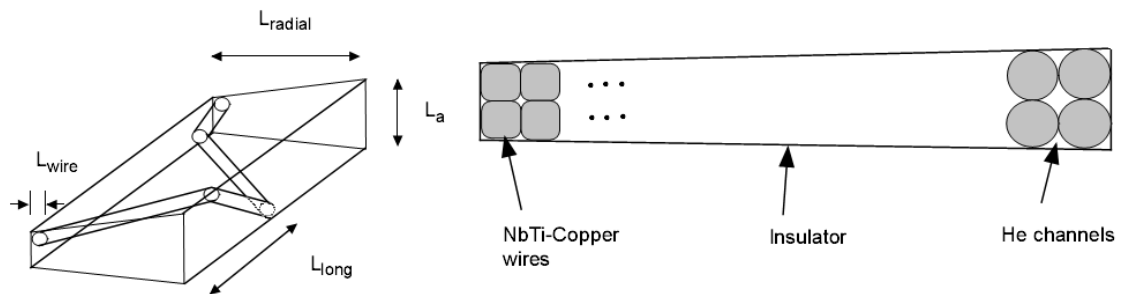


Figure 2.6. A schematic view of the a strand inside the LHC dipole cable (left) and the transverse cross section of a superconducting cable (right). The figure is taken from [7].

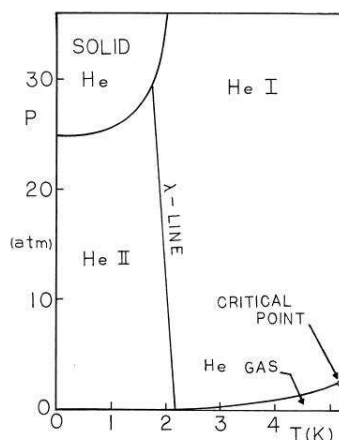


Figure 2.7. The phase diagram of helium with pressure on the y-axis and temperature on the x-axis. The superfluid is called He II and the normal fluid He I. The transition between these two phases takes place at the so called λ -line. The figure is taken from [8].

Firstly, NbTi itself is a quite brittle material, and the coils are under high pressure inside the collar. Therefore the copper is necessary in order to make the structure more robust. Also, if a part of the cable were to make a transition to the normal conducting state, the electrical resistance of NbTi would be very high, which means that a lot of heat would evolve. However, if the copper is present, the current will go through the copper part instead since it has less resistance, and less heat will develop. A third reason for its presence is that the copper improves the heat conductivity of the cable.

The coils are cooled down to 1.9 K by a constant flow of superfluid helium. Superfluidity is another state of aggregation that the helium can reach at temperatures below the so called lambda line, which can be seen in figure 2.7, where a phase diagram for helium is shown. Normally, liquid helium at low temperature is described by a two-fluid model, where one part is superfluid and the other one is normal. In the superfluid part, the viscosity and the entropy equal zero, and the heat conductivity is infinite. A zero viscosity means that the superfluid flows without resistance. At atmospheric pressure, the transition between normal fluid and superfluid helium takes place at 2.1 K. A superfluid has some very peculiar properties. A property that is very useful for the cooling of superconducting magnets, is that it can flow through very small capillaries of the order of 10^{-4} cm without resistance. Thus the helium can flow through the tiny channels inside the cable, which is a very efficient way of cooling the superconductors. Also a thicker pipe with flowing helium will pass through the yoke.

2.3 Superconductivity and quenching

Superconductivity as a phenomenon was discovered in 1911 by the Dutch physicist Kammeringh Onnes, when he noticed that the resistance of a mercury sample suddenly dropped to an immeasurably small value below a certain temperature. Superconductivity cannot be explained within a framework of classical physics and was not fully understood until the advent of the Bardeen, Cooper and Schrieffer theory (BCS) in 1957. This theory revolutionized our understanding in the area [8, 9].

According to BCS theory, a metal can transport an electrical current with practically no resistance, when it is in the superconducting state. This current, called supercurrent, is not transported by conduction electrons as in a normal conductor, but instead by pairs of electrons bound to each other, so-called Cooper pairs. A material is superconducting when the state of the material is under a three-dimensional critical surface in the space spanned by the temperature, the magnetic field in the sample and the current density. This is illustrated in figure 2.8, where the critical surface of NbTi is shown [8]. As can be seen in the figure, the material is only in its superconducting state at very low temperatures. The transition from the superconducting to the normal state is called a quench. There are several possible ways to make this transition. For instance, the magnetic field and current can be kept constant and the temperature gradually increased. The temperature at which the quench occurs is called the critical temperature. This temperature is different for different values of the magnetic field and the current density. If these quantities have large values, the starting point is somewhere in the top of the space shown in figure 2.8 and thus the distance out to the surface along a line parallel to the temperature axis is a lot smaller than if the starting point had been somewhere in the base, meaning a smaller increase in temperature will induce a quench. Analogously, one can define a critical magnetic field and a critical current.

If a quench occurs in a small volume of a superconductor, for instance through localized external heating, this volume will be normal conducting. And if there is a current flowing through the conductor, it will feel a resistance in this small normal conducting volume. This will cause Joule heating, which heats the closest surroundings of the conductor; maybe so much that they also become normal conducting. And as the normal conducting zone grows, more and more heat is developed in the resistive parts, so larger and larger parts of the superconductor will quench. In the end of such a process the whole conductor is normal conducting. So even if only a very small zone in a superconductor makes the transition, the quench will rapidly propagate. The smallest zone that can cause the whole conductor to quench is called the minimum propagating zone. This zone is normally on the order of a few micrometers [10].

There are two types of superconductors. The ones belonging to type one have a very rapid transition between the superconducting and normal conducting states. If, for instance, a homogenous magnetic field is increased until a quench occurs, the whole material will make the transition to the normal conducting state at once. For a type two superconductor this is not the case. At some value of the

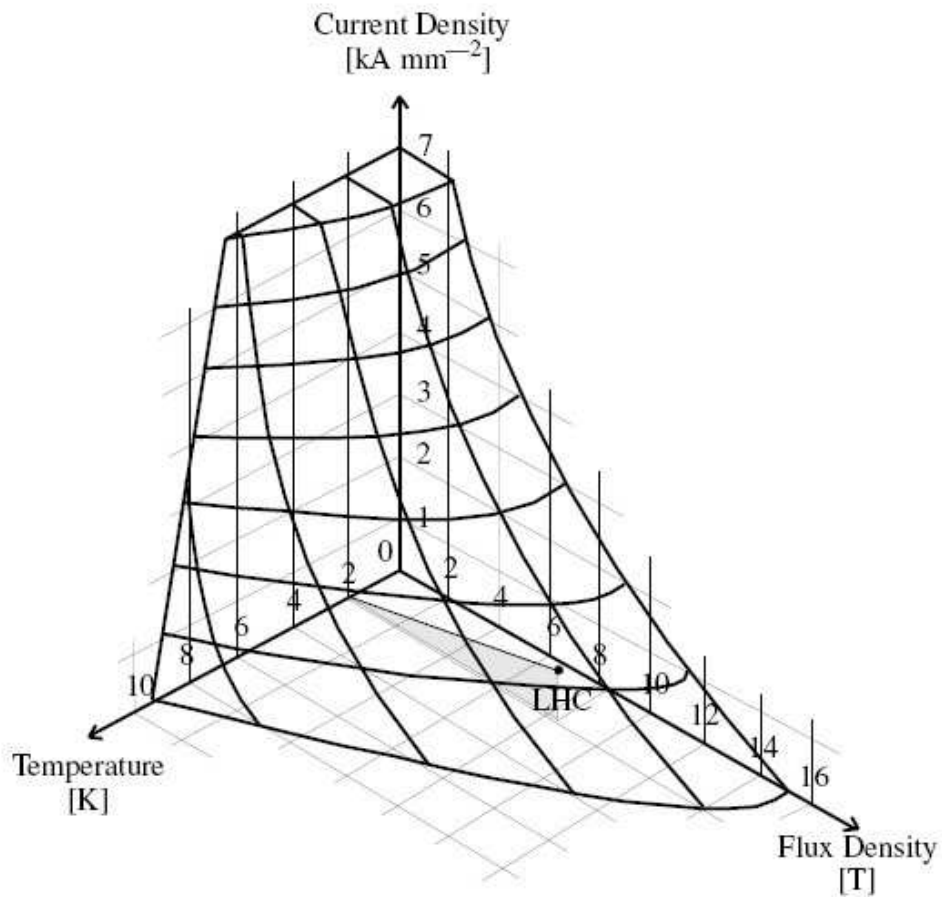


Figure 2.8. The critical surface of NbTi (the material used in the coils of the LHC dipole magnets). When the point with coordinates (temperature, magnetic field and current density) is below the surface, the material becomes superconducting. The surface has a slightly different shape for different materials but has always a qualitatively similar form, so that if the material is in the superconducting state below the surface and any of the three coordinates is increased, a quench will occur at some point. Also the load line for LHC is marked. However, the LHC cables have a slightly lower temperature margin than pure NbTi. Taken from [8].

B -field, called the first critical field, small regions will become normal conducting, and as the field is increased, more and more regions will make the transition until in the end the whole sample is back in the normal state at the second critical field. A magnetic field can not exist inside the bulk of a type one superconductor — the field lines are passing around it (the so called Meissner-Ochsenfeldt effect [9]). The current passing through a type one superconductor is a surface current, since also no currents can exist in the bulk. This is exactly the same for a type two superconductor below the first critical field. Between the first and second critical field however, in the so-called Meissner phase, parts of the material are superconducting while other parts are normal conducting. Here a magnetic flux can penetrate the bulk of the sample in the normal conducting regions, and currents are allowed around these regions. A type two superconductor is more suitable as a magnet than a type one. Typically a type one superconductor has a critical temperature of just a few Kelvin, which makes them inconvenient to use because of the needed cooling systems. Type two superconductors often have a higher critical temperature.

Superconductors are very suitable to use in magnets, where strong magnetic fields are needed. Since the superconductors can carry a very high current density with almost no resistance, only a very small power input is needed. It is also possible to achieve higher field strengths with a superconducting magnet, since a normal magnet will be saturated at some point. The magnets used in the LHC ring are superconducting, as mentioned in Section 2.1. The magnetic field of a dipole magnet in the LHC at nominal beam energy is 8.33 T. A disadvantage of superconducting magnets is that they require a very low operational temperature. In the case of LHC dipoles, the operating temperature is at 1.9 K and the quench limit at somewhere above 3.3 K at a magnetic field of 8.33 T. This requires a very powerful cooling system, which in LHC will be based on liquid helium flowing around the coils as explained in Section 2.1.

In the present problem with BFPP, which will be explained in Section 2.5, the ultimate goal is to see whether the superconducting dipole magnet quenches or not due to the temperature rise caused by the secondary ion beam. A quench in a magnet destroys the field, which in turn could make the whole beam leave its trajectory and be lost into other magnets and quench them as well. There exists a protection system that will dump the beam before it is lost in the ring and fire so-called quench heaters, but in a worst-case scenario the magnets could actually be physically damaged if they are hit directly by the beam. Replacing a broken magnet in the tunnel takes a lot of time — it is estimated to take one month [11]. This is not only very expensive but also delays the time schedule for the experiments. Even if no physical damage is done, a lot of valuable experiment time is lost, since the machine must be restarted and filled again with new bunches of particles. In the case of ions, this could take several hours. Therefore it is very important to avoid magnet quenches in the accelerator.

2.4 Cross sections and luminosity

When the particle beams collide, there are different parameters that determine which and how many reactions take place. For a given reaction, the number of events per time unit R in an accelerator is given by

$$R = \sigma \cdot L \quad (2.1)$$

where σ is the total cross section for the reaction and L is the luminosity of the collider.

The total cross section comes from the physics and is connected to the probability for a single reaction. Classically it can be described as the area of a scattering object that an incoming particle has to hit in order to be scattered. There exists also a differential cross section called $d\sigma/d\Omega$, which is dependent on the solid angle. It represents in classical physics the area that a particle has to hit to scatter in a certain solid angle $d\Omega$. Quantum mechanically, the cross section still has the dimension of an area but does not represent a physical area in the same way as in classical physics. Here the differential cross section is calculated by first solving the Schrödinger equation (or the Dirac equation in the relativistic case) for the incoming particle in the scattering potential of the other one, and then calculating the ratio of the probability current passing through the solid angle $d\Omega$ and the incident probability current density. Normally in particle physics, cross sections are given in the unit barn, where $1 \text{ barn} = 10^{-28} \text{ m}^2$.

The luminosity L is a machine parameter that tells something about how frequently the circulating particles will have an opportunity to interact. It can also be seen as a measure of the quality of an accelerator. It is proportional to the square of the number of ions N_i^2 in every bunch, the number of bunches N_b circulating in the machine and the revolution frequency f , and inversely proportional to the spread σ_x and σ_y in the transverse coordinates of the bunches [12]:

$$L \propto \frac{N_i^2 \cdot N_b \cdot f}{\sigma_x \cdot \sigma_y} \quad (2.2)$$

For the ion beam in the LHC, the luminosity is $L = 10^{27} \text{ cm}^{-2}$.

2.5 Bound Free Pair Production (BFPP)

When the ultra relativistic ion beams collide in the LHC, a lot of different physical processes take place. Apart from the wanted nuclear interactions that will be studied by the experiments, there are also a number of mostly unwanted interactions that can influence and limit the performance of the accelerator in different ways. If the collisions are peripheral, that is, the lead ions do not collide head on but pass each other by close enough to significantly influence each other, the electromagnetic interactions dominate.

The most common electromagnetic processes that can take place at the interaction points are Rutherford scattering and Free Pair Production [13]. In Rutherford scattering, the ions elastically exchange a virtual photon as they pass each other

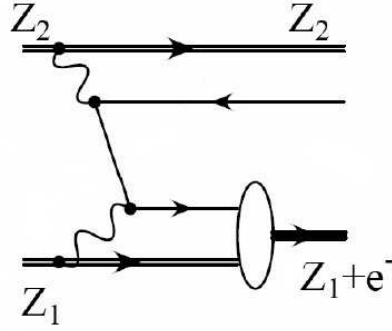
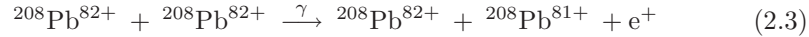


Figure 2.9. The Feynman diagram for the BFPP process. The charges of the two interacting ions are called Z_1 and Z_2 . In the case of LHC, $Z_1 = Z_2 = 82$ for the lead ions. The diagram is taken from [15], where also an overview of the physics processes for peripheral collisions with relativistic heavy ions is given.

by, which slightly changes the momenta of both particles. The change is however very small and this process has therefore very little influence on the behaviour of the beam. A very small deviation in momentum can be tolerated, and according to [14] Rutherford scattering does not change the momenta enough to cause problems for the machine operation.

In Free Pair Production, the virtual photon exchanged by the ions is converted into an electron-positron pair. The change in momentum for the involved ions is also here so small that it does not have a big effect on the behaviour of the beam.

There is however also a probability that an electron-positron pair is created, but that the electron is created in a bound state of one of the nuclei. This process is called Bound Free Pair Production (BFPP). Explicitly written, the reaction is:



The process can also be described with the Feynman diagram shown in figure 2.9.

The lead ions circulating in the machine will be fully stripped (they do not have any electrons). The magnetic field in the beam pipe is adapted to bend these fully stripped ions at a given energy so that they exactly follow the wanted path. If an ion captures an extra electron, its charge will be changed, which means that the Lorentz force acting on the ion will decrease. However, the momentum will remain approximately constant, so the radius of curvature of the trajectory will increase. These ions, which have captured an extra electron, will form a secondary beam that will leave the wanted trajectory and be lost somewhere in the machine.

The severity of this effect depends on where in the machine the ions will end up but also on the probability for the BFPP reaction. Numerous references exist [16, 17, 18, 19], where the cross section for the BFPP process is determined both theoretically and experimentally. Since the cross section depends on the energy of the particles, and no existing accelerator can even get close to the LHC-energy, the experimental reports are always based on results for lower energies that are

extrapolated to the LHC-energy. In [16], the cross section for BFPP is theoretically calculated using the plane wave Born approximation. The calculation is performed for electron capture into each atomic shell, and then the different contributions are summed up in order to get the cross section for capture to any shell.

If the two colliding ions have different charges Z_1 and Z_2 and the electron is captured by the ion with charge Z_1 , the following approximate relationship for the cross section for BFPP, σ_{BFPP} , is found:

$$\sigma_{\text{BFPP}} \propto Z_1^5 Z_2^2 (A \ln \gamma_{CM} + B) \quad (2.4)$$

Here also the coefficients A and B are slightly dependent on Z , although the main Z dependence is in the first factors. The numerical values for $AZ_1^5 Z_2^2$ and $BZ_1^5 Z_2^2$ are given in [16] for different ions, energies and atomic shells where the electron is captured. Numerically, the resulting value for the total cross section for two colliding lead ions with $Z_1 = Z_2 = 82$ at an energy of 2.76 TeV/nucleon (the nominal energy in the LHC) is:

$$\sigma_{\text{BFPP}} = 281 \text{ barn} \quad (2.5)$$

This cross section refers to electron capture to one specific ion in the pair. The cross section for electron capture to either of the two involved ions is twice as large as the value given in equation (2.5). The derivation of the formulas and value for the cross section can be found in the original paper [16].

Today this is believed to be the best estimate available, and this is also the value used in [13]. In [16] a comparison is made with other estimates and a fair agreement is found.

The value of this cross section can be compared with the total cross section for hadronic interactions between the colliding ion bunches. This cross section is $\sigma_{\text{H}} = 8 \text{ barn}$ according to Section 21.4 in [13]. This means, that the BFPP reaction is around 35 times more likely to happen than the wanted hadronic interactions that will be the main subject of study by the experiments. The very large value of the BFPP cross section gives a hint that it could cause severe problems for the accelerator operation and that a closer investigation of its consequences is necessary.

Any accelerator has a certain tolerance for deviations. If the momentum of a particle changes only slightly, it might still be that it never hits the beampipe but instead stays on an off-centre orbit. This way it is not useful anymore in the experiments, but it stays in the pipe and does no damage. But if the momentum change is too large, the particle starts to diverge so much from the wanted trajectory that it hits the inside of the pipe. If the original momentum for the particle on a closed orbit is p and it after some physical process changes its momentum to $p(1 + \delta)$, the dimensionless number δ is called the fractional momentum deviation. For the LHC, the tolerance limit is [14]:

$$\delta < 6 \cdot 10^{-3} \quad (2.6)$$

Although BFPP does not change the momentum of the ions, the condition (2.6) can be used in order to see if the affected ions will stay in the beampipe or not.

The radius of curvature ρ of a particle with charge Zq and momentum p in a magnetic field B is [12]:

$$\rho = \frac{p}{ZqB} \quad (2.7)$$

Thus if the particle changes its momentum to $p(1 + \delta)$ through some physical process, the new radius of curvature ρ_{new} will be:

$$\rho_{\text{new}} = \frac{p(1 + \delta)}{ZqB} = \rho(1 + \delta) \quad (2.8)$$

On the other hand, if the particle changes its charge to $Z - 1$ through BFPP, the new radius of curvature is instead

$$\rho_{\text{new}} = \frac{p}{(Z - 1)qB} = \rho \frac{Z}{Z - 1} \quad (2.9)$$

When a particle changes its radius of curvature, this effect can be both due to a change of momentum and a change of charge. With equations (2.8) and (2.9) it is possible to evaluate which momentum deviation δ a particle would need in order to have the same new radius of curvature as if its charge had changed through BFPP. So putting equations (2.8) and (2.9) together gives:

$$\frac{p(1 + \delta)}{ZqB} = \frac{p}{(Z - 1)qB} \Rightarrow \delta = \frac{1}{Z - 1} \quad (2.10)$$

For lead ions, $Z = 82$. Put into equation (2.10), this gives

$$\delta_{\text{BFPP}} = 0.012 \quad (2.11)$$

which does not fulfil condition 2.6. Thus it is clear that the ions that have undergone BFPP will not stay inside the beampipe. Instead, they will hit the inside of it at some point, possibly causing damage. The first step in finding out if they will do any damage is to calculate how far in the LHC they will go before they collide with the beam screen.

In [13], a tracking of the wrongly charged beam from IP2 has been done using the software MAD-X [20]. The secondary ion beam that has undergone BFPP was tracked through the magnetic field in the beam pipe, and it was concluded that it will hit the beam screen in a dipole magnet about 400 m from the interaction point. A picture from this tracking is shown in figure 2.10. The BFPP reaction will take place at each of the three IPs where the ion beams collide, with two secondary beams emerging from each IP, so in total six dipoles are affected. How this will affect the machine is difficult to tell a priori, but it is clear that the ions will deposit a large amount of energy in the beam screen and in the coils of the magnet behind it. This in turn can raise the temperature of the magnet, which eventually can lead to a quench. To see how dangerous this energy deposition is, a closer calculation is needed, and that is one of the main tasks in this report.

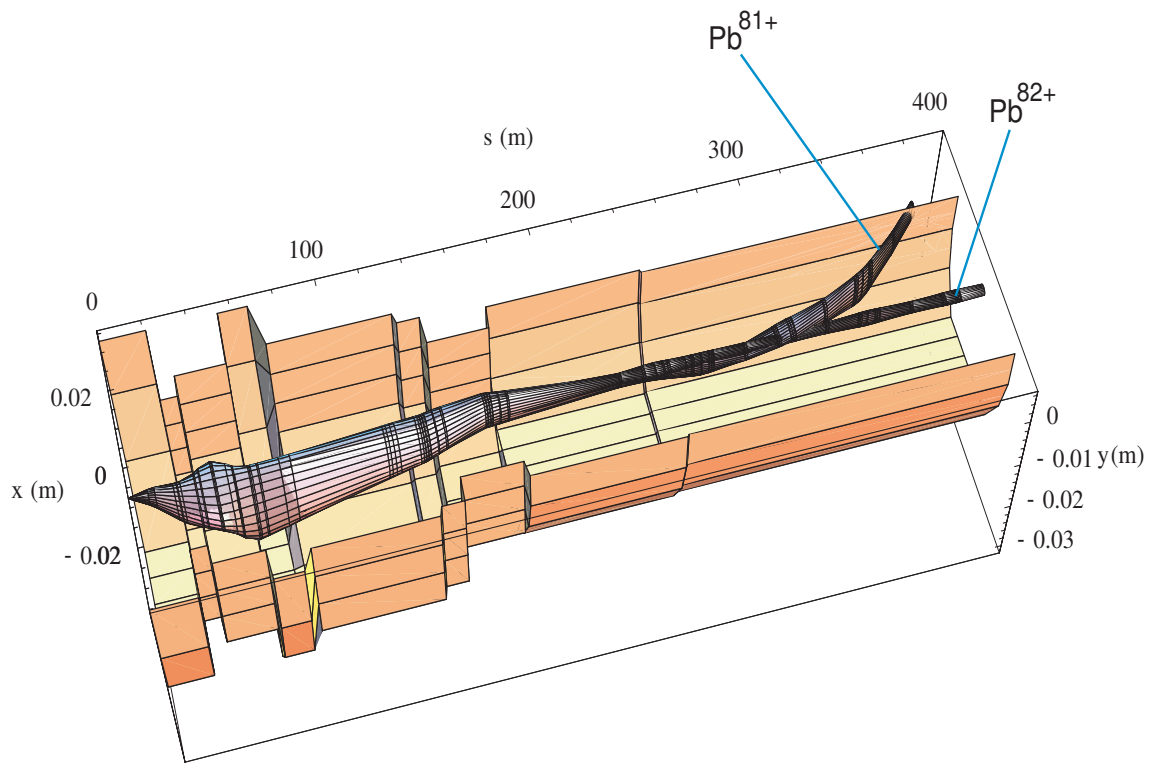


Figure 2.10. The traces of the primary beam and the secondary beam produced by BFPP through the beam pipe. The interaction point is at the left edge where the beam envelope is very small. To the right in the figure, almost 400 m from the interaction point, the main beam is going straight while the wrongly charged secondary beam leaves the trajectory and hits the beam screen. In the computer model, the original curved geometry and magnetic field were transformed to be straight. The figure is taken from [13].

2.6 Interaction between particles and matter

When the lost ions hit the beam screen and continue further into the superconducting coils, they will deposit heat, which will raise the temperature. In order to understand this, a short overview of how particles lose energy when passing through matter will be given. A more detailed description is given for instance in [21].

Particles lose energy when they pass through matter through several processes. At lower energies, the dominating loss mechanism for heavy charged particles is ionization, caused by the electromagnetic interaction between the impinging particle and the atomic electrons of the bulk. Sometimes the bulk electrons receive enough energy to become free, causing in turn secondary ionization; sometimes they only get excited to a higher atomic shell. This energy loss is very well described by the Bethe-Bloch formula [22]:

$$-\frac{dE}{dx} = \frac{Z_1^2 e^4 n_e}{4\pi\epsilon_0^2 m_e v^2} \left(\ln \frac{2m_e v^2}{I(1-\beta^2)} - \beta^2 \right) \quad (2.12)$$

Here dE/dx is the so called stopping power, meaning the energy loss of an incident particle per unit path length inside the material, Z_1 the charge number of the impinging particle, n_e the electron number density of the bulk element, I the effective ionization potential of the material, m_e the electron mass, ϵ_0 the dielectric constant, v the speed of the impinging particle and β its fraction of the speed of light as defined in special relativity.

If an impinging particle has a higher energy, above a so-called critical energy E_c , other effects become more important for the energy loss — here the energy loss is dominated by bremsstrahlung and pair production, and also photonuclear interactions come into play.

Bremsstrahlung is electromagnetic radiation emitted by charged particles that are accelerated. Often the term is however used for describing the radiation of impinging electrons deflected by the Coulomb field of the nuclei. The stopping power from bremsstrahlung is [22]:

$$-\frac{dE}{dx} \propto \frac{Z_1^2 Z_2^2}{A} \left(\frac{e^2}{mc^2} \right)^2 E \quad (2.13)$$

Here E is the energy of the impinging particle, m its mass, Z_2 is the charge number of the bulk material and A its atomic mass number. The effect is a lot more important for light particles, for instance for electrons, since the energy deposited through bremsstrahlung is inversely proportional to the square of the mass of the particle. The energy loss is also proportional to E , meaning that also for heavier particles the effect is significant at higher energies.

Also production of electron-positron pairs is an important process for energy losses. The pair is created by the electromagnetic interaction between the charged projectile and the nuclei of the target. They exchange a virtual photon that converts into a pair. The stopping power from pair production is proportional to the energy of the projectile:

$$\frac{dE}{dx} \propto E \quad (2.14)$$

The last important process for energy loss in matter is photonuclear interactions. Also in this process the projectile and a target nucleus exchange a virtual photon, but the photon excites the nucleus or even leads to nuclear break-up. Also for photonuclear interactions is the stopping power proportional to the energy of the impinging particle.

The total stopping power is the sum of the contributions from all of the above processes.

When a highly energetic particle hits a material, a so-called electromagnetic shower will develop. Through bremsstrahlung high energy photons are emitted, which later convert into electron-positron pairs. These particles in turn emit more photons through bremsstrahlung, which again convert to new electrons and positrons. Thus the number of photons, electrons and positrons increase exponentially, but in every step the energy of the particles is divided by two. And at some point the energy of a single particle is so low that the cross sections for the two involved processes, bremsstrahlung and pair production, have decreased so much that other processes dominate, for instance ionization. So just one incident particle with a very high energy can give rise to a vast number of so-called secondary particles inside the material — particles created at a later stage directly or indirectly by the first particle.

All secondary particles also scatter elastically many times, so-called multiple scattering, on the Coulomb field of the nuclei. This process slightly changes the direction, but not the energy, of the particles randomly. So the shower particles will spread out more and more transversely, defining the spatial shape of the distribution of the energy deposition. In figure 2.11, the energy deposition from a FLUKA [23, 24] simulation is shown. A single lead ion at an energy of 2.76 TeV/nucleon was shot at a solid copper block. The energy is plotted in with colour codes in the $x-z$ -plane in a 1 cm thick slice in y around the origin, where the initial ion hits. Inside the material the shape of the electromagnetic shower is clearly visible. The FLUKA code is described in more detail in Section 3.2.

For some of the mechanisms, the energy loss rises proportional to Z_1^2 , which can be seen in equations (2.12)–(2.13). This means that a heavy ion will lose more energy per unit path length in a material than for instance a proton, meaning in turn that the energy deposition from an ion will be much more concentrated. However, an ion also starts to break up when it enters a material. It splits into smaller fragments, ranging from nuclei almost as large as the initial ion down to alpha particles and single protons and neutrons, through electromagnetic and strong interactions with target nuclei. The break-up process continues until the ion is completely split into separated nucleons.

The result is a high peak in the energy deposition of an ion the first centimetres in the material before the nucleus has split—the exact distance the ion needs to break up depends on the material it enters. If instead high energy protons hit a solid, this peak will not be there. But after this first distance, the spatial distribution of the energy deposition for an ion and a proton will be practically the

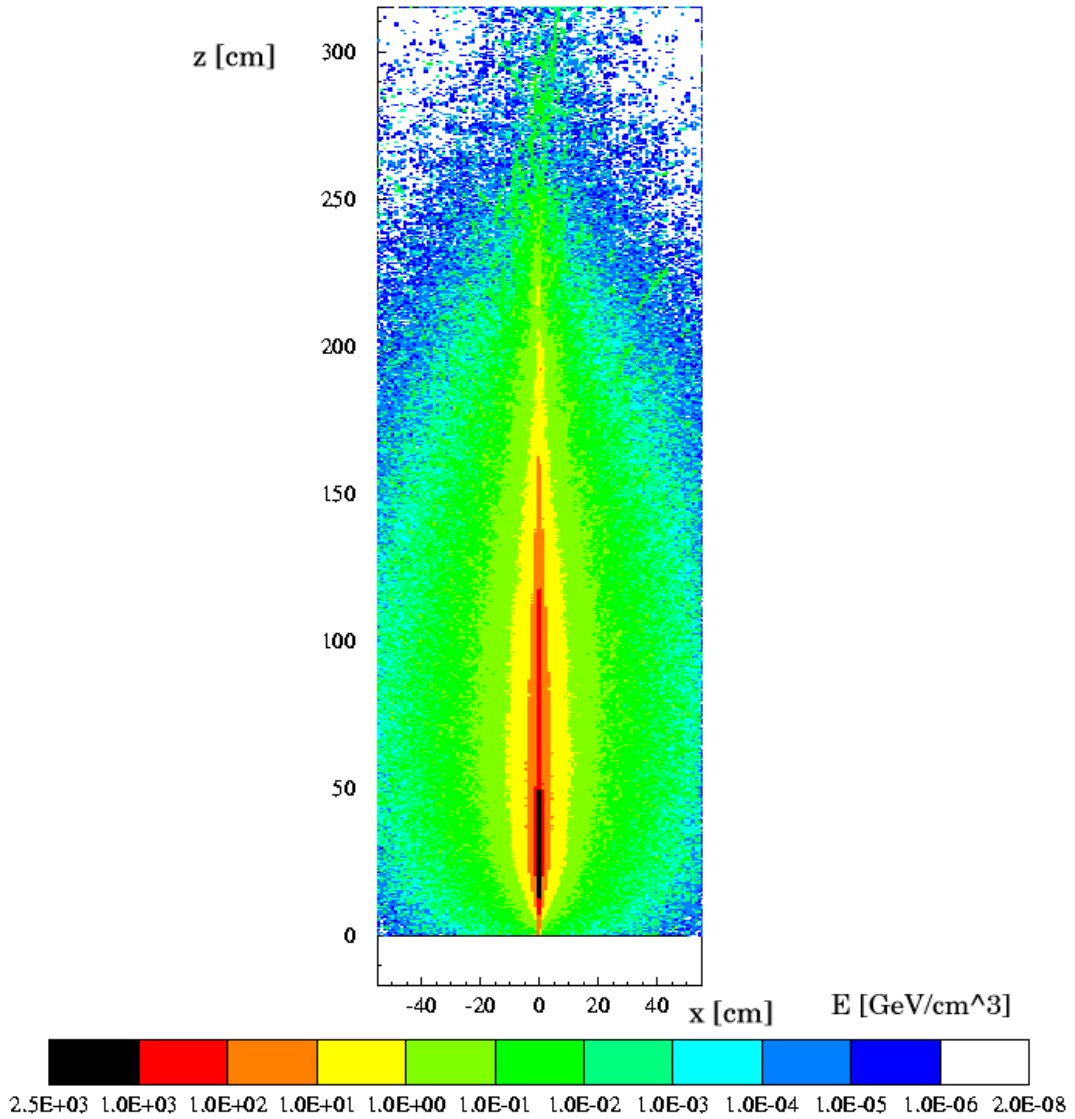


Figure 2.11. The energy deposition from a single Pb^{82+} ion at nominal LHC energy 2.76 TeV/nucleon hitting a solid block of copper under straight angle at the coordinate origin. The energy is scored in a 1 cm thick slice around the impact point. The impact was simulated with FLUKA.

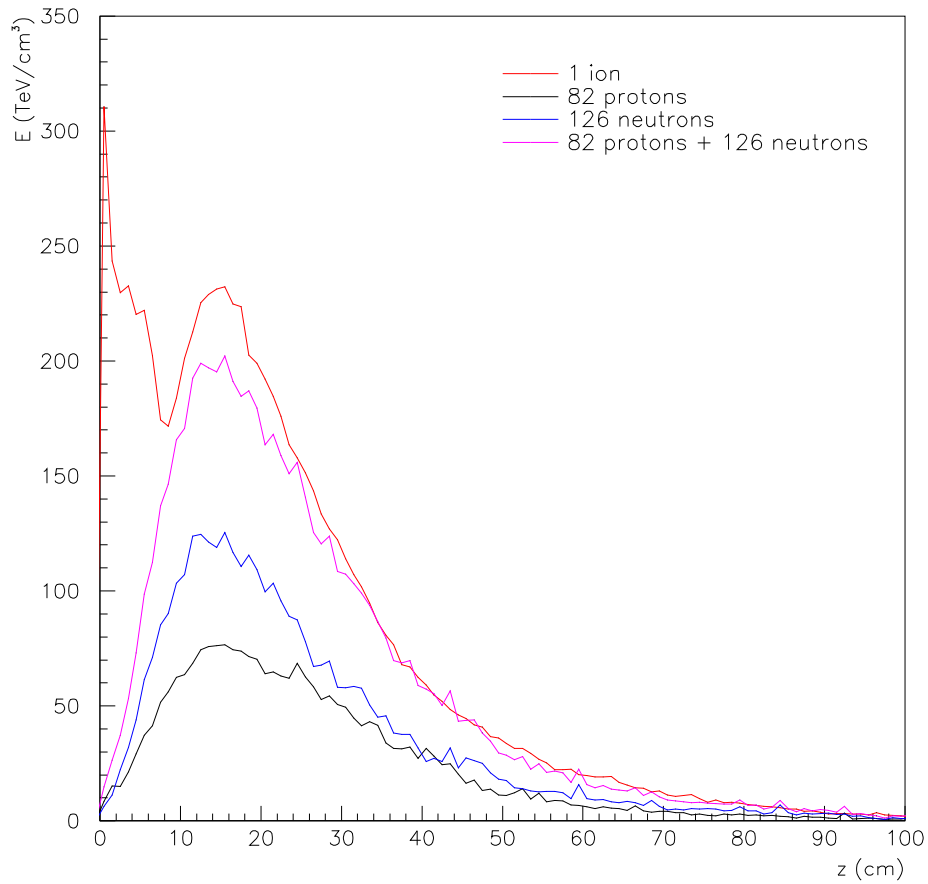


Figure 2.12. The energy deposition for one 2.76 TeV/nucleon Pb^{82+} ion in a block of copper compared with the energy deposition from its free constituents; 82 protons and 126 neutrons at the same energy, computed with a FLUKA simulation. Pencil-like beams of 2.76 TeV/nucleon lead ions, protons and neutrons were shot on a 5 m thick box of copper.

same except for a scaling factor, since the ions are now split into single nucleons. This can be seen in figure 2.12. Here the deposited energy as a function of depth in the material, in this case copper, is shown both for protons, neutrons (explained in the next paragraph) and lead ions. The sum of the energy deposition for 126 neutrons and 82 protons do not quite sum up to the energy deposition of one lead ion. This is due to the fact that the average is made in a rod with a very small area of 0.01-0.01 cm. The showers from single nucleons are more spread out than the shower from an ion, which is kept together for longer, and therefore the ion will deposit more energy in a narrow bin around the impact point.

So far only charged particles have been mentioned. Neutrons from the original impinging ion have no charge and thus no Coulomb interaction. They interact only via the strong nuclear force, but neutrons give rise to many hadronic processes in which other hadrons are produced, for instance protons or pions. The overall effect is that also high energy neutrons create an electromagnetic shower indirectly through these secondary particles. This shower has the same qualitative shape as the one for protons. When a neutron has lost most of its energy, the cross sections for creation of other particles becomes very small, which means that these low energy neutrons do not have many interactions. So low energy neutrons can penetrate very deeply into matter. Apart from hadron production, the most important ways in which neutrons lose energy are [22]: nuclear excitation, neutron capture (where the neutron is captured by a nucleus, thus producing an isotope in an excited state), neutron induced fission and emission of nuclear particles.

2.7 Choice of method

In order to find out if the dipole magnets quench or not when hit by the secondary ion beam, it is necessary to compute the temperature rise caused by the impact and then to determine if it brings the superconductor over its critical surface in a volume large enough for the quench to propagate. Several more or less realistic methods exist for treating the problem. The best would be to directly perform an experiment, where high energy ions were to be shot on a superconducting cable. This is however not very realistic. At present, neither the lead ion beam at nominal energy nor the cryogenic system used for cooling are available. And even if they were, such an experiment would be very expensive and complicated to set up. Even computer simulations of the whole process, from the beam impact to a resulting possible quench is very difficult to perform. For instance, the heat power taken out of the cable by the helium cooling system is very hard to model in a meaningful way, which is described more closely in Chapter 5. No suitable existing code was found that could perform all these steps.

Instead, the problem has to be split into several parts. Computer simulations can give an estimate of the spatial distribution of the power deposition caused by the lost particles, which is done in Chapter 4. To estimate the temperature rise in the superconductors caused by this power input turns out to be the hardest part of the problem. Due to the very complex behaviour of the heat transfer inside the cable and out through the insulation, it is very hard to model this accurately

in a computer simulation and the only realistic method is an experiment. An experiment trying to determine the power transfer through the cable insulation has however been done [25], and in Chapter 5 an attempt is made to use this experiment to determine the relation between power input in a cable and the resulting temperature. The last part, to investigate which temperature rise brings the superconductor over the critical surface, is better known. This has already been done through computer simulations by the magnet division at CERN [26], and this result will be used directly.

For the simulation of the beam impact, the Monte Carlo code FLUKA [23, 24] was chosen. It was the only particle transport code found that had a well tested implementation of the physics for heavy ions. The only option was GEANT4 [27], where however the ion physics modules are still under development. A Monte Carlo simulation, like the FLUKA program, simulates the physical processes occurring when the ions hit a material through the sampling of random numbers, which determine the outcome of each quantum mechanical process on a microscopic level. When many impinging particles are simulated, the energy deposited inside the material will converge towards an average. The Monte Carlo method is described in detail in Chapter 3.1 and the FLUKA code in Chapter 3.2.

The problem with the beam loss monitor system, described in Chapter 6, will be treated with the same method. The beam loss monitor system is a system of detectors placed outside the cryostat in the LHC, which will continuously measure the flux of secondary particles during operation. If the relation between this measurement and the temperature in the superconducting cables is known, an electronic system can decide to abort the beam before a quench occurs if the cables start to get too hot. The present design [28, 11] is based on proton operation, and the task in this thesis is to investigate if this setup is appropriate also for ions. Due to the complexity of the problem it is natural to once again do FLUKA simulations, this time with both protons and ions, and compare the energy deposited in the coils with the energy deposited in the BLMs for both cases.

In Chapter 7 finally, an attempt is made to test the FLUKA simulations through a comparison with experimental data from RHIC. There an experiment was made, where the flux secondary particles caused by BFPP was measured by a system of detectors outside the cryostat.

Chapter 3

Monte Carlo simulations

3.1 General theory of Monte Carlo simulations

Generally speaking, a Monte Carlo method is a numerical method based on random numbers [29, 30]. Monte Carlo methods can be used to solve a wide range of problems from pure mathematics and physics to finance. The idea is to first make a mathematical model using functions of random variables, and then make several trials, and in each trial sample these random variables and record some desired quantity. Then the average over all the runs will converge towards the true solution of the problem. Monte Carlo methods are implemented as computer programs and used to solve problems which are not analytically solvable and where classical numerical methods converge too slowly or are too complicated.

Quantum mechanical problems are very well suited for the Monte Carlo method, since they by nature are based on randomness. A measurement of a quantum mechanical process is never deterministic but has instead a probability distribution for a set of possible outcomes. This gives a natural connection to random variables, upon which a Monte Carlo simulation can be based.

3.1.1 Random numbers

The very basis of every Monte Carlo method is random numbers. How is it possible to obtain truly random numbers? A detailed description of how random numbers are generated is beyond the scope of this report, but a brief overview will be given.

Basically there are two types of random numbers: true random numbers and pseudo-random numbers. The first ones could theoretically be sampled from for instance white noise in an electric circuit or the decay of single atoms in a radioactive material. The use of real random numbers in computer simulations are however not practical for several reasons. Some external hardware must be connected to and interfaced with the computer, which can be quite complicated and expensive. One would also have to make periodical checks of the quality of the random numbers, since even a small technical defect could bias the result. Moreover, once a simulation is performed, the exact same simulation would be impossible

to reproduce, since the random numbers it is based on change all the time. A possibility could be to gather large tables of random numbers and record them.

A much simpler and more practical approach is to use so called pseudo-random numbers. These numbers are generated from a mathematical algorithm and thus not truly random in the sense that they can be predicted and have a deterministic behaviour. However, if the algorithm used is good, a large set of pseudo-random numbers show the same statistical properties as true random numbers. Normally the pseudo-random numbers, generated in this way by a computer code, called a random number generator, are used in Monte Carlo simulations.

In each trial in a Monte Carlo simulation random numbers have to be produced as if they were single samples from the random variable with a some probability density function (PDF). The technique to do this usually starts with sampling a random number, which is uniformly distributed between 0 and 1. This is done by a pseudo-random number generator. This generator can then be general and used in a lot of different problems involving different PDFs. Having the random number from the uniform distribution at hand, one has to somehow convert it, so that a large number of these values would be distributed with the wanted PDF from the initial problem. Call the uniformly distributed number u , let $f(x)$ be the PDF one wants to sample from and let $F(x)$ be its cumulative distribution function (i.e. its integral). According to elementary probability theory, see for instance [31], $F(x)$ is an increasing function and will take on values between 0 and 1. Therefore, if one sets

$$F(x) = u \tag{3.1}$$

and solves this equation for x , this variable will be distributed exactly as wished. The proof of this is straightforward. One can consider the probability that $x < x_0$ for some fixed x_0 and, assuming equation (3.1), show that this is equal to $F(x_0)$:

$$P\{x < x_0\} = P\{F(x) < F(x_0)\} = P\{u < F(x_0)\} = F(x_0) \tag{3.2}$$

The first equality in equation (3.2) follows from the fact that $F(x)$ is an increasing function, the second equality from equation (3.1) and the last one is true because u is uniformly distributed between 0 and 1.

So with the use of uniformly distributed random numbers from generators, it is possible to obtain an arbitrarily distributed random number by means of simple mathematical operations, as long as equation (3.1) is analytically solvable. Even if this is not the case, it is possible to do the transformation to the wanted distribution, but these methods are beyond the scope of this text.

3.1.2 Schematic Monte Carlo model of the present problem

In the problem that is treated in this report, a large flux of ions is hitting the inside of the beam pipe. There they interact with the matter in different ways as described in Section 2.6. Each of all the possible interactions has a certain probability. A Monte Carlo program that solves the macroscopic behaviour of this system could therefore be schematically modelled in the following way:

a) Consider one primary particle (this is a particle that is present from the beginning in the problem; in this case it is one of the original ions from the beam). According to some predefined and fixed initial conditions it has some momentum and position in the geometry.

b) Find the PDF of the distance that this type of particle travels inside the current medium before it interacts for the first time. This distribution is different for different types of particles and different media.

c) Use a random number generator to sample a value in such a way, that if an infinite number of values were sampled, they would be distributed as samples from a random variable with the above-mentioned PDF. This is done as described in Section 3.1.1. The sampled value will be the distance the particle travels in the material before its first interaction. Transport the particle this distance (i.e. change its coordinates).

d) Consider all the possible interactions that can take place for the particle in the present medium and give each one of them a number. Call the probability for interaction number i for P_i and suppose there are n possible interactions. It must be true that:

$$\sum_{i=0}^n P_i = 1 \quad (3.3)$$

Sample another uniformly distributed random number. If this number lies in the interval $[0, P_1[$ let interaction number one take place, if it is in $[P_1, P_1 + P_2[$ let the second interaction take place and so on. This gives the right probabilities for all possible interactions. The interaction probabilities are computed from the cross sections for the different processes.

e) Change the coordinates and momentum of the particle according to the interaction - maybe one here has to sample additional random numbers in order to determine scattering angles etc. It is also possible that new particles are created during the interaction. In this case, also these particles have to be transported. All particles that are active at the moment are placed on the computer stack along with their momenta and spatial coordinates. It is also possible that a particle is annihilated during the interaction, and then it is simply removed from the stack and its energy is deposited in some way that is recorded by the Monte Carlo-code.

f) Once the interaction of the first particle is finished and it is placed on the stack together with the possible new particles, take the first particle on this stack and go back to b) and transport it.

The transport of every particle also has to end somewhere; otherwise the simulation could run forever. For instance, a geometrical boundary could be made so that when a particle is passing this boundary it is immediately taken out of the simulation, or the geometry of the problem could be surrounded by some artificial medium where all particles are immediately eliminated from the simulation and deposit all their energy. When the stack is empty, i.e. when the first primary particle is either annihilated or has left the geometry, and the same accounts also for all secondaries (new particles created by the interactions of the primary particle), the next primary particle is loaded onto the stack and transported. The

simulation finishes when the stack is empty and all primary particles have been transported. During the simulation the Monte Carlo-code has recorded the quantities of interest. The larger the number of primary particles is, the closer the final result is to reality.

As described above, the simulation is called analogue. This means, that all physical processes are faithfully reproduced. The recorded quantities will converge towards the true average of their distributions, and also the variance and all higher moments calculated over the different trials (i.e. primary particles) will converge towards their true value. However, sometimes this convergence is very slow. If one for instance wants to study some very rare physical event, one would have to do a huge amount of trials in order to obtain enough statistics to see the convergence. Another example are some problems with high energy beams - in these cases a very large amount of secondary particles, which are quite similar to each other, are produced. To track all these particles takes a lot of time. For instance, as described in Section 4.3, a simulation of one single lead ion at nominal energy (2.76 TeV/nucleon) in the full geometry of a dipole takes more than 30 hours on a 2.4 GHz Pentium 4 computer. In the cases where the analogue calculations are slow, there are a number of so-called biasing techniques that can be used in order to speed up the simulation.

The biasing techniques are used to change some properties in the problem, often in an unphysical way, so that the total time needed to get sufficient statistics for the desired physical quantity is shortened. This could be done by either reducing the variance of the trials so that a smaller amount of primary particles is needed for convergence, or by reducing the computer time needed to handle each primary particle. Generally, the price one has to pay for this is that the statistical fluctuations and the higher moments in the real physical process are lost. It also requires a great deal of physical judgment and deeper understanding from the user. A biased Monte Carlo cannot be used as a black box. In general, the user also doesn't get definitive results after the first run, but needs to make several consecutive runs in order to optimise the biasing parameters. A large number of biasing techniques exists, and the ones relevant for the specific problem treated in this report are discussed in more detail in the Sections 3.2.1 and 4.3.

3.1.3 The role of Monte Carlo simulations

In physics, the role of Monte Carlo simulations lies between theory and experiments. In applications where confirmed theoretical models exist, but experiments are not available or too difficult, dangerous (in the case of spacecrafts or nuclear reactors) or expensive to perform, and analytical solutions are impossible, Monte Carlo simulations are often used to make predictions. For instance, in the development of machines like particle accelerators, spacecrafts or nuclear reactors, where radiation plays an important role, Monte Carlo simulations are very important. These machines have to work properly from the moment they are turned on, and the design can be thoroughly tested with inexpensive computer simulations. In the field of particle accelerators, the use of Monte Carlo simulations may seem a bit more risky, since accelerators are often constructed to work at and beyond the

limits of existing theories, upon which the Monte Carlo codes are based. The simulations only take into account the physical processes the programmer puts in to them and new phenomena will not be accounted for. However, aspects such as like radiation protection are often not so tightly connected to the new phenomena that one wants to study, but rely more on well tested theories. Also one often wants to test whether some theory is correct with an experiment, or to distinguish between competing theories. Then Monte Carlo simulations can be performed based upon the different theoretical predictions, and these results can be compared with the experimental data. But completely new phenomena can of course never be predicted by this kind of computer simulations.

In the problem treated in this report, Monte Carlo simulations are a very useful tool. A more or less well-known physical process can come into play during the LHC experiments and damage the machine. In order to avoid this and determine some limits for the different parameters of the particle beam, cheap computer simulations prove an excellent tool and the only realistic method. In this problem, the simplest approach is to use existing software, maybe with some modifications, rather than writing a new Monte Carlo code from scratch, which is very time consuming.

3.2 The FLUKA program

The software found most suitable for simulating the energy deposition of the lost ions in the magnet was FLUKA [23, 24]. An appropriate code must have a well tested implementation of ion physics and because of that FLUKA was the best option. The only alternative found, GEANT4, is still under development when it comes to heavy ion interactions.

FLUKA is a Monte Carlo code for particle interaction and transport. The first version of FLUKA was developed already in 1962 at CERN. This version handled only high energy proton beams and was used to design shieldings of high energy proton accelerators. Since then, the code has been continuously modified and improved in order to handle new particles, energy ranges and interactions. Also as the physics has evolved over the years FLUKA has been modified to use better and more accurate physics models. The name FLUKA was invented in 1970 and is short for "Fluktuierende Kaskade" in German. At that point FLUKA was used to study calorimeter fluctuations.

The present version of FLUKA has little or no remnants of older versions. It is now maintained, developed and distributed by an official collaboration between CERN and INFN¹ Milan, but also people from other institutes and universities, for instance NASA² and SLAC³, are contributing. At present, FLUKA is used for a wide range of applications. Some examples are spacecraft radiation protection, particle detectors, radiation cancer therapy, nuclear waste management and beam-machine interactions in accelerators at CERN and SLAC. For a detailed description

¹Instituto Nazionale di Fisica Nucleare

²National Aeronautics and Space Administration

³Stanford Linear Accelerator Center

of the history of FLUKA, see for instance chapter 23 in the FLUKA online manual available at [32].

FLUKA is based on five major modules, which are fully integrated with each other, for handling different interactions and particles: Hadrons, muons, electrons and photons, low energy neutrons and heavy ions. A detailed description of the different models and their implementation is beyond the scope of this text but can be found in the FLUKA reference manual.

3.2.1 General use

Detailed instructions on how to use the FLUKA program can be found on the FLUKA website [32], for instance in the online manual. Here only a short overview of the main features will be given.

In order to use FLUKA, the user has to create an input file, which contains all relevant data in the problem. The input file is a simple text file, in which the user writes so-called data cards. A data card is one or more lines in the input file that consists of a string with the name of the card followed by a number of numerical parameters and one alphanumeric. In this way all properties of the problem are defined. An example of a data card is the BEAM card. The numerical values of this card assign energy and particle type to the primary particles and also the statistical properties for beams that are normally or uniformly distributed in energy, direction or position.

The geometry of the problem is built in three dimensions using a number of standard bodies, for instance cylinders, spheres, parallelepipeds or half spaces. Each body has a data card, where the numerical parameters define its position, orientation and dimensions. The user can then define regions, which can consist of one or more bodies and one or more intersections or unions between bodies. The regions define the real geometry of the problem as it is seen by the transported particles. To each region a material should be assigned. The materials can either be defined by the user through the MATERIAL card followed by different properties and the material name, or assigned directly as a standard FLUKA material — the most common elements are already defined inside FLUKA. Also compounds consisting of several elements can be defined.

As mentioned above, the geometry of the problem has to be surrounded by so-called "black hole". This is a special material, already defined in FLUKA, in which all particles are immediately taken out of the simulation, depositing all their energy. Otherwise a simulation could run forever and the user would have to define infinite geometries.

In order to use electromagnetic interactions, the user also has to prepare a so-called pemf⁴-file containing cross sections for electromagnetic reactions for all materials present in the problem. This is a simple text file containing different properties of the materials. Then he has to run an external pre-processor that calculates the cross sections from the text file. In future versions of FLUKA this somewhat tedious procedure will disappear.

⁴Preprocessor for electromagnetic FLUKA

Another important aspect worth mentioning on the use of FLUKA is the different biasing techniques that are implemented. As described in Section 3.1.2, biasing is used to reduce the variance, that is, to speed up the simulation. The simplest biasing technique used in FLUKA is called importance biasing. Using this method, a relative importance value is assigned to each region in the geometry. The regions of interest should be assigned higher importances. When a particle is transported from a region of lower importance to a region of higher importance, it is split into several identical particles according to the quotient of the importances. And vice versa, when it goes to a region of a lower importance it is taken out of the simulation with a probability corresponding to the same quotient.

When a particle is split or removed, the statistical weight of the particles has to be adjusted so that the total weight is the same as in the analogue simulation. So in regions with higher importance, a lot of particles are transported, and thus the statistics are considerably improved here, while the statistics become worse in regions with lower importance. The importances can also be assigned differently for each particle type. In the problem with the ion beam impinging on the beam screen, it is suitable to set a high importance to the coils, which are the regions of interest, and all parts of the magnet that are close. And a lower importance can be assigned to regions further away in the periphery. In this way, a minimum of computer time is wasted on transporting large amounts of secondary particles in the outer parts of the magnet that are of little interest.

Another very effective biasing technique is leading particle biasing. The electromagnetic shower that evolves when a high energy particle beam hits matter is made up of a huge number of electrons, positrons and photons, as explained in Section 2.6, and the number of these particles increase very rapidly until they have lost most of their energy. Tracking all of these particles requires a lot of CPU time. A very good approximation to the real problem is if in each reaction, where the final state normally consists of two particles, only one of them is kept and the other one removed. The statistical weight of the particle that is transported has to be modified in an appropriate way so that the total weight is conserved. In this way, less electrons, positrons and photons are transported, which means that the statistics on the electromagnetic part becomes worse. But if the biasing parameters are tuned wisely, there are still so many of these particles being tracked that it is sufficient compared with the other interactions that also contribute to the energy loss.

A very simple but yet effective biasing method is an energy cut-off for electrons and photons. This means, that electrons and photons below a certain threshold are not transported and immediately deposits their energy. This is of course unphysical, but if the cut-off threshold is low enough it will have very little influence on the final result. Typical magnitudes of this cut-off could be between 1 MeV and 20 MeV. Higher energies and other particle types are a lot more important for the scoring. So some computer time can be saved if these low energy particles are not transported.

In order to avoid large fluctuations in the statistical weight of the particles, a weight window can be applied. The weight window should be used together with other biasing techniques that produce large variations in the statistical weights

of the particles, for instance leading particle biasing. The weight window is, like importance biasing, a combination of splitting and removing particles, but instead of being based on the relative importances of the regions, the rules for when to split or remove a particle are based on its statistical weight. The variance is negatively influenced if a single particle gains too much statistical weight, since a single process for this particle can significantly influence the final result. Therefore all particles with a weight above a certain threshold are split. Also, if a particle has a very low weight, it will have almost no influence on the final result. Therefore one can save computer time without much influence on the final result if this particle is not tracked. So all particles with a weight below another threshold are put to a random test where they can either be removed or continue being transported. The thresholds are set differently depending on the energy of the particle. The user has to give two energy thresholds and the weight limits at these energies. Then the weight window changes linearly between the energy limits to make it continuous and is constant below and above these energies.

All the above methods are quite flexible — in FLUKA most of them can be tuned for each region and particle type, and sometimes also for specific physical processes.

Chapter 4

Simulation of ion beam losses in a LHC main dipole

In this chapter the simulations of the wrongly charged ion beam hitting the dipole magnet will be described. The work that needed to be done in order to perform the simulations was:

a) Write FLUKA input, which means first make the computer model of the dipole, then determine which biasing techniques should be used and how and then set up the virtual detectors in the problem - that is, determine which physical quantities should be scored and where and how they should be scored.

b) Write additional Fortran routines for interpolating the magnetic field and injecting the source particles into the simulation and compile and link them with the main program and then run the simulation.

c) Analyze the results.

4.1 Modelling of the dipole

In order to model an LHC dipole magnet in FLUKA, some simplifications must be made. As described in Section 3.2.1, the geometry in FLUKA is built from intersections of a number of generic bodies (parallelepipeds, cylinders, half spaces etc) which makes it time consuming and difficult to accurately model all parts of a complicated object. Moreover, that a too complex geometry is not only cumbersome to implement but can also considerably slow down the simulation without significantly improving the quality of the result. In order to calculate the energy deposited in the coils it is not necessary to describe all small details. Thus some approximations of the magnet geometry can be made.

The real dipole section is slightly bent, to follow the curve of the design orbit of the beam. However, one dipole has a length of approximately 15 metres, and the LHC ring has a circumference of 27 km, so the angle covered by one magnet is only approximately 0.03 rad. Thus the dipole can be modelled as a straight cylinder instead of a small part of a torus (which is not implemented as a generic

body in FLUKA).

The interactions of interest take place in the coils of the dipole. Parts of the magnet far from the coils will have very little influence on the results. Therefore, these parts can be much simplified or even omitted in the FLUKA model. Thus the support post of the magnet, the alignment target, the instrumentation wires and the bus-bars have been completely left out, as well as some of the screws and hole in the outer part of the iron yoke.

The coils themselves were approximated as made of copper instead of the real mixture of niobium, titanium and copper. The coils consist of 62.2% copper with an atomic weight of 63.55 u, 17.8% niobium with a weight of 92.91 u and 20% titanium with a weight of 47.87 u. So the average atomic weight of the coils is 65.64 u, which is very close to the weight of copper. Thus, when considering only the weight, this approximation is very close to reality. When looking at, for instance, induced radioactivity, it is important to model the compound accurately, but for the energy deposition it is enough to use copper in the whole coils.

A transverse cross section of the computer model of the dipole can be seen in figure 4.1, and a cross section of the real dipole was shown in figure 2.4. The origin of the coordinate system was placed in the centre of one of the beampipes in the beginning of the dipole with the z -axis pointing along the pipe in the direction of the beam. One might think that also this simplified model is too complicated, since the outer parts of the geometry have very little influence on the energy deposition in the coils. However, the same computer model will be used for other studies as well, for instance for a study of the beam loss monitor system in the LHC, as discussed in Chapter 6. In these simulations also the outer parts of the dipole are important, which motivates that they are modelled already on this stage.

Also the magnetic field of the dipole had to be taken into account. In FLUKA this is done by writing a Fortran subroutine MAGFLD.f that has to be linked with the main program. The subroutine receives as input the coordinates of a point in space and returns the x -, y - and z -components of the magnetic field at that point. The routine is called as soon as FLUKA transports a particle inside a region of the geometry where a magnetic field is present.

The magnetic field in the LHC is constructed to be vertical in the beam pipe and have a magnitude of 8.33 T in order to bend the particle beam correctly. One might first think that a simple model with a homogeneous field in the y -direction might be a good approximation. But in the simulation it is important that the field is present and of correct magnitude also outside the beampipe, since the magnetic field in the coils has an influence on the secondary particle shower and thus also on the deposited energy. Therefore a detailed fieldmap from [33] was used, with values of the true magnetic field in the dipole every 0.5 cm in the x - y -plane. The z -component of the field is constantly zero. The field map that was used can be seen in figure 4.2.

Thus the routine MAGFLD.f must first read the given fieldmap and then interpolate it in order to produce the field at an arbitrary point in space. In this case, a linear two-dimensional interpolation was chosen, since it is simple to implement and still has a good enough precision.

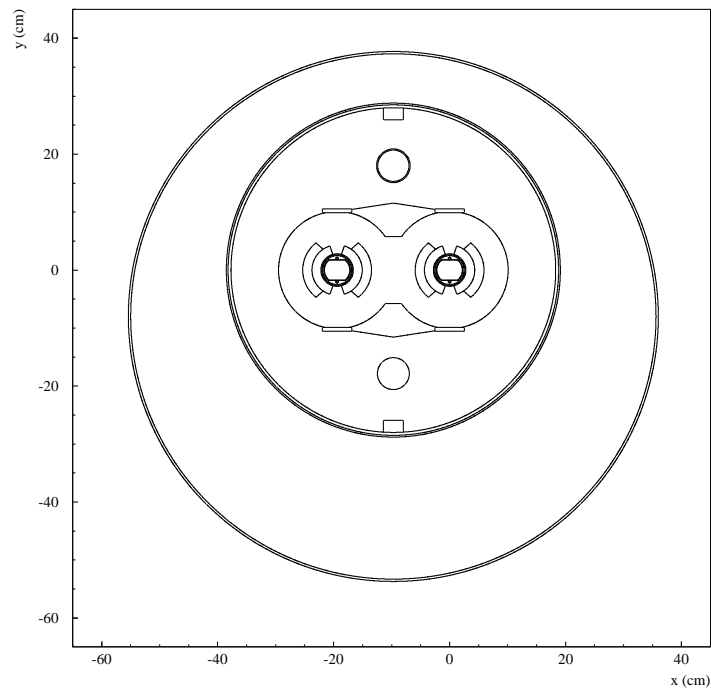


Figure 4.1. The transverse cross section of the dipole as it was modelled in FLUKA.

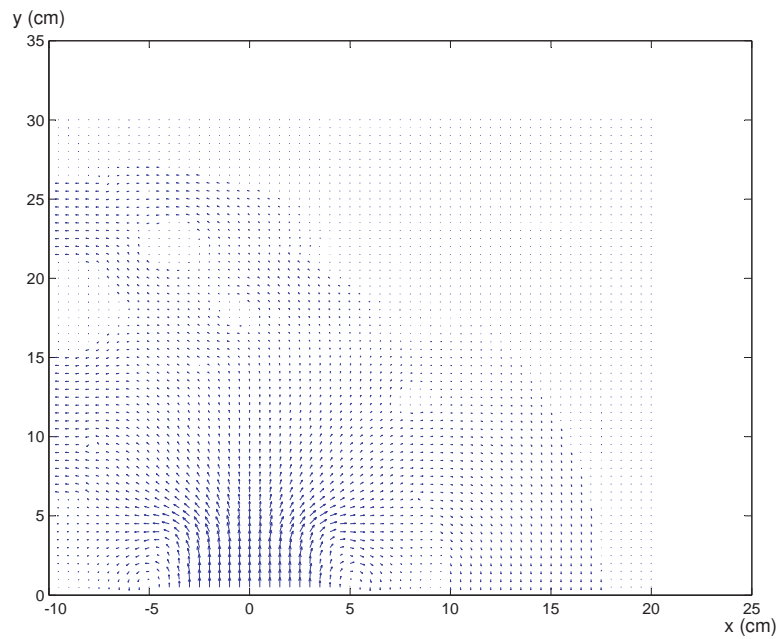


Figure 4.2. The magnetic field map that was used in the simulation. Only the first quadrant is necessary, since the other three can be calculated via symmetries from the first.

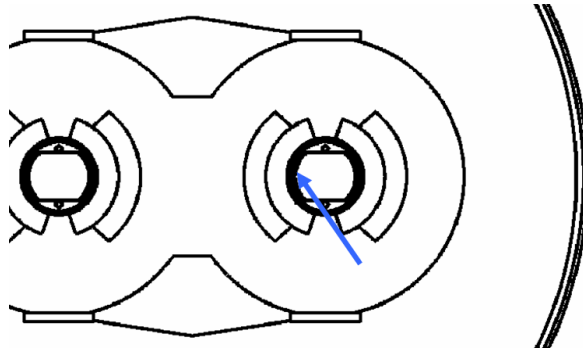


Figure 4.3. A schematic picture of how the beam hits the inside of the pipe.

4.2 Modelling of the beam

The ion beam that was used in the simulation had to correspond as well as possible to the real secondary beam of wrongly charged lead ions. According to Section 21.4 in [13], the footprint of the impinging beam on the beam screen can be approximated as a Gaussian distribution in momentum and position. So following [13], the beam was modelled as normally distributed around $z = 130$ cm with a standard deviation of 55 cm longitudinally. In the x - y plane, the angle ϕ was sampled from a normal distribution with average $-\pi$ rad and standard deviation $\pi/30$ rad. Then x and y were chosen so that every ion starts on the surface of the beam screen, on the side that faces the other beam pipe. That is, if R is the radius of the beam pipe, we set $x = R \cdot \cos \phi$ and $y = R \cdot \sin \phi$. Also the momentum of the ion beam was normally distributed around 2750 GeV/c per nucleon directed with a 0.5 mrad angle towards the beam screen. The standard deviation was 0.01% in z -direction and 2% in x and y . A schematic picture of how the beam hits is shown in figure 4.3.

The above specifications give a fair approximation of the real beam. However, the exact shape of the footprint on the beam screen may influence also the spatial shape of the energy distribution inside the coils. A better accuracy in the simulation results can be achieved by using starting conditions closer to reality. This can be achieved by using the tracking software mentioned in Section 2.5 to track the secondary ion beam from the interaction point, through the magnetic field in the beam pipe to the point where it hits the beam screen, and export the momenta and coordinates of the impinging particles directly to FLUKA.

In order to be prepared for the output from this new tracking, a Fortran routine called SOURCE.f was written and linked with the FLUKA main program. This routine overrides the BEAM data card, which is the default way of injecting primary particles into the simulation. This was done so, that whenever the main FLUKA program requests a new primary particle, the SOURCE.f routine is called. This routine then reads a file in which the momenta and spatial coordinates of all the ions are written and returns the momentum and coordinates of one particle

to the main program. In the present simulations, this file was made by a simple Mathematica[®] [34] notebook that samples the normal distributions mentioned above. However, in the future this file can instead be made by the tracking program. The reason why the output from the tracking was not used in the present simulation was that the design of the LHC beam optics has undergone some minor changes recently. And in order to give an accurate output the tracking algorithm has to be modified correspondingly. This work is under way, and when it is done new FLUKA simulations will be performed. A schematic picture of the tracking made so far was shown in figure 2.10.

4.3 Biasing methods

The need for the biasing techniques discussed in Sections 3.1.2 and 3.2.1 becomes clear when actual simulations are performed with the real geometry of the dipole and ions at nominal energy. A preliminary simulation with one single ion injected into the dipole at the nominal LHC-energy of 2.76 TeV/nucleon took more than 30 hours when run on a 2.4 GHz Pentium 4 computer. In order to get sufficient statistics, it is necessary to have at least hundreds of ions. With this in mind, the use of different biasing techniques to speed up the simulation is essential. However, the biasing has to be carefully tuned, since a poor choice of the biasing parameters may actually slow down the convergence instead of speeding it up, or in the worst case give unphysical results.

First a simple importance biasing was applied, where the regions in the geometry were divided into four classes. The first class, with the most important regions, consisted of the coils of the superconducting magnets and the surrounding parts. This class was given the highest importance. The second class was the collar, and the third class the remaining parts of the dipole. The fourth class consisted of the regions outside the cryostat — the tunnel and tunnel wall. Between the different classes a factor $1/3$ was chosen as scaling factor of the relative importances. A much lower ratio would induce unnecessary fluctuations, while a much higher ratio would be too close to one and therefore not speed up the simulation enough.

Also a cut-off for electrons and photons was used, that was set differently in the different regions, and a leading particle biasing with different thresholds was applied throughout the whole geometry. A weight window was used for all particles except for neutrons in order to compensate for the statistical weight fluctuations caused by the other biasing methods. The energy limits were chosen to be 100 and 500 GeV. An overview of the biasing settings for the different importance classes is given in table 4.1.

With all these biasing options turned on, the time needed to transport one primary ion and all its secondary particles decreased to 11 minutes on the same computer. With the biasing options turned on, the statistics for the outer parts of the magnet in the lower class regions are a lot worse, but a good result of the scoring in the coils without big fluctuations is achieved more quickly.

Importance class	1	2	3	4
Relative importance	1	1/3	1/9	1/27
Cut-off γ [MeV]	0	1	10	10
Cut-off e^- [MeV]	0	20	100	100
Lead bias below [MeV]	2	5	10	10

Table 4.1. The biasing parameters applied in the different region classes.

4.4 Scoring methods and results

In order to determine the power density deposited by the secondary ion beam in the coils, one can use the USRBIN card in FLUKA. This option defines a spatial mesh in some desired part of the geometry (in this case the coils of the magnet), and after that different quantities can be recorded throughout the simulation in each of the small cells in the mesh. For instance, one can score the energy deposition per primary ion in the mesh and from that calculate the corresponding power.

This is done by multiplying the energy density per ion with the number of ions per time unit that undergo BFPP — that is, the cross section σ_{BFPP} for the reaction times the luminosity L of the lead ion beam according to equation (2.1). So, with the numerical values for the cross section and the full design luminosity from Section 21.4 in [13], the total power $P(\mathbf{r})$ deposited per volume at position \mathbf{r} in the coils corresponds to an energy deposition $E(\mathbf{r})$ per volume and primary lead ion through:

$$\begin{aligned}
 P(\mathbf{r}) &= E(\mathbf{r}) \cdot \sigma_{\text{BFPP}} \cdot L = E[\text{J}/\text{cm}^3] \cdot 281 \cdot 10^{-24}[\text{cm}^2] \cdot 10^{27}[\text{cm}^{-2}\text{sec}^{-1}] \Rightarrow \\
 P(\mathbf{r}) &= E(\mathbf{r}) \cdot 2.81 \cdot 10^5[\text{W}/\text{cm}^3]
 \end{aligned}
 \tag{4.1}$$

A problem that arises quite soon is to determine the appropriate size of the cells in the mesh. The non-homogenous distribution of the secondary beam means that the power is not homogeneously distributed in the superconductors. If, for instance, one took the whole magnet as one cell, the value of the deposited energy per volume would be much lower than if one instead considered a very small cell around the place where the centre of the beam hits the coil. So with a smaller mesh the highest value of the deposited energy per volume is larger. This also leads to a higher maximum temperature in the coil. Moreover, if the mesh is made finer and finer, the value of the maximum energy deposition will converge if the area of the beam is finite. Also the fact that the minimum propagating zone is of the order of micrometres implies that a very small cell volume should be used.

On the other hand, too fine a mesh will also result in troubles. Since only a limited number of primary particles are simulated and averaged over, there will be statistical fluctuations. So the distribution of the spots on the beam screen where an ion hits will not be smooth. Also, in this particular case where the variance of the longitudinal beam coordinate is quite large, these fluctuations will be even

greater. The spots in the coils located exactly behind the points on the beam screen where an ion hits will therefore get a very high average energy deposition, while spots lying in between will get a lower average. If the mesh is made very fine, some cells will cover only these peaks where an ion hits, and these cells will therefore have a very high average value of the deposited energy.

In reality, there are 281 000 ions per second undergoing BFPP according to equation (4.1), so the distribution will be practically smooth. This means that the real maximum will be lower than the peaks discussed above. If one takes too small a mesh, and therefore arrives at a higher maximum, it is possible that the result of the simulation is that the magnet quenches, when in reality it may actually not. And if that is likely, one must take certain precautions in order to avoid it. So too fine a mesh should also be avoided, in order not to have too pessimistic results.

So what is then the best mesh to use, in which the cells are small enough to resolve the peak, but large enough not to zoom in on the statistical fluctuations? The answer is hard to determine a priori, although some knowledge about the physical processes involved can give rise to an educated guess. If steady state is considered, it turns out to be necessary to average the power over the radial dimension of the cable in order to compare the result with the experiments performed in [25]. This is explained further in Section 5.1. So in steady state, only one cell is needed in the radial direction, and thus the δr is set to 1.55 cm. In the ϕ -direction, a superconducting cable can be well approximated as one thermal body, while the heat transfer rate between different cables is low due to the cable insulation. Therefore the dimension of the thickness of a cable, around 2 mm according to table 7.1 in [13], is a suitable length of the arc in the cell. This gives appropriate intervals in ϕ . Longitudinally, a first estimate of a suitable cell length is 1/3 of a nuclear interaction length in copper, which is 15 cm according to [21]. This will capture a large part of the energy deposition originating from one primary lead ion inside one cell, thus considerably suppressing the effect of the statistical fluctuations without making the volume unnecessarily large. Another interesting longitudinal binning is a Δz of 15 cm, since this was the length of the plates used in [25].

But when very short timescales are considered, the peak value of the energy deposition is needed. How to choose the mesh here is not obvious. Therefore, in one FLUKA run five different meshes in the inner coil were used simultaneously. Four of them used cylindrical coordinates with the z -axis in the centre of the beam pipe and in the direction of the beam, with the particles impinging at $-\pi$. One mesh had Cartesian coordinates. The dimensions of the different binnings are given in table 4.2. The *old* mesh is the one described above. The other meshes are finer in order to see how the maximum converges and the fluctuations come into play. The *old* and *medium* meshes were also used in the outer coil.

In order to avoid huge output files the z - and r -directions in the finer meshes were limited to cover only a short distance around the point where the maximum value was reached in earlier simulations. To get exactly the maximum was not important at this stage — the purpose here was just to compare the shape of the energy distributions in order to choose an appropriate binning. In ϕ the whole 2π had to be binned, since the USRBIN card in FLUKA does not allow anything

Binning:	Old cylindrical	Medium cylindrical	Small cylindrical	Xsmall cylindrical	Cartesian
Δz [cm]	5	1	0.1	0.01	1
z_{min} [cm]	-4460	-4460	-4310	-4302	-4460
z_{max} [cm]	-3000	-3000	-4290	-4300	-3000
Δr [cm]	1.55	1.55	0.1	0.01	
r_{min} [cm]	2.8	2.8	2.8	2.8	
r_{max} [cm]	4.335	4.335	3.5	2.9	
$\Delta\phi$ [rad]	$2\pi/88$	$2\pi/88$	$2\pi/176$	$2\pi/176$	
Inner arc [cm]	0.2	0.2	0.1	0.1	
Outer arc [cm]	0.310	0.310	0.125	0.104	
Δx [cm]					0.25
Δy [cm]					0.25

Table 4.2. The dimensions of the meshes used in the inner coil. The Δz , Δx , etc are the lengths of the cell in z - or x -direction. The inner arc is the inner length of the arc in the innermost cell, and the outer arc is the length of the outer arc in the outermost cell.

else. To score only between certain angles in the geometry would require extra user-written routines.

The beam distributed as described in section 4.2 was used, and 250 primary particles were transported in the simulation. In order to perform the simulation more efficiently, ten different runs with 25 particles in each were launched on different computers on a cluster. After the simulations were finished, all runs were combined together and averaged using simple software that had to be written for this special purpose. The results were analysed and visualized using Physics Analysis Workstation (PAW) [35].

The results were plotted as power deposition per volume against z for a fixed r and ϕ for the different binnings in figure 4.4. The standard FLUKA output unit $\text{GeV}/(\text{cm}^3 \cdot \text{ion})$ was converted to power density with equation (4.1) with the GeV converted to Joule. In figure 4.6 the energy deposition scored with the medium binning used for determining quenching is shown for the inner and outer coils. The energy deposition is plotted with colour codes in the $\phi - z$ -plane. The black spot where the beam hits the beampipe is the hottest part and the place where the danger of a quench is largest.

As can be seen in figure 4.4, the *old* and *medium* binnings oscillate a lot less than the *small* and the *xsmall* ones. The maximum energy deposition per lead ion and volume for the innermost r -value at $\phi = -\pi$ for the *xsmall* binning is over $225 \text{ mW}/\text{cm}^3$, while the maximum for the *old* and *medium* binnings is around $7.2 \text{ mW}/\text{cm}^3$. From the shape of the *xsmall* curve it is however clear that this high peak is a statistical fluctuation. So the maximum values of the *small* and the *xsmall* meshes should not be taken too literally. However, the average values of the *small* and *Cartesian* binnings are fluctuating around straight lines higher than

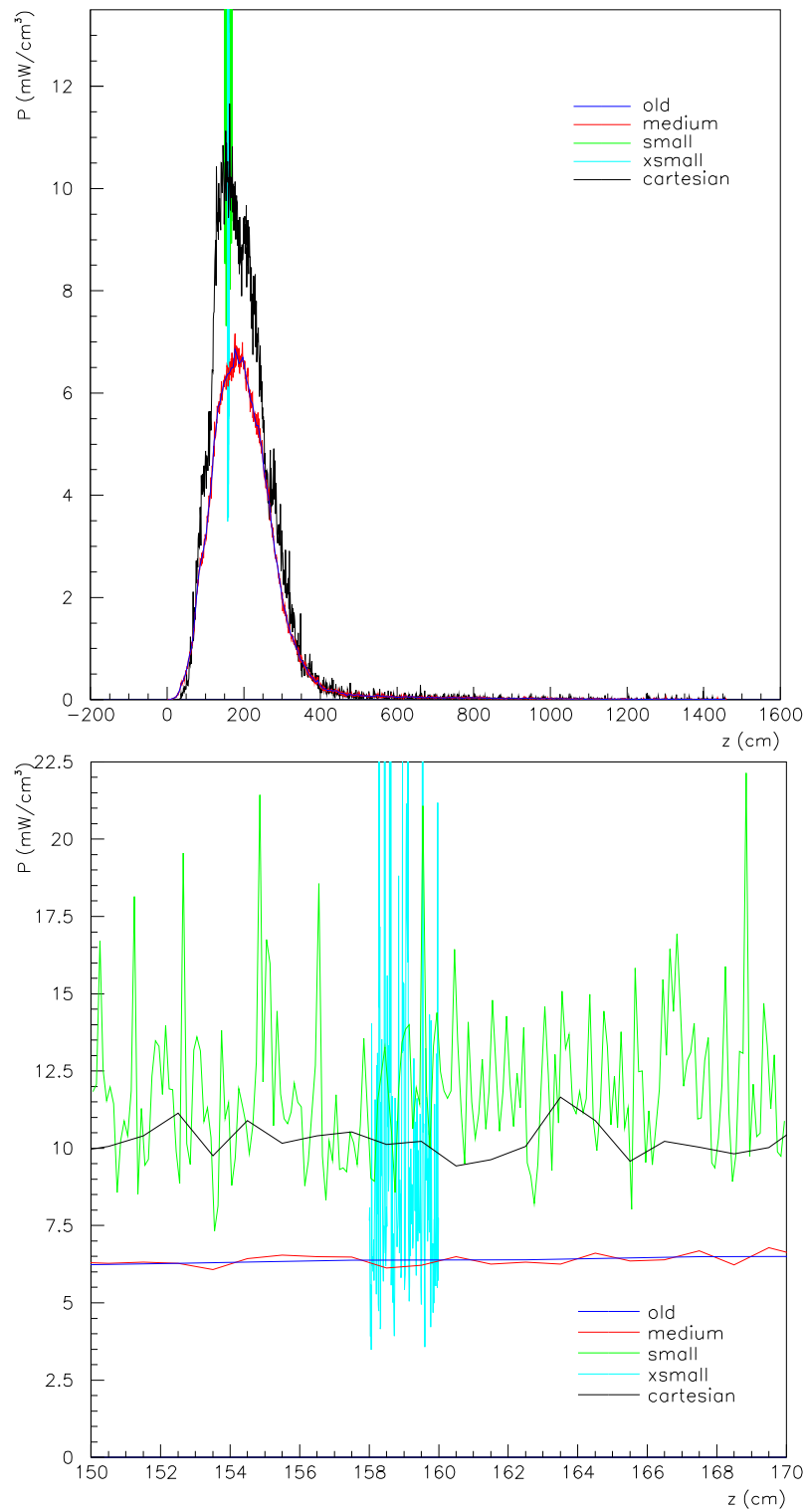


Figure 4.4. The power density for the *old*, *medium*, *small* and *xsmall* meshes plotted against z for $\phi = -\pi$ rad and the smallest possible r (at the hot spot).

Binning:	Old	Old 2	New 1	New 2	New 3
$\Delta r(\text{cm})$	1.55	1.55	1.55/4	1.55/8	1.55/16
$\Delta z(\text{cm})$	5	15	5	5	5

Table 4.3. The dimensions of the new meshes used. The other dimensions were the same as for the *old* mesh.

the average of the larger binnings. This is due to the binning in r , which raises the mean and which is not present in the *medium* and *old* mesh. So the higher averages give a warning that if the binning in r is made finer, the maximum could grow, maybe without introducing large fluctuations.

Thus the conclusion is that the *old* mesh and the *medium* mesh have good longitudinal and azimuthal binnings for avoiding the spiky behaviour of the curve, but that a finer radial binning may raise the maximum. So for the steady state case, where no radial binning is needed, the *old* and the *medium* meshes are sufficient. However, for the transient case, it is necessary to obtain the maximum. Therefore another FLUKA run with three new meshes was launched. These meshes all have the same radial and angular binning as the *old* mesh, but differ radially. The different radial binnings can be seen in table 4.3. Also one mesh with the 15 cm longitudinal binning called *old 2* was used in order to compare directly with the heat flow determined in [25].

The result can be seen in figure 4.5. It is clear from this figure that the absolute maximum converges to 13.5 mW/cm^3 as the binning in r is made finer. For the steady state case, the *old*, *old 2* and *medium* binnings give very similar results. As maximum for the radial both the *medium* and the *old* binnings have a maximum power density of 7.2 mW/cm^3 . Both maxima occur as can be expected in the inner coil at the spot where the beam hits, which can be seen in figure 4.6.

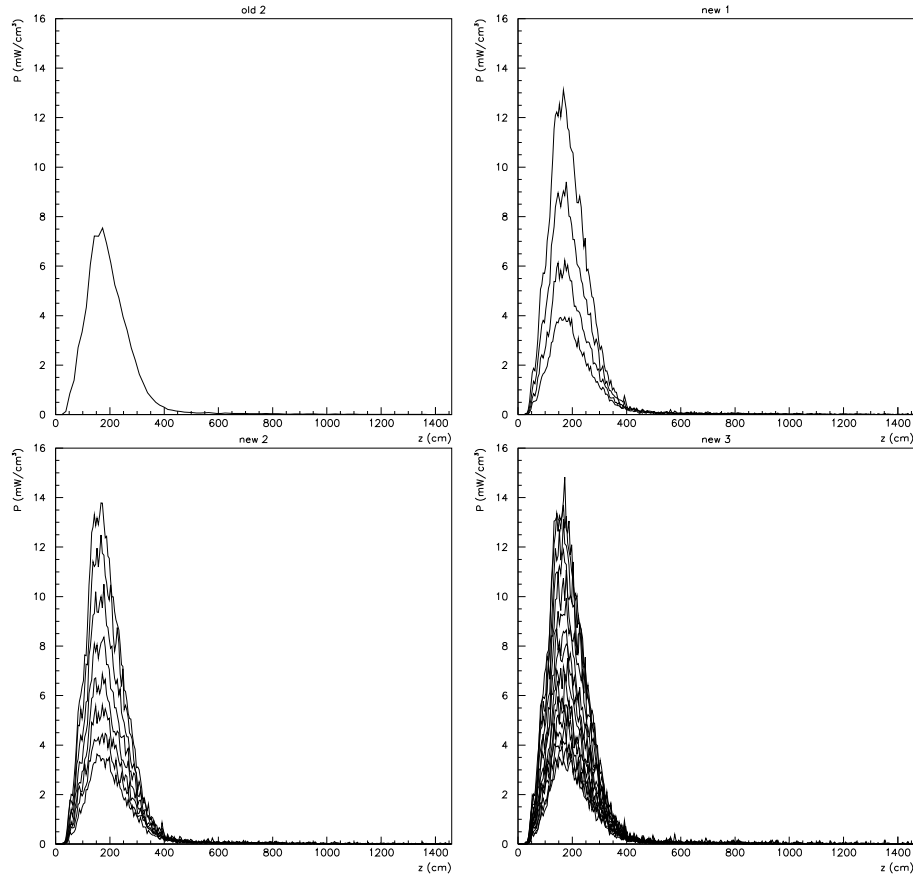


Figure 4.5. The energy deposition for the *old 2*, *new 1*, *new 2* and *new 3* meshes plotted against z for $\phi = -\pi$ rad for all possible values of r . The highest curve is for the smallest r -value in each diagram. As the radial binning is made finer, the maximum power density converges to $13.5 \text{ mW}/\text{cm}^3$. The peak in the curve for the smallest r -value in the *new3* mesh is clearly a statistical fluctuation and therefore ignored.

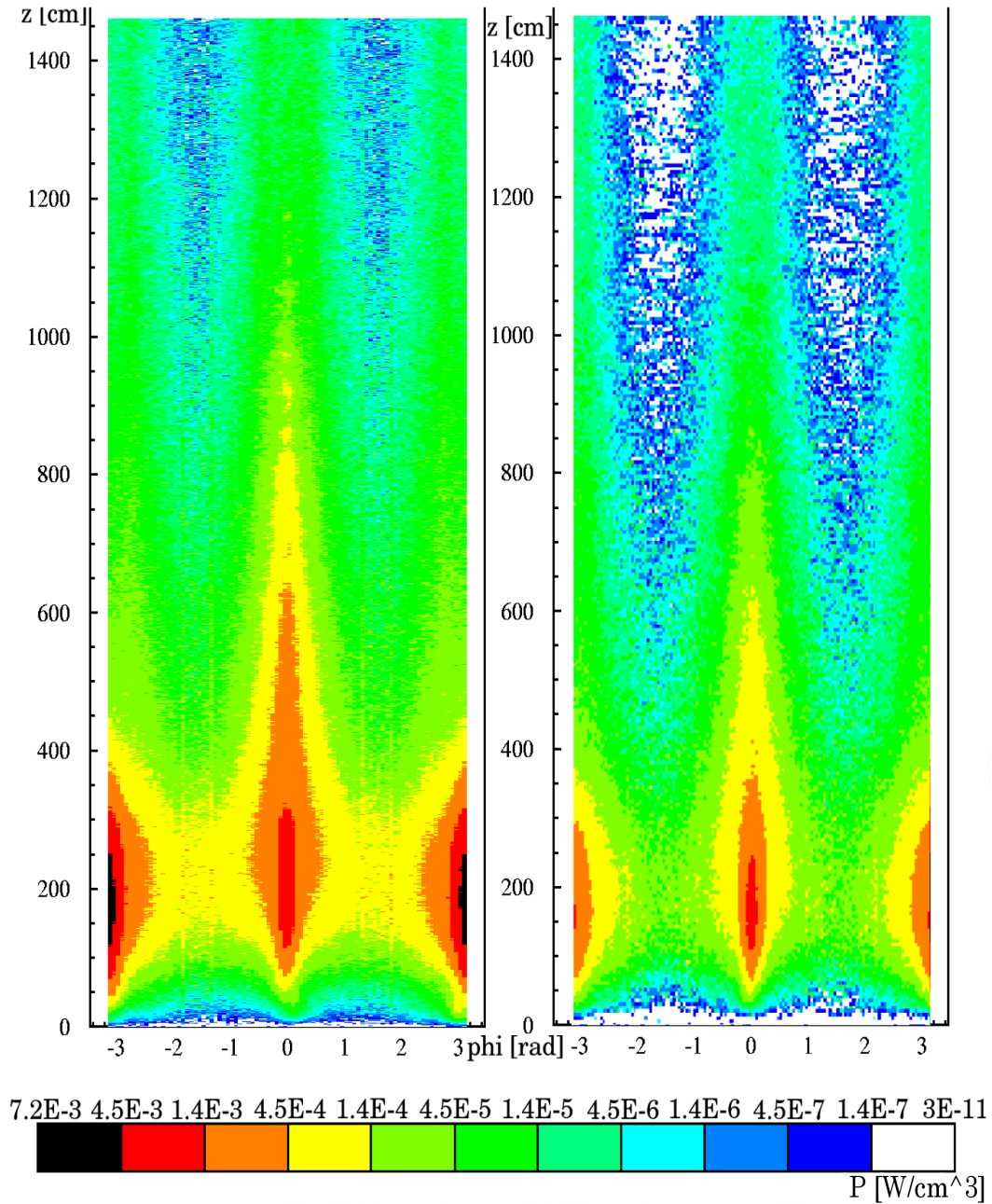


Figure 4.6. The energy deposition in the inner coil (left) and outer coil (right) scored with the medium mesh plotted with colour codes in the ϕ - z plane (only one bin was used in the radial direction). The incident ions are normally distributed around $-\phi = \pi$ rad.

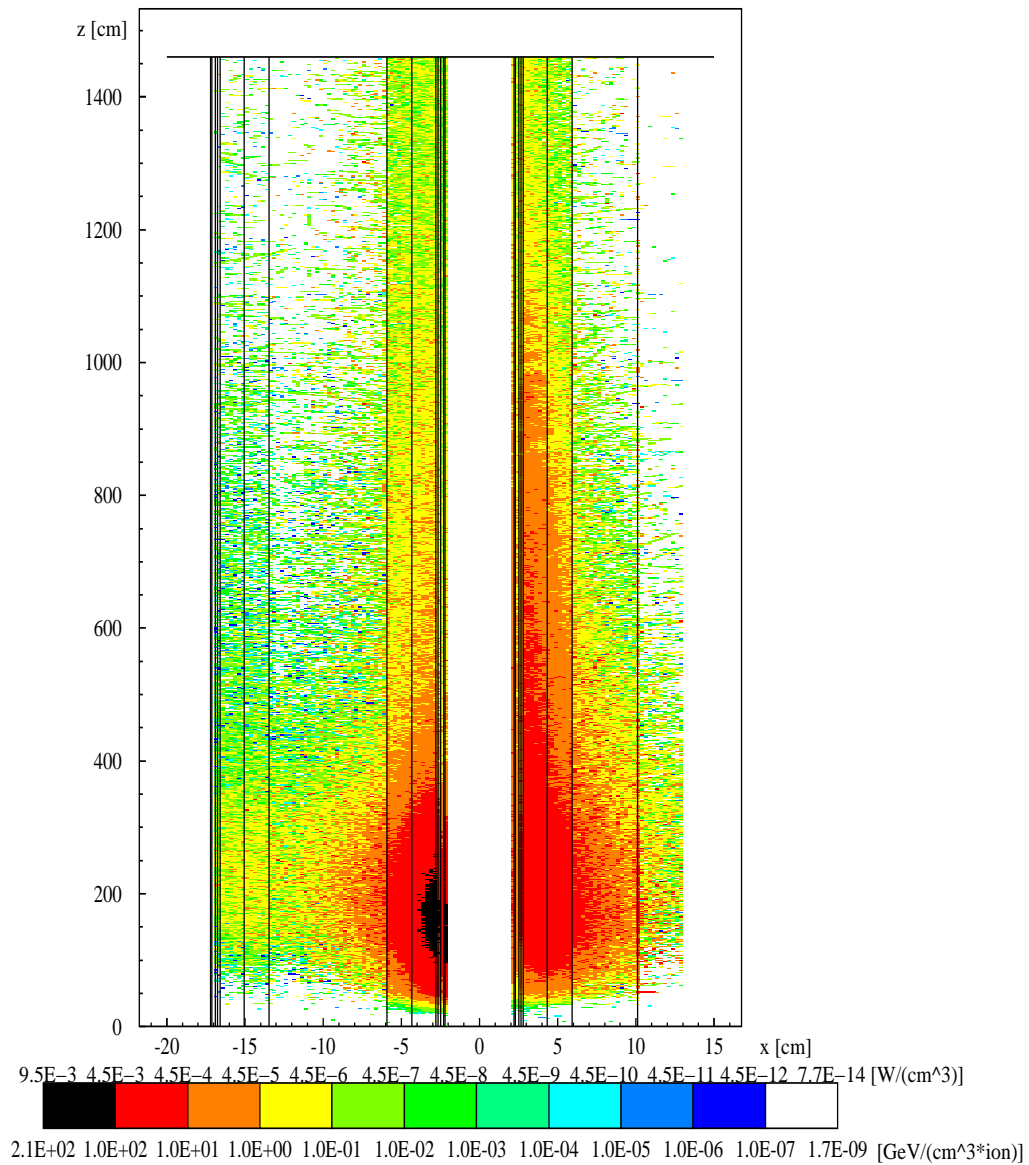


Figure 4.7. The energy deposition from BFPP scored with the *cartesian* mesh plotted with colour codes in a horizontal plane of width 0.25 cm around the vertical centre of the dipole. The white vertical stripe is the beam pipe where no energy is deposited, and the two stripes on each side are the coils. The black spot to the left is the hottest part where most of the ions hit the beam screen. The other beam pipe is to the left of the region shown.

Chapter 5

Quench limit and conclusion

In this chapter, an attempt is made to understand how the temperature rises in the superconducting LHC cables when some power is deposited. From that it is possible to draw conclusions about the maximum power that the cable can tolerate before it quenches. This is done in Section 5.1. After that, in Section 5.2, these results are compared with the results from Chapter 4 in order to draw conclusions about whether the dipoles will quench because of BFPP. In order to further investigate the probability of a quench, also the transient case, that is the first instants of time after the beam has been put into collision, is considered in Section 5.3.

5.1 Quench limit for the LHC main dipoles

In order to determine if a dipole magnet quenches or not due to the energy deposition from the BFPP, one has to compute if the temperature rise inside the superconductor is high enough to bring the superconductor over the critical surface described in Section 2.3. From thermodynamics, the heat δQ per volume needed to cause a temperature rise δT is

$$\delta Q = C \cdot dT \tag{5.1}$$

if the material has a specific heat C , which is normally a function of temperature. C can be given as a fixed number for a specific body, or per weight or volume unit. In this report, C will have the dimension $\text{J}/(\text{cm}^3 \cdot \text{K})$, meaning that also the energy δQ will be given per volume with the unit J/cm^3 . On very short timescales, on the order of milliseconds, one can assume that no heat is transported away from the local point where it is deposited and that the temperature rise is a local process [7]. This can be useful when analyzing what happens during the first moments of operation after the LHC beams have been put into collision. Then equation (5.1) can be integrated directly and one can put Q equal to the energy

deposited by the lost ions during a certain time interval:

$$Q = \int_{T_1}^{T_2} C dT \quad (5.2)$$

Here T_1 is the starting temperature, that is the temperature of the helium bath, and T_2 is the final temperature. The integral can be solved for T_2 and compared with the critical temperature of the superconductor.

However, if steady state is considered, the situation is more complicated and the full heat flow has to be taken into account. The amount of heat δQ per volume transferred between two bodies with temperature difference δT in the time δt connected with a heat conductor with cross sectional area A and length L is [36]

$$\delta Q = \frac{A \cdot k(T) \cdot \delta T}{LV} dt = \frac{k(T) \cdot \delta T}{L^2} dt \quad (5.3)$$

where $k(T)$ is the heat conductivity. This is a material parameter with the dimension $W/(cm \cdot K)$ and normally a function of temperature. The normalization over the volume V of the heat conductor is done in order to express the transferred energy per volume, and the expression was thus simplified using $V = AL$.

Consider now instead the case, where the two bodies are two neighbouring infinitesimal segments inside a larger body with a temperature independent of the y - and z -directions, for instance inside a thin homogenous rod along x . The temperature inside the body as a function of position x and time t can be written as $T(x, t)$ and the distance between the neighbouring infinitesimal elements as dx . If δQ is defined as the heat flowing in in the x -direction, the temperature difference is $T(x, t) - T(x + dx, t)$ and the transferred heat between the two elements becomes:

$$\begin{aligned} \delta Q &= \frac{1}{dx} k(T(x, t)) \frac{T(x, t) - T(x + dx, t)}{dx} dt \\ &= -\frac{1}{dx} k(T(x, t)) \frac{\partial T(x, t)}{\partial x} dt \end{aligned}$$

The total heat increase per unit volume through conduction in an infinitesimal element of length dx in time dt is the sum of the flow into the volume at the left and the right boundaries (with the heat flowing in negative x -direction at the right boundary). This is:

$$\begin{aligned} \delta Q &= \frac{1}{dx} \left(k(T(x + dx, t)) \frac{\partial T(x, t)}{\partial x} \Big|_{x+dx} dt - k(T(x, t)) \frac{\partial T(x, t)}{\partial x} \Big|_x dt \right) \\ &= \frac{\partial}{\partial x} \left(k(T) \frac{\partial T}{\partial x} \right) dt \quad (5.4) \end{aligned}$$

To this, also external sources of heat and heat removal can be added. This is, in the case of the superconducting cable in the dipole, the power density deposited by the lost ions during the time dt , $P_{loss}(x)dt$, which will depend on the spatial coordinate. The external heat removal is the heat transported away per time

and volume by the liquid helium, $-P_{He}(T)dt$, which depends on the temperature difference between the conductor and the helium. Both $P_{loss}(x)$ and $-P_{He}(T)$ have the dimension W/cm^3 .

Now when it is clear how the heat flows inside an infinitesimal volume of a material, one can use equation (5.1) to see how this added heat changes the local temperature during the time interval dt . So, combining equations (5.1) and (5.4) and dividing with dt , one arrives at a differential equation for the temperature:

$$\begin{aligned}
 C(T) \cdot (T(x, t + dt) - T(x, t)) &= \\
 \frac{\partial}{\partial x} \left(k(T) \frac{\partial T}{\partial x} \right) dt + P_{loss}(x)dt - P_{He}(T)dt &\Rightarrow \\
 C(T) \frac{\partial T(x, t)}{\partial t} &= \\
 \frac{\partial}{\partial x} \left(k(T(x, t)) \frac{\partial T(x, t)}{\partial x} \right) + P_{loss}(x) - P_{He}(T(x, t)) &\quad (5.5)
 \end{aligned}$$

This is the full heat flow equation in one dimension. If three dimensions are considered instead, the x -derivatives have to be replaced by ∇ . If steady state is considered, the time derivative on the left hand side can be set to zero.

The power deposited by particle losses was determined through Monte Carlo simulations of the particle shower in Chapter 4. In order to solve the heat flow equation, one also has to know the characteristics of the heat transfer between the superconductor and the superfluid helium. This turns out to be very hard. Not only is there a large number of helium channels inside each cable, with the area between the helium and the conductors being very hard to calculate, but also the thermal behaviour of the helium is very complex. The structure of the wires inside the cable was shown in figure 2.6. Normally the heat flow between a surface and a liquid is directly proportional to their temperature difference, where the proportionality coefficient is called the heat transfer coefficient. In this case however, it is more complicated. Firstly, the heat transfer coefficient for a superfluid depends on the cube of the temperature of the solid — this phenomenon is known as the Kapitza resistance. Secondly, if the surface temperature of the conductor is high enough, helium will start to boil next to the surface of the conductor, thus creating thin films of vapour next to the surface. This will also change the heat transfer characteristics. Moreover, the heat transfer inside the helium pipe has a very complex behaviour. The helium will be a mixture of superfluid, fluid and some vapour next to the conductor interface, and the heat transport is a counterflow process [10]. At the hot surface, superfluid helium will pick up thermal energy and become normal fluid and flow in one direction, while the superfluid phase will flow in the other direction. It is also not well known how the heat flows out of the cable, through the insulation.

So the heat transfer process is extremely hard to model mathematically in a meaningful way. However, there are ways to make estimates. In 1999, some experiments were performed by C. Meuris et al [25], in order to test the characteristics of different cable insulations. In these experiments, five plates made of stainless

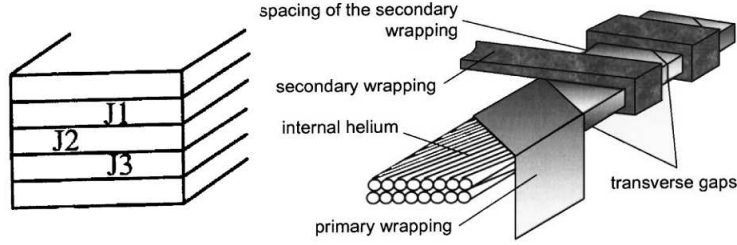


Figure 5.1. Schematical picture of the stack of five conductors in the experiment [25] (left) and a drawing of one of the conductors used (right). The figures are taken from [25].

steel with a length of 15 cm were machined so as to resemble the geometry of the superconducting cable with the helium channels and insulated with different types of insulation. In the middle of each plate a temperature sensor was mounted. Then the plates were enclosed in a pressurized cryostat containing liquid helium, which was kept at a constant bath temperature. A drawing of one of the plates is shown in figure 5.1.

In order to resemble the heating induced by the lost beam particles, a current was run through the plates, causing Joule heating. For a lot of different types of insulation, the temperature difference between the central conductor in the stack and the helium bath was measured as a function of the power input. This can be seen in Figure 5.2, which is taken directly from [25]. These curves can also be inverted, in order to see the power conducted away from the conductors as a function of the temperature difference, which one can use as the function $P_{He}(T(x, t))$ in equation (5.5).

Since only one temperature sensor was mounted in the middle of the cable, it is not meaningful to solve the heat flow equation radially. Although it is an approximation, it has to be assumed that the temperature is constant radially and one has to average the power input $P_{in}(x)$ over the width of the cable. Also some physical reasons exist that could motivate this averaging, since the coils are not homogenous solids. If that were the case, a non-homogenously distributed energy deposition would result in a non-homogenous temperature profile in steady state, which can be realized when solving equation (5.5) in simple cases. In the case of the coils, there is superfluid helium with an extremely high heat conductivity flowing in channels inside the cables, rapidly distributing the heat and transporting it away. Thus a cable can be more regarded as a wet sponge in a flow of water than a homogenous solid. There will still be a small temperature difference between the inner and outer radius, but the effect is a lot smaller due to the helium [37]. Thus the coil can be regarded approximately to have constant temperature radially.

The azimuthal flow of heat between adjacent cables is small but not very well known in detail. Therefore a good first approximation of the problem could be to solve the heat flow equation in one coordinate along the longitudinal direction. It is also worth noting that solving the full heat flow equation in three dimensions imposes severe numerical difficulties. No suitable mathematics software package has been found for the integration of this equation numerically in three dimensions,

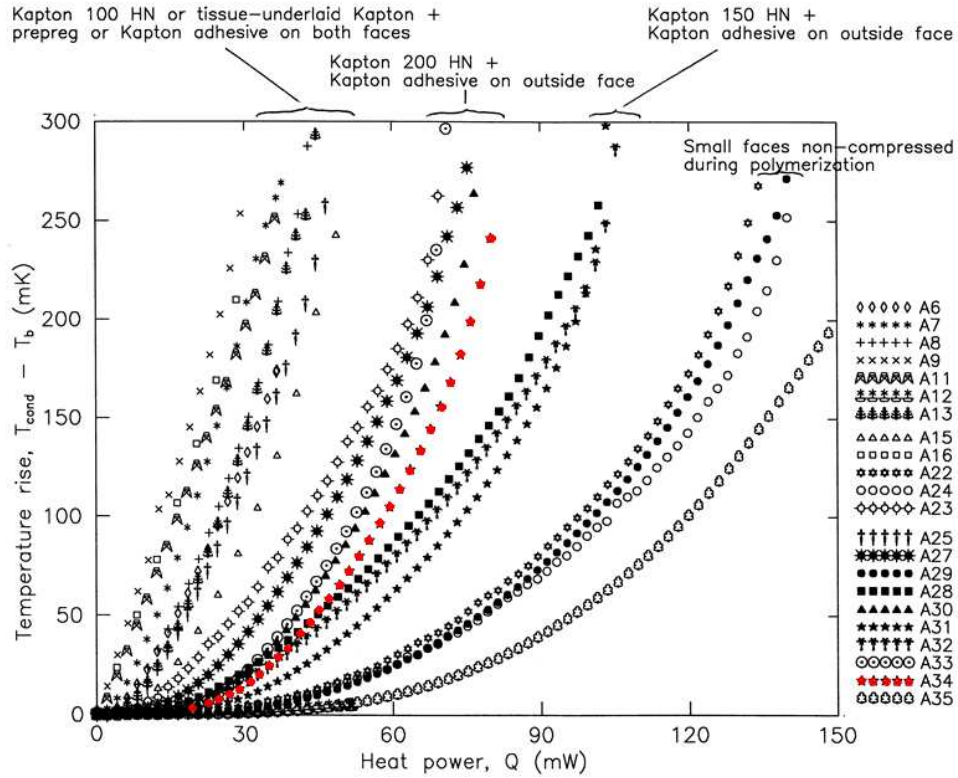


Figure 5.2. The temperature rise in the central conductor as a function of the power input for different cable insulations in the experiment described in [25]. The insulation that was actually chosen for the cables in the LHC dipoles is called A34. The power input is given as an absolute power — in order to get the power per volume one has to divide the scale with the volume 6.375 cm^3 that was used in the experiment. The figure is taken from [25].

which means that a solution algorithm would have to be programmed.

It is also worth noting that a rough first estimate of the temperature rise inside the conductors can be taken directly from Figure 5.2 if one neglects also the longitudinal heat flow. Then the expected temperature rise can be directly read in the diagram if the power input from the particle losses is known. One can even easily put up an upper quench limit for the magnet — if the power deposition is lower than the power needed to raise the temperature to the critical one, neglecting the longitudinal heat flow, the magnet will not quench.

In fact, the LHC design report [13] states 4.5 mW/cm^3 as a limit for the maximum allowed power deposition inside the coils due to beam losses, with a reference to [25]. According to [13] it should have been concluded in [25] that a power input of 4 mW/cm^3 should cause a 1 K temperature rise, which through a linear extrapolation gives at hand that an input of 4.5 mW/cm^3 causes a rise of

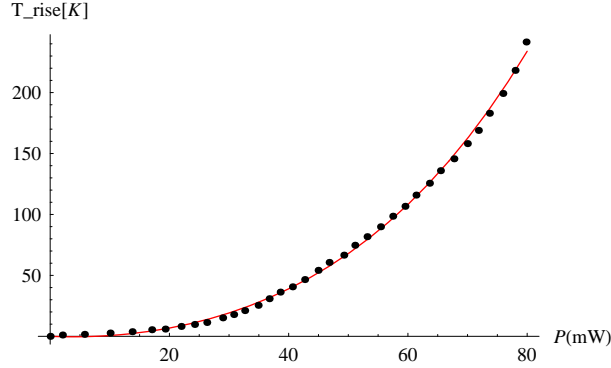


Figure 5.3. The fitted curve from Mathematica and the original data points for insulation A34 in [7].

1.12 K. This is the allowed maximum rise due to beam losses if the temperature margin is 1.4 K, which also can be seen from Table 7.3 in [13]. However, if one examines the curve for the correct LHC insulation A34 shown in Figure 5.2, one can see from the highest point on the curve that an input of 79 mW in the reference plate (with a volume of 6.375 cm^3), which corresponds to 12.4 mW/cm^3 , only causes the temperature to rise by 241 mK.

The points for insulation A34 from Figure 5.2 were also loaded into Mathematica and fitted with a fourth degree polynomial. The resulting fitted polynomial was

$$T_{rise}(P_{in}) = -0.451P_{in} + 0.0434P_{in}^2 - 0.000358P_{in}^3 + 4.31 \cdot 10^{-6}P_{in}^4 \quad (5.6)$$

and the graph is shown in figure 5.3. If one extrapolates this result beyond the range of the experiments, one arrives at temperature rise of 1.12 K for a power deposition of 19.3 mW/cm^3 . This is more than four times higher than the limit proposed in the LHC design report [13]. However, this extrapolation is not very trustworthy, because the transition temperature at 2.167 K where helium goes from superfluid to fluid is passed. Normal fluid helium has a lower heat transfer coefficient, lower heat capacity and lower thermal conductivity than superfluid [10], meaning that the helium will take less heat away from the cable. Thus the real value of the power input should be lower than 19.3 mW/cm^3 . But even if one does not fully trust the extrapolation, it is clear that 12.4 mW/cm^3 only causes a temperature rise of 241 mK. This power is three times higher than the 4 mW/cm^3 that according to [13] should cause a rise of 1 K. The real quench limit derived from the experiment in [25] should thus be somewhere between 12.4 mW/cm^3 and 19.3 mW/cm^3 .

A closer investigation showed that this discrepancy between [13] and [25] can be explained by the fact that before the experiments were done, it was postulated

as a requirement on the machine performance that a power input of 4 mW/cm^3 should not cause a higher temperature rise in the conductor than 1 K. After that the experiments in [25] were performed in order to confirm that this requirement was met. And these experiments showed that the thermal characteristics of the cable and insulation were actually even better, but the original number remained in the LHC design report in order to impose extra safety margins [37].

There are some uncertainties in the experimental results that could motivate the extra safety margins. First of all, the cooling conditions were not exactly the same as in the real dipole magnet. In the experiment, the cables were completely surrounded by a large helium bath with a temperature close to constant. In the LHC cables, the flow of helium around the cables is limited and therefore less efficient. On the other hand, in the experimental setup there were no helium channels inside the cables — they were made of solid stainless steel. Just the surface of the plates was machined to resemble the real cable. These two effects could change the temperature rise a little in both directions. Also the shape of the cable is not exactly the same as the shape of the one in the experiment. As can be seen in figure 2.6 the transverse cross section of the cable is not symmetrical — the end facing the beam pipe is thinner than the outer end. This was not the case in the experiment. How this would influence the thermal behaviour is not clear, but it should not make a major difference.

On the other hand, a recent calculation of the critical temperature in the magnet shows that the magnet should be able to stand more than the 1.4 K mentioned above [26]. This calculation is described in Section 5.3 and shown in figure 5.6. This should slightly increase the quench limit, but it is very hard to say quantitatively how much, since the curve in figure 5.2 cannot be extrapolated because of the phase transition of helium. But due to the worse heat transfer characteristics of helium above the phase transition described above, the gain is probably small.

Another thing worth noting is that the magnetic field in the coils decreases close to the ends of the magnet, thus increasing the quench margin. However, the helium cooling is not as efficient as in the centre due to the gluing of the end caps, which all in all makes the quench limit lower. But the losses from BFPP hit at 1/3 of the magnet length, so this issue is not a big concern in the context of BFPP.

The conclusion of the study of the quench limit is that there is a large uncertainty in the function $P_{He}(T(x, t))$. The best approximation available comes from [25]. But some uncertainties exist that could motivate extra safety margins. However it is very unlikely that the quench limit has to be decreased as much as to the number given in [13]. In order not to have a too pessimistic limit, 10 mW/cm^3 was proposed by [37].

5.2 Conclusion for the steady state case

As was concluded in Section 5.1, the appropriate mesh for studying steady state losses has no radial binning. And as was shown in Section 4.4, the maximum for this type of mesh converges to 7.2 mW/cm^3 . Comparing this value with the

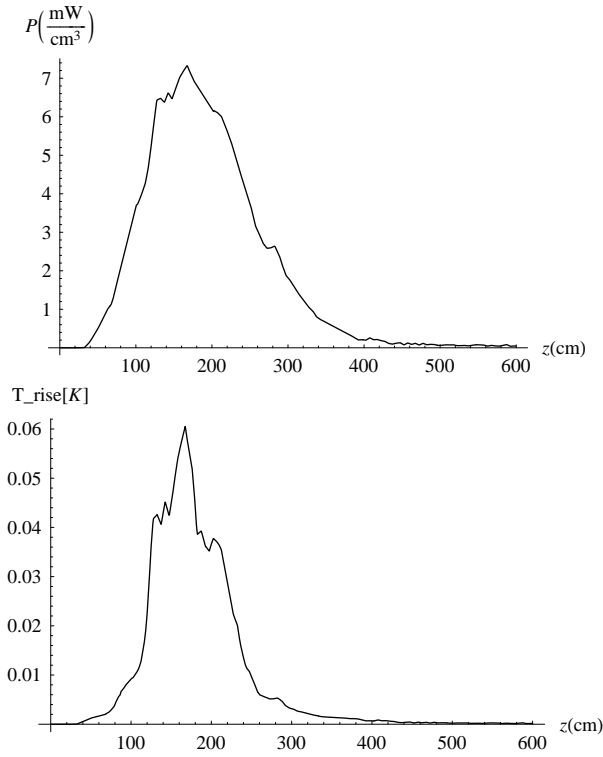


Figure 5.4. The power density in the hottest cable from the FLUKA simulation (top) and the resulting temperature profile (bottom) if no longitudinal heat conduction is taken into account.

suggested quench limit of 4.5 mW/cm^3 in [13] directly, it is clear that the power deposition is too high. However, as was discussed in Section 5.1, there are strong reasons to believe that this limit is too pessimistic.

A first rough estimate of the temperature profile caused by BFPP can be made directly with the data from figure 5.2. If the longitudinal heat flow is neglected at first, each data point in the FLUKA output can be used as input to the correct function in this figure, which will return the temperature rise at that point. This has been done for the hottest cable in figure 5.4. In the upper part, the power deposition scored with the *old* mesh is shown, and in the lower part the resulting temperature profile. As can be seen in the figure, the maximum temperature rise is only around 60 mK, which is an order of magnitude below the temperature margin of 1.12 K quoted in [13]. And so far no longitudinal heat flow has been taken into account.

A better estimate of the temperature profile is obtained through the solution of the full heat flow equation in steady state, that is equation 5.5 with $\partial T/\partial t = 0$. As explained in Section 5.1, strong reasons exist for reducing the heat flow equation to only one direction. The function $P_{loss}(z)$ can be taken directly from

the FLUKA output and the function $P_{He}(T)$ is given by the curve for insulation A34 in figure 5.2.

However, even when solving the one-dimensional equation, numerical difficulties arise due to limited numerical precision. In order to demonstrate this, and also to investigate the qualitative effect of the heat transfer and see if it is worth writing a special numerical integrator for the heat flow equation, a very simplified model can be considered. The maximum power deposited in the cable is 7.2 mW/cm^3 , but the shape of the curve for the power deposition as a function of z is rather complicated. In this oversimplified model the power deposition along the 1460 cm cable was approximated as a square function with the same integral of 1.22 W as the original FLUKA curve:

$$P_{in}(z) = \begin{cases} 0 \text{ mW/cm}^3, & 0 \leq z < 645 \text{ cm} \\ 7.2 \text{ mW/cm}^3, & 645 \leq z < 815 \text{ cm} \\ 0 \text{ mW/cm}^3, & 815 \leq z \leq 1460 \text{ cm} \end{cases} \quad (5.7)$$

The sharper distribution concentrates the heat more in the cable, which together with the fact that this distribution was placed in the middle of the cable makes the heat flow more important. In order to make the helium cooling less important it was modelled as a straight line

$$P_{He}(T) = P_0 T \text{ mW/cm}^3 \quad (5.8)$$

with initially $P_0 = 50 \text{ mW/cm}^3\text{K}$ if T is the temperature rise and not the absolute temperature. Also the heat conductivity of the cable has to be taken into account. This is the weighted sum of the conductivities of copper and NbTi, with the copper to NbTi ratio 1.65 [7]. The heat conductivity for NbTi at temperature T is given by [40]:

$$k_{\text{NbTi}} = 7.5 \cdot 10^{-3} \cdot T^{1.85} \text{ mW/(cm K)} \quad (5.9)$$

The heat conductivity for copper is not such a straight forward expression. At temperature T and magnetic field B it is given by [40]:

$$\begin{aligned} k_{\text{Cu}} &= \frac{2.44 \cdot 10^{-8} \cdot T}{\rho_{\text{Cu}}(RRR, T, B)} \text{ mW/cm K} \\ \rho_{\text{Cu}}(RRR, T, B) &= (1+r) \left(\rho_i + \rho_0 + 0.4531 \frac{\rho_i \rho_0}{\rho_i + \rho_0} \right) \\ \rho_0 &= 15.53 \cdot 10^{-9} / RRR \\ \rho_i &= \frac{1.171 \cdot 10^{-17} \cdot T^{4.49}}{1 + 4.498 \cdot 10^{-7} \cdot T^{3.35} \cdot \exp(-(50/T)^{6.428})} \\ \ln r &= -2.662 + 0.3168 \ln s + 0.6229 (\ln s)^2 - 0.1839 (\ln s)^2 + 0.01827 (\ln s)^4 \\ s &= \frac{15.53 \cdot 10^{-9} \cdot B}{\rho_0 + \rho_i + 0.4531 \frac{\rho_i \rho_0}{\rho_0 + \rho_i}} \end{aligned} \quad (5.10)$$

Here ρ_{Cu} is the resistivity and RRR the residual resistivity ratio. This is a dimensionless parameter and a measure of the impurity of the specific material sample. For the copper in the LHC dipole cables, $RRR = 250$ [13]. In the simplified model, the heat conductivity was assumed to be constant. And in order to overestimate the influence of heat conduction compared with convection through helium this constant was chosen to be

$$k = 80 \text{ mW}/(\text{cm K}), \quad (5.11)$$

which is higher than all the real values in the actual temperature range and the real magnetic field in the coil, which is roughly between 1 and 8 T.

Putting equations 5.7, 5.8 and 5.11 into the heat flow equation (5.5) with $\partial T/\partial t = 0$, the following differential equation is obtained:

$$k \frac{d^2 T}{dz^2} - P_0 T = -P_{in}(z) \quad (5.12)$$

Worth noting is that T in this equation is actually the temperature rise and not the absolute temperature due to the definition of P_{out} . Equation (5.12) has the same form as for instance the Schrödinger equation for a free particle encountering a potential barrier and its solution is well known:

$$T(z) = C_i e^{\sqrt{\frac{P_0}{k}} z} + D_i e^{-\sqrt{\frac{P_0}{k}} z} + P_{in}(z)/P_0 \quad (5.13)$$

Here C_i and D_i are integration constants. The index $i = 1, 2, 3$ is needed to distinguish the three zones determined by P_{in} . So in total there are six integration constants that need to be calculated through boundary conditions. Four boundary conditions are, just as in the case of the Schrödinger equation, given by the constraint that T and dT/dz must be continuous at $z = 645 \text{ cm}$ and $z = 815 \text{ cm}$. Yet another way of increasing the importance of the heat flow is to also demand that the edges of the cable at $z = 0$ should be kept constant at the bath temperature $T = 0$. In reality it is not that simple: since the cables are wound in several turns, a more realistic boundary condition would be to demand that the end temperature of one cable should equal the temperature in the beginning of the next cable on the other side of the beam pipe and so on, which requires that the heat equation is solved in all cables, which is not done in this simplified model.

The above mentioned boundary conditions give in total six equations that allow the integration constants to be determined numerically. However, when attempting to solve the equation system with the initially proposed $k = 80 \text{ mW}/(\text{cm K})$ and $P_0 = 50 \text{ mW}/\text{cm}^3 \text{K}$ numerical difficulties arise due to limited precision. This is due to the fact that for these values the resulting temperature profile is very similar to the profile one would arrive at without any heat flow—that is, the solution of equation (5.12) if $k = 0 \text{ mW}/\text{cm K}$. As can be seen by inspection, this profile is also a square wave with height $7.2/P_0 = 0.144 \text{ K}$.

If one gradually increases k the heat flow slowly becomes important and starts influencing the shape of the temperature profile. This is shown in figure 5.5, where the solution to equation (5.12) is shown for several values of k . As can be seen

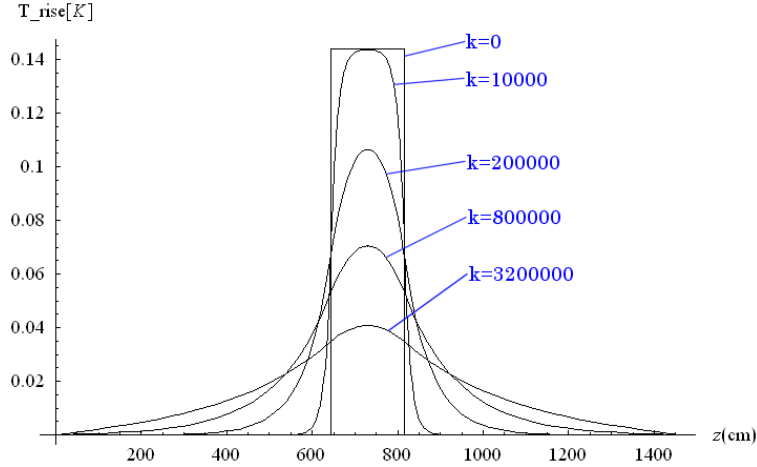


Figure 5.5. The temperature rise in the cable for different values of the thermal conductivity k [mW/(cm K)] calculated with the simplified model of the energy deposition and transfer.

in the figure, the heat conduction does not lower the maximum temperature in the cable significantly until k becomes very large. For $k = 200000$ mW/cm K the maximum temperature in the cable has decreased with roughly 20%. Such large values of k are totally unrealistic, even if the temperature varies and the magnetic field changes. And one should also bear in mind that the heat conduction was consequently overestimated and the heat transported away by the helium underestimated in the rough approximations in this very simplified model. Therefore it can be concluded that the longitudinal heat conduction is negligible as source of heat removal when compared to the convection through the helium. It is a very good approximation to simply solve the equation $P_{He}(T) = P_{in}(z)$, which was done in figure 5.4, and it is not necessary to solve the full heat flow equation. Here the maximum temperature rise in the hottest cable is 60 mK and taking into account the heat conduction along the cable does not change this value significantly.

The uncertainty lies instead in the function $P_{He}(T)$ which is not well known but where the best existing estimate is given by [25] as explained in Section 5.1. Although some extra safety margins should be taken into account, it is however unlikely that the actual temperature rise is an order of magnitude higher. Thus it can be concluded that the risk of quenching the magnet with losses from BFPP in steady state is very small, if one trusts the FLUKA simulation.

It is also worth mentioning that by the time of writing, the need of a deeper understanding of the quench limit of the LHC magnets has become clear to more and more people at CERN. Therefore, the magnet division at CERN has started the development of a computer code that simulates the temperature rise due to a power input inside an LHC cable. It is to be hoped that this project will be successful and that it will bring more clarity also to the possible quenches due to the BFPP process.

Another uncertainty is that the 7.2 mW/cm^3 calculated in Section 4.4 has an error bar which is very difficult to estimate. Because of numerical errors, possible errors in the physics models used and approximations of these models, this number can not be fully trusted. FLUKA specialists [33] suggest a safety margin of a factor two. This would mean instead a maximum power density of 14.4 mW/cm^3 , which when used as input to the curve in figure 5.2 instead gives a temperature rise of 0.39 K . But in order to arrive at this value extrapolation must be used. A temperature rise of 0.39 K means a final temperature of 2.29 K , which is above the lambda point for helium at 2.167 K . At this temperature and atmospheric pressure, helium undergoes a phase transition from superfluid to fluid, meaning that some extra energy is needed to make the transition but also that the heat capacity drastically decreases afterwards. The total effect could be that the final temperature is higher. A power density of 14.4 mW/cm^3 is also above the limit suggested by [37].

Yet another uncertainty factor lies in the radial averaging of the power input, which is necessary in order to compare with the experiments done in [25]. If instead the maximum power deposition of 13.5 mW/cm^3 is taken, and one also takes into account the safety margin of a factor two, it is clear that the magnet is probably over the quench limit.

So although a magnet quench due to BFPP is not likely to occur, it is impossible to exclude one due to the uncertainties in the quench limit and the simulation result itself. So far it has also been assumed that only the BFPP process causes ion losses at this particular spot. If other physical processes cause more power to be deposited in the coils, there danger of a possible quench increases. Therefore it is very important that more work is carried out in order to determine the effect of other loss mechanisms, that at a first glance may seem less dangerous.

There are however some safety measures that can be taken in order to further lower the risk of a quench. First, it could be possible to change the shape and size of the footprint of the beam impinging on the beam screen. The beam will crash in a dispersion suppressor dipole, and between this magnet and the interaction point there are some other magnets whose fields could be adjusted. First, the main quadrupoles could be adjusted. These magnets are focussing the beam in one plane and defocusing in the other. The field in these magnets could be slightly modified, for instance in order to defocus the beam more in one of the planes. This would spread out the spatial distribution on the beam screen and therefore also the distribution of the energy deposition in the magnet, which could help to prevent a quench. Also the dipole magnets, which bend the beam, could be adjusted a little, so that the radius of curvature decreases. This would make the secondary beam crash further down in the beam line instead, for instance in a quadrupole magnet. A quadrupole magnet has a higher temperature margin than a dipole and can therefore withstand more heat before it quenches.

Also the beam screen could be modified. The main function of the beam screen is to shield the coils from the synchrotron radiation created by the charged beam. But if the beam screen is made thicker, a larger amount of the energy carried by the ions will be deposited in there instead, and if it is made thick enough, it will absorb so much heat that a quench can be avoided. The problem is that if

the beam screen is made thicker, the beam pipe will be smaller, and the particles propagating through it will be closer to the walls, resulting in more interactions with the beam screen through for instance induced currents. Maybe there could be some way of keeping the cross sectional area of the pipe constant while increasing the thickness of the beam screen. However, such modifications are difficult and expensive to implement, since they require changes in the magnet design. In order to tell exactly how the beams would be affected by a thicker beam screen, one would have to do deeper studies which are beyond the scope of this report.

Last, as can be seen from equation (4.1), the power deposited into the coils depends linearly on the luminosity and the cross section for BFPP. The luminosity is the parameter in the equation that is easiest to change, since it is a design parameter of a collider that can be changed or lowered according to the technical limits discovered during the construction or the operation. Reducing the luminosity by some factor would reduce also the number of ions undergoing BFPP with the same factor. However, since all other reaction rates also depend on the luminosity, the interaction rate for the processes that are wanted in order to study new physics phenomena will also be reduced by the same factor. On the other hand, a lower luminosity also implies a longer lifetime of the beam (due to the above mentioned lower interaction rates). The time it takes to fill the LHC is comparable to the beam lifetime, and therefore the efficiency in wanted interactions per time will not decrease as much as one first might think. So maybe the luminosity can be lowered without too high a decrease in the total number of physics interactions. Further investigations are necessary in order to clarify this issue.

So some possible safety measures exist. A good way to further investigate the danger of a quench is to look on BFPP on a very short timescale and consider what happens the first instants of time after the beam has been put into collision. On a very short timescale, the heat does not have sufficient time to spread along the cable or to be transported away by the helium. Thus this consideration does not involve a steady state limit and the function $P_{He}(T)$. If it shows consistency with the results above, it is a good way of confirming the above calculation.

5.3 BFPP Energy deposition on short timescales

In order to validate further the results for the quench limit and the temperature rise calculated in the previous section, one can take a different approach and consider a very short time scale after the beam has been put into collision. Since it takes a certain time for the heat to migrate out of the cable and be conducted away by the helium, one can choose a timescale so short that one can assume that all deposited heat stays within the cable and that the flow of heat can be neglected. If a quench is likely to occur already on this time scale, it is certain that a quench will occur also if steady state is considered. The opposite is however not true. A similar calculation has already been performed for homogenous losses of protons [7], and this section will follow this calculation in broad outline but with some appropriate modifications and also improvements.

In order to understand if a magnet quenches or not on a short time scale, one

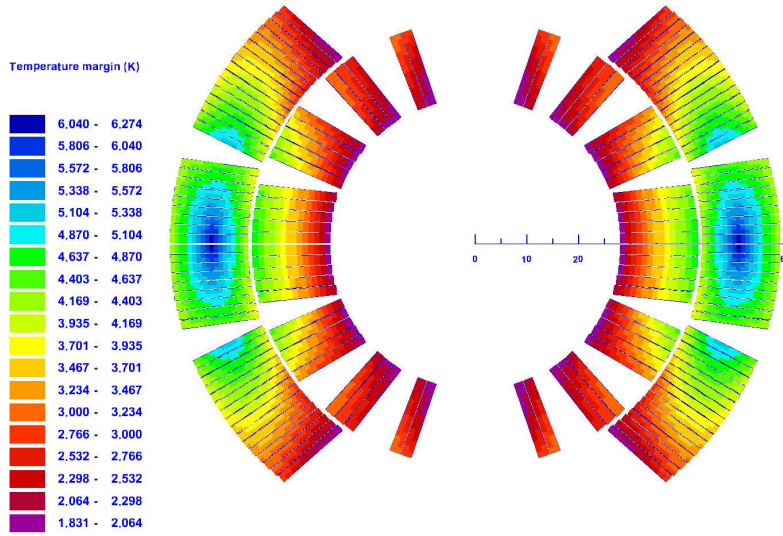


Figure 5.6. The temperature margin in K up to a quench in the coils of an LHC dipole magnet as calculated by [26].

must calculate the temperature rise caused by the energy deposition and then compare it with the minimal temperature rise that brings the superconductor outside the critical surface at the present magnetic field and current, as explained in Section 2.3. A detailed map of this temperature margin T_{margin} in a fine grid in the coils has been computed for the nominal magnetic field and current by [26] and is shown in figure 5.6.

One can note that the minimum temperature margin in this map is 1.8 K. In Table 7.3 in the LHC design report [13] another number — 1.4 K — is given. This discrepancy is due to some recent changes in the design of the coils. In Table 7.3 in [13] also some extra terms are listed, which decrease the temperature margin. The measurement precision, dissipation and ramping losses mentioned there, decreasing the margin with in total 0.34 K, had thus to be subtracted from every point in the temperature margin map given by [26].

The amount of heat required to raise the temperature in the cable by a certain value is given by equation 5.2. In this case, the wires are almost free to expand locally since they are surrounded by liquid helium. Thus for the wires the specific heat at constant pressure, C_P , should be used. However, for a limited low temperature range in metals, $C_V \approx C_P$ [7], and the calculations become significantly simplified if instead C_V is used. Therefore C_V will be used throughout the calculations.

In the superconducting cable, C_V is a function of temperature. Therefore the energy needed to raise the temperature in the superconductor from the normal working temperature, which is the same as the temperature of the helium bath

$T_{bath} = 1.9$ K to the temperature at the critical surface $T_{bath} + T_{marg}$ is:

$$Q = \int_{T_{bath}}^{T_{bath}+T_{marg}} C_V dT \quad (5.14)$$

Since the coil is made up of several different materials, the total specific heat of it is a weighted sum of the specific heat for each material. The coils in a dipole consist of superconducting NbTi inserted in a Cu matrix as explained in Section 2.1. The copper takes up 56.6 % of the volume and the NbTi 35.4 %. The remaining 8 % of the volume is taken up by superfluid helium and insulation. Following [7], the insulation has a specific heat close to that of NbTi and a very small relative volume. Therefore it contributes very little to the total heat reserve and can therefore be neglected in this estimation.

The helium on the other hand contributes substantially to absorb the added heat - in this temperature range the specific heat of helium is orders of magnitude larger than the one of NbTi. So although it only occupies 5 % of the volume it has to be taken into account. However, if very short timescales

$$t \ll 8 \cdot 10^{-3} \text{s} \quad (5.15)$$

are considered, as pointed out in [7], the heat does not have enough time to spread to the helium, since the flux of heat from the wire to the helium is limited. Thus, when looking at for instance the very first 100 μs , a timescale proposed by [41] which fulfils the restriction (5.15), the influence of the helium can be neglected.

Therefore two different timescales can be considered — first the 100 μs scale, where the helium does not contribute, and then the 8 ms scale, where also the helium contributes. This corresponds to the cases a) and c) in [7].

5.3.1 Calculation without helium

The specific heat for copper at low temperatures can be described as a sum of a term proportional to T and another one proportional to T^3 . The linear term is connected to the free conduction electrons, which can be calculated within the Fermi free electron model, and the cubic one to the phonons, which can be calculated using Debye theory [9]. Thus, the specific heat of copper can be parameterized as

$$C_{V,Cu} = \gamma_{Cu} \cdot T + \alpha_{Cu} \cdot T^3 \quad (5.16)$$

where

$$\begin{aligned} \gamma_{Cu} &= 9.686 \cdot 10^{-2} \text{ mJ/cm}^3\text{K}^2 \\ \alpha_{Cu} &= 6.684 \cdot 10^{-3} \text{ mJ/cm}^3\text{K}^4 \end{aligned}$$

according to [7].

More care needs to be taken in order to find the specific heat for the superconducting NbTi. The electronic heat capacity changes in the superconducting state,

since some other effects, which cannot be described within the free electron model, come into play. The conduction electrons bound in Cooper pairs no longer contribute to the heat capacity. This has been thoroughly investigated in theoretical papers, see for instance [42], and here only the result will be used. The specific heat for the superconducting NbTi is

$$C_{V,NbTi} = \gamma_{NbTi} \cdot \frac{B}{B_{c2(0)}} \cdot T + \alpha_{NbTi} \cdot T^3 \quad (5.17)$$

where

$$\begin{aligned} \gamma_{NbTi} &= 0.87 \text{ mJ/cm}^3\text{K}^2 \\ \alpha_{NbTi} &= 4.464 \cdot 10^{-2} \text{ mJ/cm}^3\text{K}^4. \end{aligned}$$

Furthermore, B is the magnetic field and $B_{c2(0)} = 14 \text{ T}$ is the second critical field at $T = 0$.

The total specific heat is then obtained by weighting C_V for Cu and for NbTi according to their relative volume fractions:

$$C_{V,tot,noHe} = \frac{C_{V,Cu} \cdot V_{Cu} + C_{V,NbTi} \cdot V_{NbTi}}{V_{Cu} + V_{NbTi}} \quad (5.18)$$

So the energy required to raise the temperature to the critical surface is, with use of equation (5.14):

$$Q = \int_{T_{bath}}^{T_{bath}+T_{marg}} C_{V,tot,NoHe} dT \quad (5.19)$$

Thus, with a working temperature of $T_{bath} = 1.9\text{K}$ an energy margin — that is the maximum energy per volume that can be added before the magnet quenches — was calculated for every point on the temperature margin map. The minimum energy margin in the whole magnet was found to be 1.636 mJ/cm^3 .

Now this margin has to be compared with the energy deposited by the lost ions. When considering a very short timescale, as stated in [7], the heat does not have sufficient time to migrate radially through the wire. This means that the correct value of the energy deposition to compare with is the very peak of the energy deposition as a function of radius at the hottest longitudinal coordinate, and not the radial average. According to Section 4.4, this value converges to 13.5 mW/cm^3 . If this power is deposited in the coil during $100 \mu\text{s}$, $1.35 \cdot 10^{-6} \text{ J/cm}^3$ is deposited in the hottest part of the magnet. This is three orders of magnitudes below the lowest energy margin. Thus it can be concluded that there is no risk of the heat deposition from BFPP quenching the magnets on the $100 \mu\text{s}$ timescale.

Indeed, even if the high heat capacity of the helium is not taken into account, and it is supposed that the highest energy density is deposited in the weakest part of the coil, the wire itself could stand this power for

$$\frac{1.636 \text{ mJ/cm}^3}{13.5 \text{ mW/cm}^3} = 0.12 \text{ s} \quad (5.20)$$

which gives plenty of time to dump the beam.

5.3.2 Calculation with helium

If one considers timescales large enough to allow heat to flow from the wire to the helium, but not large enough to let the heat be transported away by the helium flow, then also the specific heat of the helium has to be taken into account. The total specific heat of the cable is then

$$C_{V,tot,He} = \frac{C_{V,Cu} \cdot V_{Cu} + C_{V,NbTi} \cdot V_{NbTi} + C_{V,He} \cdot V_{He}}{V_{Cu} + V_{NbTi} + V_{He}} \quad (5.21)$$

and the energy needed to raise the temperature to the critical value is

$$\begin{aligned} \Delta Q &= \int_{T_{bath}}^{T_{bath}+T_{marg}} C_{V,tot,He} dT \\ &= \frac{V_{Cu} + V_{NbTi}}{V_{Cu} + V_{NbTi} + V_{He}} \cdot \int_{T_{bath}}^{T_{bath}+T_{marg}} C_{V,tot,noHe} dT \\ &\quad + \frac{V_{He}}{V_{Cu} + V_{NbTi} + V_{He}} \cdot \int_{T_{bath}}^{T_{bath}+T_{marg}} C_{He} dT. \end{aligned} \quad (5.22)$$

The first integral was already calculated in the previous section. It only has to be summed up with the second integral with the appropriate weights.

The second integral is more problematical to evaluate. The specific heat of liquid helium as a function of the temperature has a complicated shape. In [7] the integration was performed using tabulated data for C_P in the approximation that the density was constant. In this report a different approach was used. The specific heat was calculated with the software HEPAK 3.4 [43] instead to achieve much higher accuracy.

For superfluid and fluid helium, C_V and C_P are qualitatively different, which can be seen in Figures 5.7 and 5.8, so the choice really matters and is not obvious. Although the cables are under high pressure inside the cryostat, the superfluid helium is at atmospheric pressure, since it can flow without resistance through the microscopic channels. Thus the helium starts at 1.9 K and approximately 1 atm before the heat deposition. The density of helium at this pressure and temperature is 0.147 g/cm³ [7]. In Figure 5.8, C_V is shown as a function of temperature at this constant density. And in Figure 5.7, C_P as a function of temperature at constant pressure 1 atm is shown. Both curves were calculated using HEPAK up to 9 K. It is worth noting, that in the C_V curve there is only one phase transition, between fluid and superfluid, whereas there are two transitions in the C_P curve. If the pressure is kept constant the transition to gas can also be seen. The phase transitions are the peaks in the diagrams — when the curve is integrated over a peak, the integral has a large value corresponding to the energy needed for the transition.

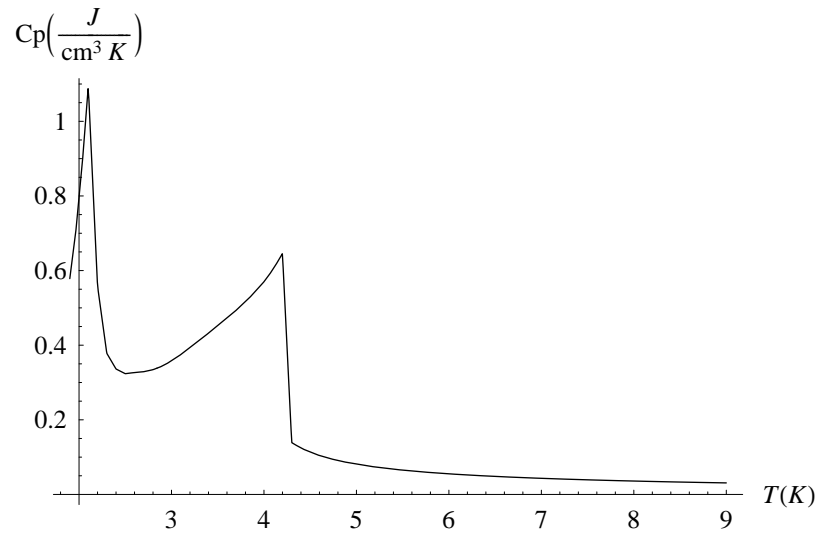


Figure 5.7. The specific heat C_P [$\text{J}/(\text{cm}^3 \text{K})$] at constant pressure 1 atm as a function of temperature [K].

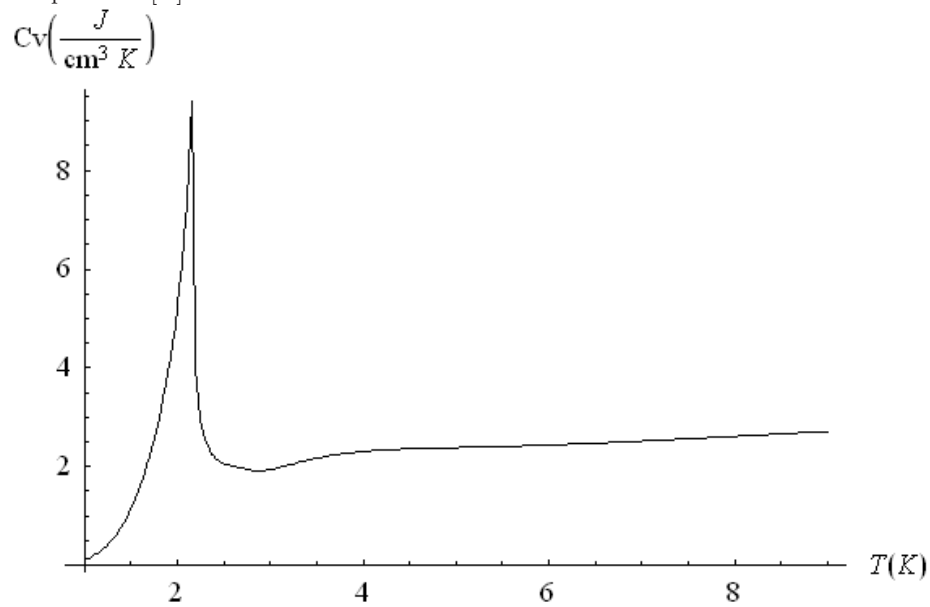


Figure 5.8. The specific heat C_V [$\text{J}/(\text{cm}^3 \text{K})$] at constant density $0.147 \text{ g}/\text{cm}^3$ as a function of temperature [K].

For a correct choice of integration path in the $P - V$ plane, the underlying physical processes have to be investigated in more detail. The cable is surrounded by an insulation which can stand some pressure but, if the pressure becomes too high, helium will evaporate out through the insulation. A fair model would thus start the integration at constant volume but then, at the maximum pressure P_c that the cable insulation can stand, switch to an integration with constant pressure. If the temperature of the helium is $T(P_c)$ at this critical pressure, the second integral in equation (5.22) becomes

$$\int_{T_{bath}}^{T_{bath}+T_{marg}} C_{He} dT = \int_{T_{bath}}^{T(P_c)} C_{V,He} dT + \int_{T(P_c)}^{T_{bath}+T_{marg}} C_{P,He} dT. \quad (5.23)$$

The value of P_c is not known and is very hard to estimate. The only hints known are observations in some experiments that thin films of helium actually starts to boil close to the cable surface at quite low temperatures well included on the temperature axis in the shown diagrams [44]. This means that the critical pressure is well below the final pressure at 9 K in the C_V diagram, which according to the HEPAK calculation is 34 atm. It seems plausible that the cable could not hold this pressure inside.

In [7], the specific heat for helium was integrated from the bath temperature at 1.9 K to three temperatures — 2.168 K (the lambda point), 2.8 K and 9 K. In order to compare with these results, the specific heat for helium was integrated between the same points for several different cases: The extreme cases with only C_V or only C_P all the way, and several cases starting with C_V , and then when a critical pressure is reached, switching to C_P . The C_P integration has to start at the pressure and temperature where the C_V integration stopped. Thus a different C_P had to be calculated for each critical pressure. The values of C_V and C_P in units of J/(K cm³) were calculated every 0.1 K from 1.9 K to 9 K using HEPAK and then put into Mathematica[©] [34]. There the points were linearly interpolated to a continuous curve that could be numerically integrated. The achieved values are given in Table 5.1 together with the reference values from [7].

The highest energies are obtained for critical pressures between 6 and 10 atm. This is due to the fact that the specific heat is a lot lower for gaseous than for liquid helium. So if, for instance, C_P is integrated all the way, the helium is in gaseous state over a larger temperature range where it does not absorb a lot of energy. If the critical pressure is increased, also the boiling point is increased, and the temperature range where the helium is in gaseous state decreases, thus yielding a higher value of the integral. On the other hand, if the critical pressure is set to infinity, that is C_V is integrated all the way, the helium does not start to boil before 9 K. This means that it does not go through the second phase transition where a lot of energy is needed, thus lowering the value of the integral again. So the maximum energy needed should be at a critical pressure where the boiling point is displaced to a position right before 9 K.

P_c [atm]	Integral to 2.167 K	Integral to 2.8 K	Integral to 9 K
1	0.22	0.46	1.40
2	0.22	0.44	2.41
5	0.22	0.44	3.96
6.25	0.22	0.44	4.07
7.5	0.22	0.44	4.09
8.125	0.22	0.44	4.07
8.75	0.22	0.44	4.04
10	0.22	0.44	3.97
20	0.22	0.44	3.31
∞	0.22	0.44	2.67
Report 44 [7]	0.23	0.58	6.3

Table 5.1. The energy values obtained by integrating the specific heat as shown in equation (5.23) up to three different temperatures. P_c is the pressure where the helium is assumed to start leak out through the cable insulation. At a critical pressure of 1 atm, C_P is used through the whole integration, and at a critical pressure of ∞ only C_V is used. The last line gives the values calculated in [7].

As can be seen in table 5.1, the integrated energies do not differ substantially at the lower integration boundaries depending on whether C_V or C_P is chosen. But the integral to 9 K varies a lot depending on how the critical pressure is chosen. Especially worth noting is the large value that was obtained in [7]. Regardless of how the critical pressure is chosen (the true value is not known as pointed out above), it is not possible to get a value as high as this using the HEPAK data. The discrepancy comes from the fact that a less accurate method was used in [7] due to lack of data. The integral up to 9 K comes in to play when looking at quench limits for the injection energy (450 GeV for protons), and the results above thus imply that the magnet will quench more easily than was earlier thought for this type of loss. Depending on the true value of the critical pressure, the energy that the helium can absorb should be decreased by at least a factor 1.5. In reality it may also well be the case that the process follows a different path in the $P - V$ plane, where none of these variables is constant. An investigation of this case is however beyond the scope of this text.

For the present problem with BFPP, it is not necessary to know the exact value of the critical pressure, and the lower temperature range, where the results are consistent, is the one of interest. In order to have safety margins, the most pessimistic case can be chosen, which is the case where C_P is integrated all the way. Physically, this would mean that the helium would start to leak out through the cable insulation as soon as it is heated, which is not the case in reality. However, choosing this integration path gives a pessimistic estimation.

So using equation (5.22) and C_P for helium an energy margin was once again calculated for every point in the coils. It was found that the minimum energy margin in the magnet was 34.9 mJ/cm³. When considering this slightly larger timescale, the relevant value of the power deposition is not the peak value, but the

radial average, since the heat has sufficient time to migrate radially in the cable [7]. This is, as mentioned earlier, 7.2 mW/cm^3 in the hottest part of the coil. Thus, during 8 ms, the energy density deposited in the cable is $7.2 \cdot 8 \cdot 10^{-3} = 0.0576 \text{ mJ/cm}^3$. This is again orders of magnitude below the quench limit, so there is no risk quenching the magnet on this timescale either. So, even if the maximum energy density was deposited at the weakest spot in the magnet, it would still take

$$\frac{34.9 \text{ mJ/cm}^3}{7.2 \text{ mW/cm}^3} = 4.85 \text{ s.} \quad (5.24)$$

before the magnet would quench.

The conclusion that can be drawn is that the magnet will not quench due to BFPP before the cooling system comes into play. This is consistent with the result for the steady state case. Since it will take seconds before enough heat to induce a quench is accumulated even without helium flow, it will take much more time when this cooling is present. So if the magnet would after all quench in steady state, it will be a slow process where more and more heat is accumulated in the magnet over time, provided that no other processes increase the heat deposition.

Chapter 6

The beam loss monitor system

In order to protect the magnets from quenches caused by beam losses, that in the worst case could even damage the magnets, a beam loss monitor system will be installed around the LHC [28, 11]. The system will consist of small ionization chambers that will be placed just outside the cryostat. These beam loss monitors (BLMs) will detect secondary particles from the showers induced by beam losses. The correlation between the signal in a BLM and the energy deposited in the magnet coils has been determined for protons through simulations [28]. If the signal corresponds to a too high energy deposition, a signal will be given to the beam dump system, which dumps the beam within one turn.

For lead ions however, the correspondence between the signal in the BLM and the energy deposition in the magnet was not known. Because of the physical reasons explained in Section 2.6, the ions deposit more energy per volume before the nuclear breakup. This could mean that the same amount of detected shower particles outside the cryostat corresponds to a higher energy density in the coils in the case of ions. In order to investigate this problem more closely, FLUKA simulations were performed in order to determine whether the present design, optimized for protons, also could be suitable for lead ions.

6.1 Ionization chambers

An ionization chamber is a cavity filled with a gas that is kept between two electrodes [46, 12]. A high voltage is applied to the electrodes in order to create an electric field inside the chamber. If a charged particle passes through, it will ionize the gas. The energy needed to do this is taken from kinetic energy of the particle and is normally very small — typically a particle loses a few keV per centimetre gas it passes [46]. Because of the force from the electric field, the created ions will drift to the cathode and the electrons to the anode. This will induce a current that gives the signal that a charged particle has passed the detector.



Figure 6.1. One of the ionization chambers that will be placed around the LHC ring in order to monitor the beam losses.

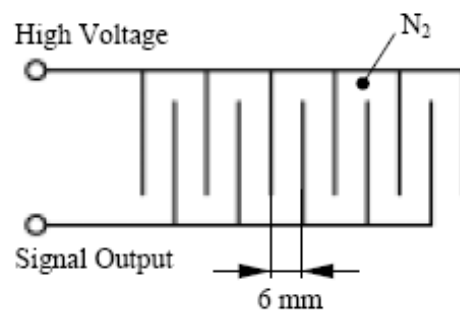


Figure 6.2. Schematic view of an ionization chamber. The figure is taken from [45].

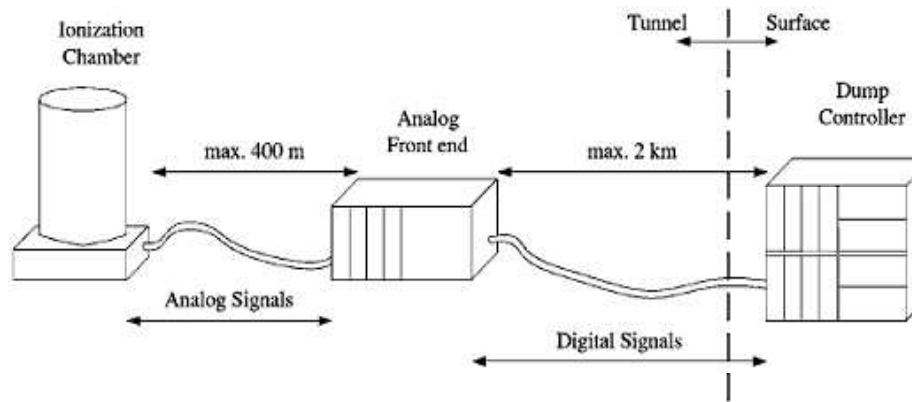


Figure 6.3. Schematic view of readout chain for the LHC beam loss monitor system. The figure is taken from [45].

The ionization caused directly by the charged particle is called primary ionization. Here one or more electrons are freed from a gas atom by the passing particle. Most of the electrons and ions that reach the poles are however created by secondary ionization. This occurs when the electrons created by primary ionization in turn collide with other atoms and ionize them. If the detector is built in such a way that the electrical field is strong enough to accelerate the free electrons to a sufficiently high energy, this process can grow exponentially, with more and more electrons ionizing more and more atoms. For instance, if the anode is replaced by a thin wire, the cylindrical geometry will imply a $1/r$ dependence for the electric field, so the field is very strong close to the wire. Thus, the process will accelerate the closer the electrons get to the anode and induce a so-called avalanche. This effect can amplify the originally quite weak signal by as much as 10^4 to 10^6 times [12].

Secondary ionization can also take place if the charged particle passing through the gas excites an atom, which in turn ionizes another atom during its de-excitation. Sometimes there are two gases in a detector — one that is meant to capture energy from the passing particles through nuclear excitation, and another gas, called the quencher, that is meant to de-excite the first gas and produce electrons and ions that in turn induce the current.

The LHC beam loss monitor system consists of cylindrical ionization chambers filled with N_2 [11]. They are 19 cm long and have a surface of 80 cm^2 . The applied voltage can be varied between 800 V and 1800 V. In order to minimize the drift time of the ions and electrons created in the chamber, and thus make the system respond faster to beam losses, there are 31 parallel plates inside the cylinder with alternating polarity. The distance between the neighbouring plates is 6 mm.

The signal from the beam loss monitors goes first through the analog front end electronics, where it is converted into a digital signal that continues to a threshold controller, which is located in a surface building. The threshold controller checks the integrated signal on different timescales and is programmed to calculate the

actual energy deposition in the coil from this. The correlation between the power losses in the magnet coil and the signal from the BLM induced by shower particles was determined through simulations in the case of protons [28]. If the power density is found to be too high, either a warning or a signal to dump the beam is sent to the beam abort system. Then the beam will be extracted from the main LHC ring and deposited in a beam dump.

For a closer description of the readout electronics see [11] and for the beam abort system see chapter 17 in [13]. A picture of one of the ionization chambers can be seen in figure 6.1, and a schematic view of the detector and the whole readout chain can be seen in figures 6.2 and 6.3.

6.2 Simulation setup

The most straight-forward way of finding out if the setup for protons is suitable also for ions is to simulate the impact of both ion and proton beams in an LHC magnet and then compare the ratio between energy deposition in the coil and in a detector outside the cryostat for both particle types. The energy deposition in the BLM is approximately directly proportional to the output signal. The particles hitting the BLMs have a low energy, so the dominating source of energy loss in the gas is ionization, which in turn gives rise to the output signal. The model of the BLM does not need to be exact in this case, since the ratio and not the absolute number is the interesting quantity. In [11] the BLMs were modelled as thin rectangular chambers with iron walls filled with N_2 . This is not the real shape, but this approximation is good enough also for this purpose.

For convenience, the dipole model from the simulation of the BFPP shower was used again, with the modelled BLMs added outside the cryostat. The transverse cross section of the computer model is shown in figure 6.4. Also the same magnetic field map was used. At first one might suspect that this fieldmap, which only covers the cold mass, is not precise enough, since the particles giving rise to the signal in the BLMs have to traverse the void outside the cold mass, where there is a weak magnetic field, on the order of μT . This field could bend low energy charged particles in such a way that the signal changes. Therefore a larger magnetic fieldmap extending 30 cm outside the cryostat was obtained from [26]. However, two otherwise identical FLUKA simulations showed that this difference is negligible. Therefore the smaller fieldmap was used in the following simulations, because the tracking in FLUKA is faster and more accurate in regions without magnetic field.

The biasing requires some closer attention. The biasing used in the BFPP simulation was set up to produce a very accurate scoring in the coils and a lot less accurate one in the outer regions of the dipole. Thus this biasing introduces a large uncertainty in the particle flux in the BLM and is therefore not appropriate. On the other hand, if the biasing was tuned to set the priority on the BLM, the scoring in the coils would be inaccurate. And an unbiased simulation would require far too much computer time. The found solution to the problem was to run every the simulation twice — once with the old biasing, which is accurate in the coils, and

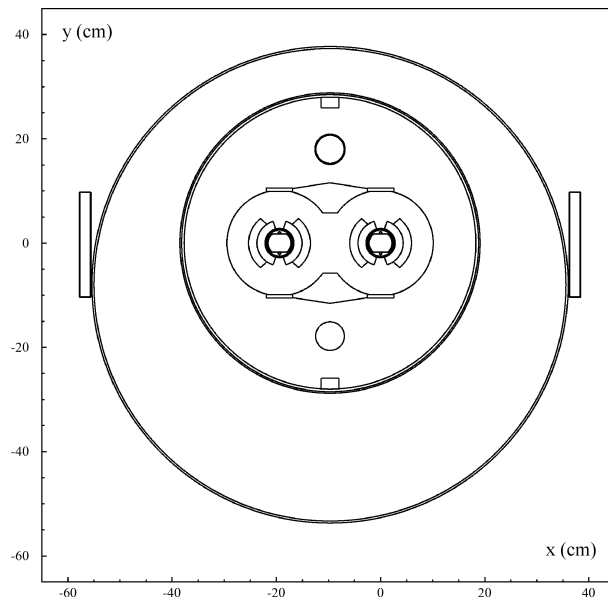


Figure 6.4. The transverse cross section of the computer model of the dipole with the BLMs.

once with a new biasing, which instead is accurate in the BLMs. Then the energy deposition in the coils could be taken from the first simulation and the deposition in the BLMs from the second one.

The new biasing applied was based on the same idea as the one described in Section 4.3. The regions were divided into four different importance classes with the same biasing parameters as in table 4.1, but this time the most important regions were the BLMs themselves and the air around them, the second class consisted of the cryostat wall, the air inside and the yoke, the third class was the remaining inner parts of the magnet and the fourth class, finally, consisted of the tunnel and the tunnel wall.

So four different FLUKA runs had to be performed — both 7 TeV protons and 2.76 TeV/nucleon lead ions with the two different biasing settings. The beam used was a pencil like beam—that is, all particles hit in the same point, in this case at $z=0$ in the beginning of the magnet at an azimuthal angle of $-\pi$ and with an incident angle of 25 mrad. A pencil beam is the simplest type of beam to simulate and the same beam that was used in [11]. Using the same shape and composition of the BLMs and the same beam, the FLUKA simulation will be easier to compare with [11]. The pencil beam, used as a δ -function, can symbolize any beam loss. It is very unlikely that the change of beam distribution should substantially change the ratio between energy deposition in the coils and in the BLMs.

The scoring was again done with the USRBIN card recording energy deposition. In the simulations with biasing priority on the coils, the *old* mesh described in table 4.2 was used. And in the simulations with the priority set to the BLMs, a

cartesian mesh with $\Delta z = 5$ cm and $\Delta x = \Delta y = 1$ cm was set up in both BLMs throughout the full length of the magnet.

6.3 Results

In figure 6.5 the results from all four FLUKA simulations are shown. The curves have quite similar shapes. This becomes even more clear when regarding figure 6.6, where the function

$$f(z) = \frac{E_{\text{ions,coil}}(z)/E_{\text{ions,BLM}}(z)}{E_{\text{protons,coil}}(z)/E_{\text{protons,BLM}}(z)} \quad (6.1)$$

is plotted. Here E is the energy deposition per volume and primary particle. As can be seen in the figure, this curve is fluctuating around 1 or even below, meaning that the ratio between energy deposited in the coil and in the BLMs is approximately the same for ions and protons. The peak in the beginning of the curve is clearly a statistical fluctuation. It is also not as important as one might think, since figure 6.5 shows that the absolute maximum for both curves, which is the critical part for determining quenching, is located at $z=25$ cm.

It is clear from figure 6.5 that the shapes of the curves for ions and protons do not differ much. Physically, one might expect a difference, since the ions have much higher cross sections for electromagnetic interactions as described in Section 2.6. So before the nuclear breakup, the ions should lose their energy faster, thus increasing the top value in the coils. But in figure 6.5 this first large energy loss can not be seen.

The explanation is that the ion beam hits the pipe with a very small angle around 25 mrad. Therefore the peak in the energy deposition from before the nuclear fragmentation is already in the beam screen and because of the angle it never reaches the coils. A new set of FLUKA simulations, where the energy deposition also in the beam screen was scored, confirms this. The result for both ions and protons is shown in figure 6.7. The curve for protons was scaled with the energy ratio 2.76/7 between ions and protons and then multiplied with the number of nucleons, 208, in one lead ion in order to simplify the comparison. The resulting number of protons to compare with is 82.

So the conclusion of the simulation is that the lead ions and protons at LHC energies will have the same energy to signal ratio, meaning that the thresholds for the BLMs do not need to be changed. However, this conclusion is based also on the assumption that the losses for ions and protons occur in the same places around the LHC, since there is a certain spacing between the BLMs. For instance, at the spot where the lost ions from BFPP hit, there is no BLM placed in the present design. This means that the BLM catching the traces from BFPP will be too far away and therefore not make a correct estimation of the power deposition in the coil. Therefore, in order to safely operate the LHC, it is essential to place a BLM at this spot but also to investigate other sources of ion losses and trace the loss locations.

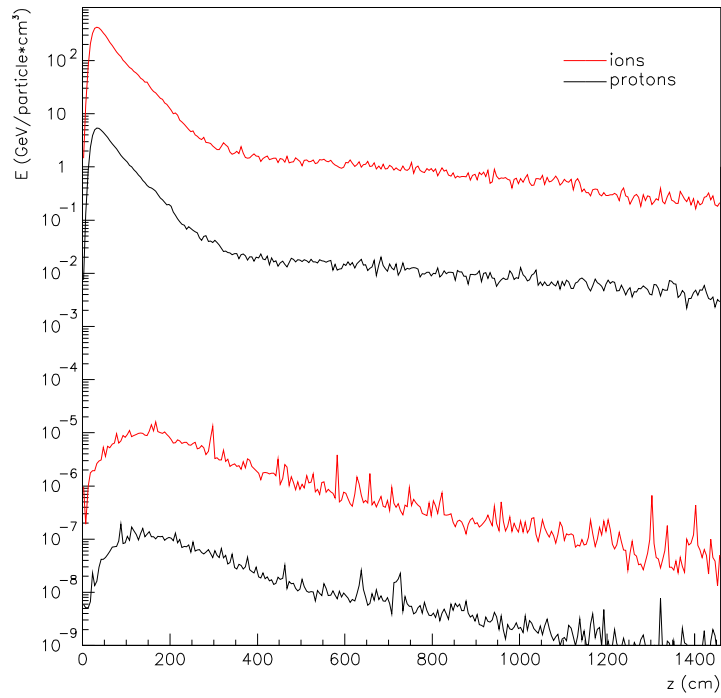


Figure 6.5. The two upper curves show the energy deposition in the hottest part of the inner coil for ions and protons, and the two lower curves the energy deposition in the BLMs.

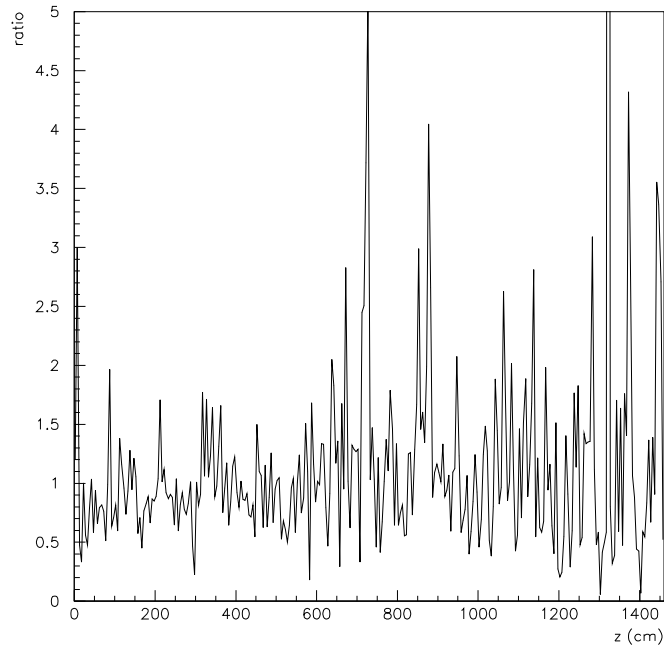


Figure 6.6. The ratio between ion and proton losses and signals as described by equation (6.1).

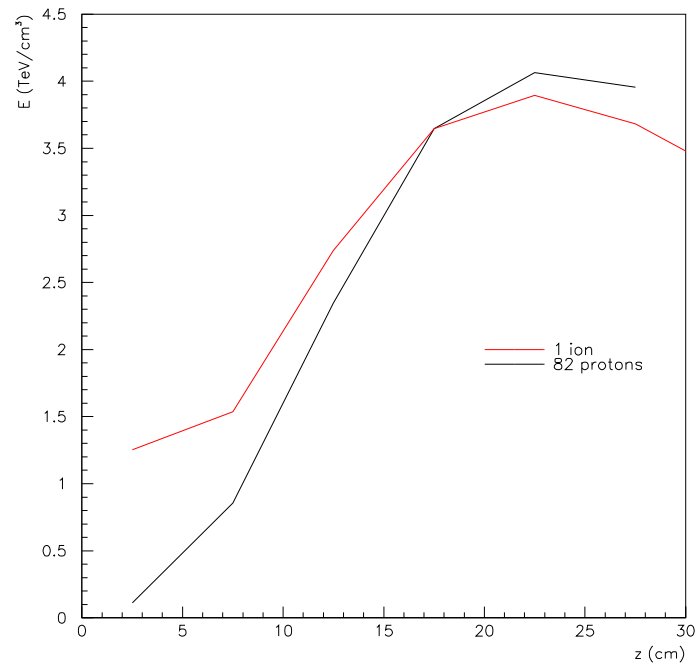


Figure 6.7. The energy deposition for one ion and 82 protons in the beam screen. In the very beginning, before the nuclear fragmentation, the energy deposited by the ion is higher due to the large cross sections for electromagnetic interactions.

Chapter 7

Comparison with experimental data from RHIC

RHIC (Relativistic Heavy Ion Collider) [6] is a heavy ion collider situated at the Brookhaven National Laboratory near New York in the USA. It was put into operation in year 2000. It is the first large-scale machine ever capable of colliding ultra-relativistic heavy ions. RHIC consists of two six-fold symmetric storage rings, called the blue and the yellow ring, which are located at ground level and have a circumference of 3.8 km. Two ion beams are circulating in opposite directions in the two rings, and they can be brought into collision at six interaction points around the ring. At four of these points experiments called STAR, PHENIX, PHOBOS and BRAHMS have been built. The other two interaction points are for the moment not being used for particle experiments. RHIC has collided a variety of ions from polarized protons to Au⁷⁹⁺ at a maximum energy of 100 GeV/nucleon for ions.

Also at RHIC, superconducting magnets made of NbTi are being used. However, there are two separated rings at RHIC, while at LHC there is only one with both beampipes inside. So the design of the magnets is slightly different since the magnet only has to accommodate one beampipe. The coils also have only one layer, while the coils in the LHC dipoles have two. The transverse cross section of a RHIC dipole magnet can be seen in figure 7.1. The operating temperature of the RHIC dipoles is 4.67 K and the highest operational magnetic field is 3.46 T. The fieldmap of a RHIC dipole magnet is shown in figure 7.2.

7.1 The BFPP experiment

When running beams with gold ions at RHIC, the problem with BFPP does not appear. Since gold and lead ions have almost the same charge, $Z = 79$ for gold and $Z = 82$ for lead, the fractional momentum deviation will be approximately

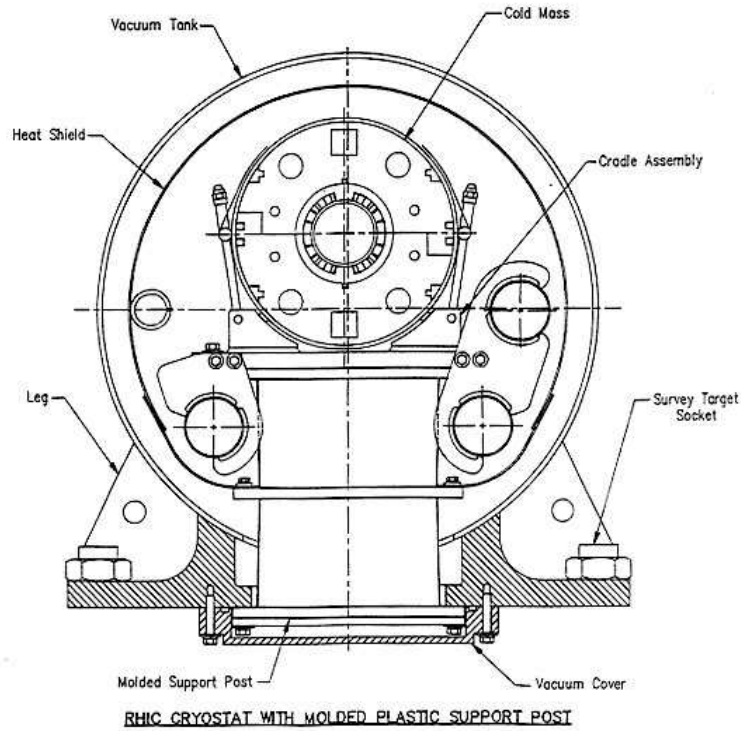


Figure 7.1. The transverse cross section of a dipole magnet at RHIC. The beam pipe can be seen in the centre, surrounded by the coil and the cold mass.

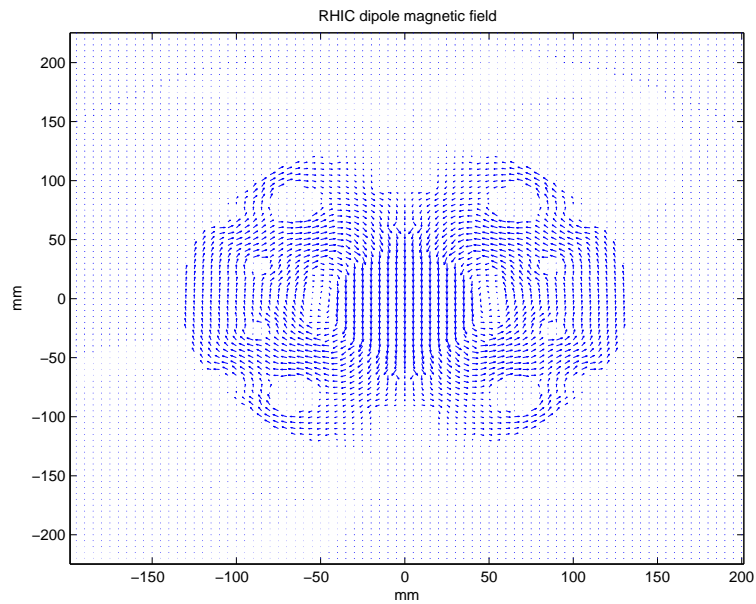
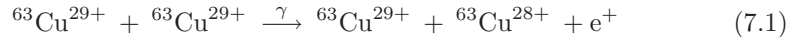


Figure 7.2. A vector plot of the magnetic fieldmap in the $x - y$ plane of the RHIC dipole.

the same according to equation (2.10). But the beampipe at RHIC has a diameter of 6.91 cm and is thus larger than the beampipe at the LHC, which is only 4.4 cm, which in turn makes the acceptance of the fractional momentum deviation higher. This difference among other things turns out to make the wrongly charged ion beam travel longer inside the pipe and thus be lost in a more homogenous way. Thus BFPP was never a critical issue in the runs with Au⁷⁹⁺ ions, although it significantly contributed to the decrease in luminosity with time.

However, in order to study the new state of hadronic matter at RHIC, also copper Cu²⁹⁺ were being brought into collision for a few weeks in the beginning of 2005. Also copper ions undergo BFPP:



Since the charge of copper is only 29, the fractional momentum deviation due to BFPP will be significantly larger than in the case of lead or gold. This can be seen in equation (2.10). And the larger beampipe is in this case not enough to accommodate this larger momentum deviation. So the copper ions will hit the beampipe and form a spot.

It is however also worth noticing that the cross section for BFPP at 100 GeV/nucleon is much smaller, only 0.1 barn, than for lead at 2.76 TeV/nucleon, where $\sigma_{\text{BFPP}} = 281$ barn. This seems plausible when looking at equation (2.4) and when put into equation (2.1) it means that the rate of wrongly charged ions impinging on the beam screen is lowered by a factor 2800.

However, the runs with copper at RHIC gave a unique opportunity to actually measure the effect of BFPP. If the approximate location of the spot in the beampipe is known, detectors can be placed outside the cryostat to measure the flux of secondary particles. Then the experimental data can be used first to see if there are any effects caused by BFPP and then also for a comparison with FLUKA simulations. Such an experiment was thus performed by a collaboration between CERN and RHIC teams, where the task treated in this report is to simulate the shower of secondary particles outside the cryostat in FLUKA.

In order to find the appropriate position for the detectors, a tracking similar to the one described in Section 2.5 was performed through the RHIC beam optics [47]. This tracking shows that the secondary ion beam will hit the inside of the pipe 135 metres from the PHENIX interaction point. A visualization of this tracking is shown in figure 7.3.

In order to measure the flux of secondary particles, PIN diodes were strapped onto the outside of the cryostat on the same side as where the secondary beam hits. PIN diodes are detectors made of silicon or a similar semiconductor material, and a voltage is applied between its ends. When a charged particle passes through the detector, it will ionize the atoms of the diode, which in turn will create free electrons inside the material. These electrons will move due to the voltage, creating a small current that can be measured. The used diodes had an area of 1 cm² and were placed every three metres around the expected impact position. A photo of a PIN diode mounted outside the cryostat is shown in figure 7.4.

During operation of the machine, the signals from all detectors were recorded. The luminosity was varied and, when compared to the signals from the diodes, a

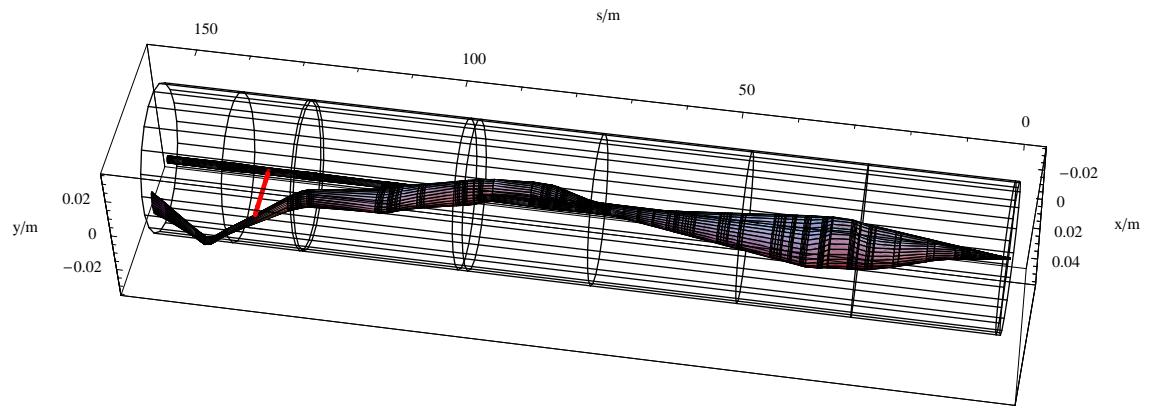


Figure 7.3. The tracking of the primary and secondary beam at RHIC. The interaction point is to the right. To the left, the two beams are separated and the secondary beam hits the pipe after 135 m. The original curved geometry and magnetic field was transformed to be straight in the computer model. The red line indicates the spot where the secondary beam hits the inside of the pipe.



Figure 7.4. A photo of a PIN diode mounted on the outside of the RHIC cryostat.

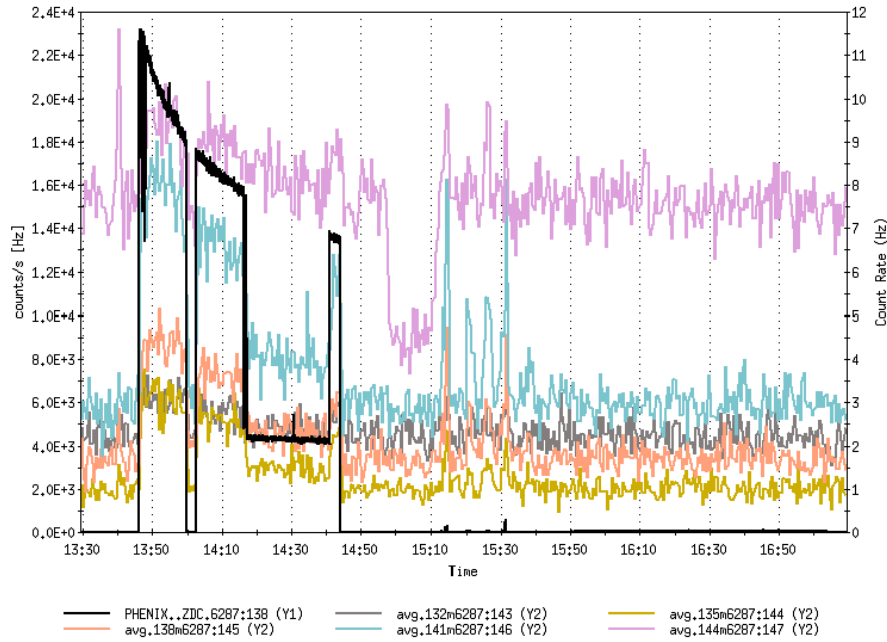


Figure 7.5. The signals from the different PIN diodes in the RHIC experiment as a function of time. The black curve is the luminosity. The pin diode at 141.6 m was the one that gave the highest signal.

clear correspondence was found. This is shown in figure 7.5, which represents the first measurement ever of BFPP on a high energy collider.

When the luminosity, the black curve, equals zero, the PIN diodes still gave a signal caused by the background noise. Thus this background level has to be subtracted from the absolute value of the signal.

7.2 Simulation setup

The BFPP experiment at RHIC gave a unique opportunity to compare the FLUKA simulations with real data and in this way evaluate the calculations for the LHC. Thus a simulation of the particle shower caused by the BFPP copper ion beam in the RHIC magnets was performed.

The calculated impact point at 135 m from the interaction point is in the middle of a dipole. The transverse cross section of a dipole at RHIC was shown in figure 7.1. This magnet was modelled in FLUKA, with some simplifications analogous to the ones made for the LHC dipole. The legs and supports outside the cryostat were not modelled, neither the cradle assembly inside. These parts are far from the path of the secondary shower particles and will have little impact on the energy deposition in the PIN diodes. The coils were also modelled as made

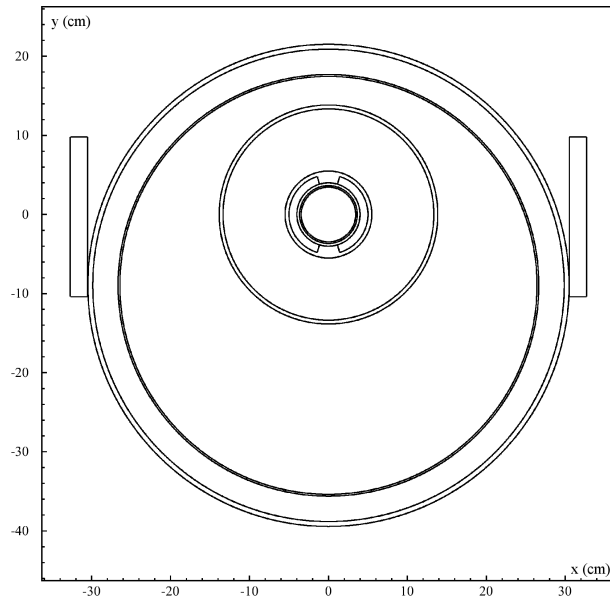


Figure 7.6. The transverse cross section of the FLUKA model of the RHIC dipole.

of copper instead of NbTi in a copper matrix and the magnet as straight. This last approximation is however not as obvious in this case as with the LHC dipole. The reason is that the cold mass has a different radius of curvature than the cryostat with a quite large sagitta of 3 cm relative to the cryostat [48]. However, since the torus is not implemented as a generic body in FLUKA, this is a necessary approximation. This is however a possible source of errors for several reasons, which will be further discussed in Section 7.3.

Also the magnetic field of the dipole had to be taken into account. The field was calculated by [48] and implemented and linearly interpolated in FLUKA through a Fortran program. The computer model of the dipole is shown in figure 7.6 and the magnetic fieldmap in figure 7.2. The cross section of the real dipole is shown in figure 7.1.

The calculated impact point is 4 m away from the end of the dipole magnet. Since the shower extends further than that, the lattice magnet after the dipole has to be modelled too. The dipole ends at 139.04 m, then there is a short drift area and after that a quadrupole starts at 140.6 m. The RHIC quadrupole magnet is however very similar to the dipole in its shape except for the coils. And the exact shape of the coils several metres away from the impact point does not play a significant role in the shower development. Therefore, the quadrupole magnet was approximated as a copy of the dipole, but without any magnetic field. The field of the quadrupole outside the beampipe is much weaker than the field of the dipole and therefore it is a fair approximation to neglect the quadrupole field. Also the magnetic field in the empty drift area between the two magnets was neglected.

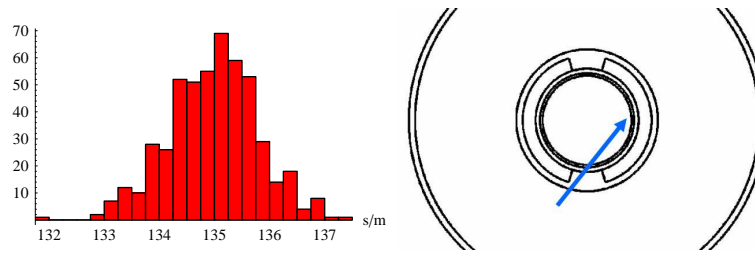


Figure 7.7. The longitudinal distribution, the number of particles versus impact point, of the impinging Cu ions at RHIC (left). A schematic picture of how the secondary beam hits the inside of the pipe (right).

This field is also weaker than the dipole field and it is also not known in detail. This approximation could however be too simplistic, which is further discussed in Section 7.3.

The coordinates and momenta of the impinging particles were taken directly from the tracking. The longitudinal distribution is shown in figure 7.7. In total 500 particles were simulated. The impact angle is distributed around 2.5 mrad to the beam pipe. However, there is an uncertainty in the initial distribution of the beam particles. In the tracking program MAD-X [20] that produced the distribution, all magnetic elements along the beam line are represented by transfer matrices that transform the beam coordinates and momenta accordingly. In this abstract description of the collider, the actual geometry of the machine is not present and all coordinates are given relative to a reference orbit. In an ideal machine, this reference orbit is in the middle of the beam pipe, but it can be displaced due to imperfections and small optical errors. If there is an angle between the reference orbit and the tangent of the beam pipe, also the incident angle of the beam on the vacuum chamber changes. Also the actual position where the beam hits can change slightly due to this uncertainty. In a dipole magnet, the field in the beam pipe is close to homogenous, which means that the transfer matrix does not change if the reference orbit is slightly displaced from the centre of the vacuum chamber. At the time of writing the reference orbit was still not known at CERN, and the large sagitta of the beam pipe relative to the cryostat implies that the effect of an off-centred reference orbit is enhanced, meaning that the uncertainty in angle increases.

Also the PIN diodes had to be modelled. This was done geometrically in the same way as the BLMs were modelled in Chapter 6. They were simulated as rectangular silicon blocks located outside the cryostat. If they were given the natural small size of 1 cm^2 , they would not be useful for scoring due to statistical fluctuations. The Monte Carlo simulation used can not generate enough statistics in reasonable computer time to produce data of use for such small detectors. Therefore the detectors were made larger, extending 10 cm vertically on each side of the centre of the beam pipe. They were also modelled all along the cryostat instead of being present only every third metre as in the experiment in order to get a more complete overview of the physical processes. Since the absolute calibration

of the PIN diodes is not known, it is not possible to reconstruct their signals in absolute numbers. However the ratio between the signals from different detectors can be studied and compared with the simulations. And this ratio will not change because of the different shape of the diodes in the simulation.

The scoring was performed in the same way as the scoring in the BLMs by the LHC dipole. The USRBIN card in FLUKA was used to score the energy deposition in the silicon blocks in a mesh with dimensions $\Delta z = 5$ cm and $\Delta x = \Delta y = 1$ cm. Also biasing had to be used in the simulations, since they would require too much time and computer resources otherwise. The biasing was done in the exact same way as for the LHC dipole when the priority was set to the BLMs. The geometry was divided into four different importance classes with the detectors and the air around them in the first class, the cryostat, the air inside it and the yoke in the second class, the inner parts of the magnet in the third class and the tunnel and wall in the fourth. These importance classes were then assigned biasing parameters according to table 4.1.

7.3 Results and conclusion

As explained in Section 7.2, the real signal from the PIN diodes is not possible to reconstruct. But the ratio between the signal from different PIN diodes after the assumed background noise has been subtracted is shown in figure 7.8. Worth noticing is the fact that the maximum in the signal is actually recorded by the PIN diode at 141.6 m, which is located after the magnet where the beam is lost.

The first FLUKA run with the initial 2.5 mrad angle did not reproduce this shape. Therefore, due to the uncertainty in angle, new FLUKA simulations were performed, where the angle of incidence was gradually decreased. This changes the ratio between the peak signals of the detectors outside the the first and the second magnet. The results from the simulations for different angles and both sides of the cryostat are shown in figure 7.9.

But even if the incident angle is decreased the shape does not correspond very well to the experimental results. Several reasons are identified that may explain this. First of all, as already mentioned, there is an uncertainty in the incident angle and position of the beam. Small optical errors along the beam line can amplify this effect. Furthermore, the relative calibration of the PIN diodes is not known. So far it has been silently assumed that all PIN diodes have the same zero level. This is however not necessarily true. The read out chain includes electronics that need to be calibrated and tuned. Since the experiment was set up very quickly it has not been possible to obtain this calibration information.

Yet another error source is that the signal from other losses could be superimposed on the signal from BFPP. Other loss mechanisms exist and the distribution of the lost particles is not yet known. Also the fact that no magnetic field was implemented in the empty section between the magnets could contribute to the discrepancy, since the field could contribute through bending secondary charged particles emerging out of the first beampipe towards the outside and the detector.

The conclusion is that the detailed correspondence so far between possible

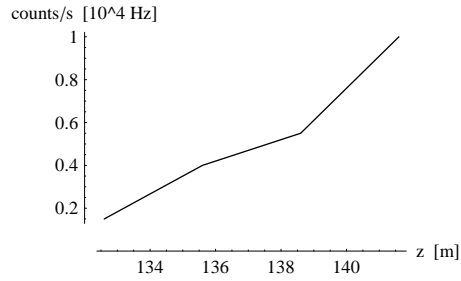


Figure 7.8. The profile of the signal in the PIN diodes versus z . The values are extracted from figure 7.5 with the zero level subtracted. The diode at 144.6 m was not included since the signal from this diode did not follow the luminosity, as can be seen in figure 7.5.

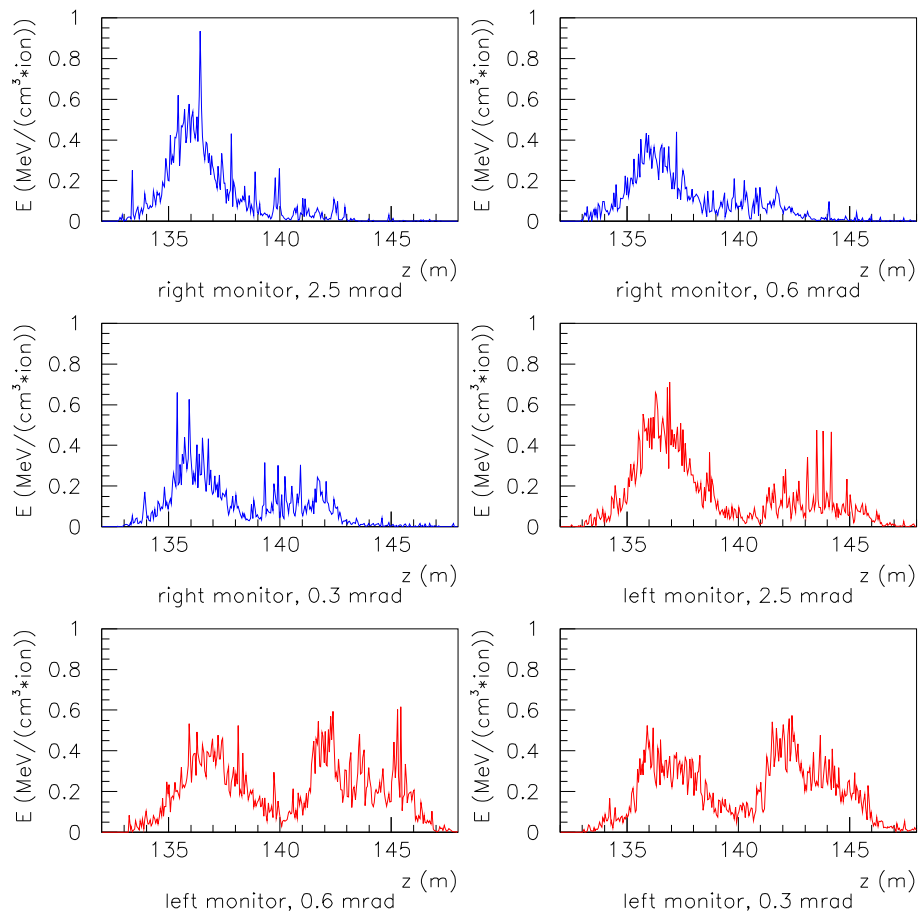


Figure 7.9. The energy deposition in the silicon detectors as a function of z for different angles of incidence of the beam. The PIN diodes were placed on the side labelled "right", towards the outside of the ring.

simulations and the experimental data is relatively poor, but several causes for this discrepancy have been identified. Because of these uncertainties, the simulation of the RHIC dipole is not yet a good benchmarking test of the previous FLUKA simulations. However, the most important conclusion is mentioned in Section 7.1. Figure 7.5 shows that there is a clear correspondence between the luminosity and the signal on the PIN diodes in a very localized position. Most likely this is the first experimental evidence of BFPP in colliding beams and it means that BFPP will take place also in the LHC. But it remains to understand more in detail the discrepancies between the simulation and the experiment.

Chapter 8

Concluding remarks

As described in Chapter 1, the main task in this thesis was to investigate whether the secondary ion beam caused by BFPP risks to quench the superconducting magnets in the LHC. Another task was to determine if the present setup for the BLM system, adapted for protons, is suitable also for ion operation. Finally a simulation of the shower caused by the secondary BFPP copper beam at RHIC was made and compared with experimental data.

The BFPP problem was much more complicated than it was initially believed, since the knowledge of the actual quench limit for the LHC dipole turned out to be limited. In [13] there is a given limit of 4.5 mW/cm^3 for the power density in the magnet. FLUKA simulations showed that the maximum power density caused by BFPP is 7.2 mW/cm^3 and therefore above the limit. But after a closer investigation of its origins, it was concluded that the given limit is probably too conservative. So although some uncertainties exist, both in the quench limit and in the simulation result, it can be concluded that the magnet is not likely to quench due to BFPP at design luminosity. A hypothetical consideration of the first instants of time after the beam has been set into collision, with no heat conduction and no convection, showed that the magnet can withstand the power deposition from BFPP for several seconds. This means that when also the cooling comes into play, it will take much more time before there is any danger. A quench is not likely to occur but can not be excluded.

The FLUKA simulations of the BLM system showed that the ratio between power density in the superconductors and expected signal on the BLMs is almost identical for ions and protons. The simulations showed that the peak in power deposition expected for ions, when they enter a material, occurs in the beam screen and not in the coils. Thus the same BLM thresholds can be used, provided that the ion and proton losses occur at the same places in the machine. The present placement of the detectors is adjusted to the expected loss locations for protons. Thus it is very important that further work be carried out in order to calculate expected loss locations for ions.

The simulations of the secondary ion beam at RHIC did not agree in detail with the experimental results. However, several possible error sources were identified,

for instance in the angle of incidence between the beam and the beam pipe as well as in the impact point. Also the signal caused by other sources is not known, as well as the absolute calibration of the PIN diodes used in the experiment. More work is still left to do on the analysis of the data from RHIC, and it is to be wished that this will aid in getting better understanding of the discrepancies.

Bibliography

- [1] <http://www.cern.ch>.
- [2] G. Bayatian et al. CMS technical proposal. *CERN/LHCC 94-38, LHCC/P1*, 1994.
- [3] Atlas TDR. *CERN/LHCC/99-14*, 1999.
- [4] LHCb technical proposal. *CERN/LHCC 98-4, LHCC/P4*, 1998.
- [5] F. Carminati et al. Alice: Physics performance report. *J. Phys. G: Nucl. Part. Phys.*, (30):1517, 2004.
- [6] <http://www.bnl.gov/rhic>.
- [7] J.B. Jeanneret et al. Quench levels and transient beam losses in LHC magnets. *LHC Project Report 44*, 1996.
- [8] Superconductivity in particle accelerators. *Proceedings of the Cern Accelerator School, CERN 96-03*, 1996.
- [9] N. W. Ashcroft and N. D. Mermin. *Solid State Physics*. Brooks Cole, 1976.
- [10] M. Wilson. *Superconducting magnets*. Clarendon Press Oxford, 1983.
- [11] E. B. Holzer et al. Design of the beam loss monitoring system for the LHC ring. *LHC Project Report 781*, 2004.
- [12] J. Mnich. Elementarteilchenphysik.
<http://www.physik.rwth-aachen.de/~roth/eteilchen/ETeilchen.pdf>. 2004.
- [13] O.S. Brüning, P. Collier, P. Lebrun, S. Myers, R. Ostojic, J. Pool, and J. Proudlock (editors). LHC design report v.1 : the LHC main ring. *CERN-2004-003-V1*, 2004.
- [14] J. M. Jowett. Ions in the LHC ring. *Proceedings of the LHC Performance Workshop, Chamonix XII*, 2003.
- [15] G. Baur et al. Coherent $\gamma\gamma$ and γA interactions in very peripheral collisions at relativistic ion colliders. *Phys. Rept.*, (364):359, 2002.

- [16] H. Meier et al. Bound-free electron-positron pair production in relativistic heavy-ion collisions. *Phys. Rev. A*, (63), 2001.
- [17] S.R. Klein. Localized beam pipe heating due to e^- capture and nuclear excitation in heavy ion colliders. *Nuclear instruments and Methods in Physics Research A*, (459):51, 2001.
- [18] H.F. Krause et al. Electron capture and ionization of Pb ions at 33 TeV. *Phys. Rev. Letters*, 80(6):51, 1998.
- [19] S. Datz et al. Measurement of electromagnetic cross sections in heavy ion interactions and its consequences for luminosity lifetimes in ion colliders. *CERN SL-99-009*, 1999.
- [20] <http://mad.home.cern.ch/mad/>.
- [21] S. Eidelman et al. Review of Particle Physics. *Physics Letters B*, 592:1+, 2004.
- [22] O. Zimmer. Introduction to nuclear and particle physics. <http://www.e18.physik.tu-muenchen.de/zimmer/>. 2004.
- [23] A. Fasso et al. *Electron-photon transport in FLUKA: Status, invited talk in the Proceedings of the MonteCarlo 2000 Conference*, page 159. Springer-Verlag Berlin, 2001.
- [24] A. Fasso et al. *FLUKA: Status and Prospective for Hadronic Applications, invited talk in the Proceedings of the MonteCarlo 2000 Conference*, page 955. Springer-Verlag Berlin, 2001.
- [25] C. Meuris et al. Heat transfer in electrical insulation of lhc cables cooled with superfluid helium. *Cryogenics*, (39):921, 1999.
- [26] S. Russenschuck, private communication, 2004.
- [27] <http://wwwasd.web.cern.ch/wwwasd/geant4/geant4.html>.
- [28] E. Gschwendner et al. The beam loss detection system of the LHC ring. *CERN SL-2002-021*, 2002.
- [29] I. M. Sobol. *A primer for the Monte Carlo Method*. CRC-Press, 1994.
- [30] A. F. Bielajew. Fundamentals of the Monte Carlo method for neutral and charged particle transport. <http://www-personal.engin.umich.edu/~bielajew/mcbook/book.pdf>. 2001.
- [31] G. Blom. *Sannolikhetsteori och statistikteori med tillämpningar*. Studentlitteratur, 1989.
- [32] <http://www.fluka.org>.

- [33] M. Magistris, private communication, 2004.
- [34] <http://www.wolfram.com>.
- [35] <http://paw.web.cern.ch>.
- [36] J. H. Lienhard IV and J. H. Lienhard V. *A heat transfer textbook*. Phlogiston Press, 2003.
- [37] D. Leroy, private communication, 2005.
- [38] R. Bruce, S. Gilardoni, and J. M. Jowett. Luminosity limit from bound-free pair production in the LHC. *Proceedings of the 2005 Particle Accelerator Conference, Knoxville, Tennessee*, 2005.
- [39] R. Bruce, S. Gilardoni, and J. M. Jowett. Ion operation and beam losses. *Proceedings of AMT 01 - Beam generated heat deposition and quench levels for LHC magnets*, 2005.
- [40] F. Sonnemann and M. Calvi. Quench simulation studies: Program documentation of SPQR Simulation Program for Quench Research. *LHC Project Note 265*, 2001.
- [41] A. Siemko et al. Beam loss induced quench levels. *Proceedings of the LHC Performance Workshop, Chamonix XIV, CERN-AB-2005-014*, page 296, 2005.
- [42] S. A. Elrod et al. The specific heat of NbTi from 0 to 7 T between 4.2 and 20 K. *Advances in Cryogenic Engineering*, (28), 1982.
- [43] <http://www.users.uswest.net/~varp/hepak.htm>.
- [44] J-B Jeanneret, private communication, 2005.
- [45] B. Dehning et al. LHC Beam Loss Monitor System Design. *Proceedings of the Beam Instrumentation Workshop 2002: Tenth Workshop, American Institute of Physics*, page 229, 2002.
- [46] W. Blum and E. Rolandi. *Particle detection with drift chambers*. Springer-Verlag, 1993.
- [47] J. M. Jowett, private communication, 2005.
- [48] R. Gupta, private communication, 2005.

Appendix A

Common acronyms

ALICE	A Large Ion Collider Experiment
ATLAS	A Toroidal LHC ApparatuS
BCS	Bardeen, Cooper and Schrieffer
BFPP	Bound Free Pair Production
BLM	Beam Loss Monitor
BRAHMS	Experiment at RHIC
CERN	Conseil Européen pour la Recherche Nucléaire
CMS	Compact Muon Solenoid
FLUKA	FLUktuierende KAskade
IP	Interaction Point
LEP	Large Electron-Positron collider
LHC	Large Hadron Collider
PDF	Probability Density Function
PEMF	Preprocessor for ElectroMagnetic FLUKA
PHENIX	Experiment at RHIC
PHOBOS	Experiment at RHIC
PS	Proton Synchrotron
PSB	Proton Synchrotron Booster
RHIC	Relativistic Heavy Ion Collider
SLAC	Stanford Linear ACcelerator